Thesis

The role of NOX4 in SIRT4-driven worsening of pathological cardiac hypertrophy

submitted by

Carolin Költgen

in partial fulfillment of the requirements for the degree of

Doktorin der gesamten Heilkunde

(Dr.^{in} med. univ.)

at the

Medical University of Graz

executed at the

University department of Internal Medicine

Division of Cardiology

Under the supervision of

Assoz. Prof. Priv.-Doz. Dr. Heiko Matthias Bugger

and

Nikole Byrne, PhD

Graz, 23.08.2024

I. Statutory Declaration

I solemnly declare that I have independently and without external assistance authored this present work, have not utilized sources other than those indicated, and have clearly identified passages taken verbatim or in content from the used sources.

Graz, 23.08.2024 **Carolin Költgen eh.**

II. Acknowledgements

First, I would like to thank my supervisor, Assoz. Prof. Priv.-Doz. Dr. Heiko Bugger, for his invaluable guidance and support. I am deeply grateful for the opportunity to undertake this compelling work under his mentorship.

Next, I would like to thank my second supervisor, Dr. Nikole Byrne, whose support at every juncture has been instrumental and I appreciate her continued support tremendously.

Special thanks go to Dipl.-Biol. Katharina Pfeil, who was always there to help and advise me and whose technical support was crucial for the successful completion of this project.

I would also like to express my gratitude to my family, for their unwavering support and boundless encouragement.

Lastly, I want to thank my partner and great support Alexander, who stood by my side at all times and who I could always rely on.

III. Zusammenfassung

Oxidativer Stress trägt nachweislich zur Ausbildung einer kardialen Hypertrophie bei. Die mitochondriale NAPDH-Oxidase 4 (NOX4) kann durch Produktion reaktiver Sauerstoffspezies (ROS) direkt mit oxidativen Stresses in Herzmuskelzellen in Verbindung gebracht werden. Sirtuin 4 (SIRT4) ist eine mitochondriale Deacetylase, die an der Regulierung der ROS-Homöostase beteiligt ist und das hypertrophe Wachstum des Herzens beschleunigt. Vorläufige Daten unserer Gruppe zeigen, dass eine Überexpression von SIRT4 eine kardiale Hypertrophie durch vermehrten oxidativen Stress verschlimmern kann, möglicherweise vermittelt durch eine erhöhte NOX4-Expression. Um die Rolle von SIRT4 in der Regulation der NOX4-Expression in der Herzhypertrophie zu untersuchen, wurde in dieser Studie untersucht, ob eine SIRT4-Überexpression die NOX4-Expression als Reaktion auf pro-hypertrophe Signale im Zellkulturmodell erhöhen kann. Kardiomyoblasten der Ratte (H9c2) wurden mit einem Vektor für die Überexpression von humanem SIRT4 transfiziert und anschließend mit Angiotensin II (ANG II) oder Isoproterenol (ISO) stimuliert, um eine hypertrophe Reaktion auszulösen. Die Zellgröße wurde anhand einer Fluoreszenzfärbung quantifiziert. Die mRNA- und Proteingehalte von natriuretischem Hirnpeptid (BNP) und NOX4 wurden mittels RT-qPCR bzw. Immunoblotting analysiert. Die Transfektion führte zu einer erfolgreichen Expression humaner SIRT4-mRNA, jedoch nicht in Zellen mit Kontrolltransfektion. Die Expression von Ratten-SIRT4-mRNA war in SIRT4-transfizierten Zellen fast signifikant verringert (p=0,05), was auf eine kompensatorische Unterdrückung der endogenen SIRT4-Expression hinweist. Im Gegensatz zur ANG II Behandlung führte die Behandlung mit ISO zu einer Vergrößerung der Kardiomyozyten und einem erhöhten Bnp-mRNA-Spiegel, was auf eine erfolgreiche Induktion einer Hypertrophie hindeutet. Während die SIRT4-Überexpression allein die BNP-Spiegel im Vergleich zu Kontrolltransfektionen erhöhte, führte die Kombination von SIRT4-Transfektion und ISO-Behandlung nicht zu einer synergistischen Erhöhung der Bnp-mRNA-Spiegel. Die NOX4 mRNA- oder Proteinexpression wurden durch die ISO-Behandlung der Kontrollzellen nicht verändert. Darüber hinaus waren die NOX4-mRNA-Spiegel in SIRT4-überexprimierenden Zellen nicht signifikant erhöht, weder in Gegenwart noch in Abwesenheit von ISO. Daraus schließen wir, dass a) eine erhöhte Expression von SIRT4 zu Hypertrophie in H9c2-Kardiomyoblasten führt und b) die NOX4-Expression in H9c2-Kardiomyoblasten nicht von SIRT4 gesteuert wird.

IV. Abstract

Pathological hypertrophy leads to systolic and diastolic dysfunction and ultimately to heart failure. Oxidative stress has been shown to contribute to hypertrophic remodeling of the heart. Mitochondrial NAPDH oxidase 4 (NOX4) can be directly linked to the increase in oxidative stress in cardiac muscle cells through its production of reactive oxygen species (ROS). Sirtuin 4 (SIRT4) is a mitochondrial deacetylase that has been involved in the regulation of ROS homeostasis and is known to accelerate hypertrophic growth of the heart. Preliminary data from our group show that overexpression of SIRT4 drives aggravation of pressure overload-induced cardiac hypertrophy by oxidative stress, potentially mediated by markedly increased NOX4 expression. To evaluate the potential of SIRT4 to mediate NOX4 expression in cardiac hypertrophy, this study investigated whether SIRT4 overexpression increases NOX4 expression in response to pro-hypertrophic signaling in a cell culture model. Rat cardiomyoblasts (H9c2) were transfected with a vector for human SIRT4 overexpression and then stimulated with angiotensin II (ANG II) or isoproterenol (ISO) to induce a hypertrophic response. Cell size was quantified using wheat germ agglutinine (WGA) fluorescence staining. mRNA and protein levels of brain natriuretic peptide (BNP) and NOX4 were analyzed by RT-qPCR and JESS-automated immunoblotting, respectively. Transfection of rat cardiomyoblasts resulted in successful expression of human *SIRT4* mRNA, whereas human *SIRT4* expression was not detectable in cells undergoing control transfection. Expression of rat *SIRT4* mRNA was almost significantly decreased ($p=0.05$) in SIRT4 transfected cells, indicative of compensatory suppression of endogenous SIRT4 expression. While ANG II treatment did not increase cardiomyocyte size or *Bnp* mRNA levels, ISO treatment resulted in increased cardiomyocyte size and increased *Bnp* mRNA levels, indicative of successful induction of cardiomyocyte hypertrophy. While SIRT4 overexpression alone did increase BNP levels compared to control transfections, combining SIRT4 transfection and ISO treatment did not synergistically increase *Bnp* mRNA levels. NOX4 mRNA or protein expression was not altered by ISO treatment of control cells. In addition, *Nox4* mRNA levels were not significantly increased in SIRT4 overexpressing cells, neither in the presence or absence of ISO. Thus, we conclude that a) increased expression of SIRT4 leads to hypertrophy in H9c2 cardiomyoblasts, and b) NOX4 expression in H9c2 cardiomyoblasts is not driven by SIRT4.

V. Publications

Byrne NJ, Koentges C, Khan E, Pfeil K, Sandulescu R, Bakshi S, **Költgen C**, Vosko I, Gollmer J, Roth G, Hoffmann MM, Odening KE, Horstmann H, Potter LA, Bode C, Wolf D, Ljubojevic-Holzer S, Wallner M, Rainer PP, Sedej S, Scherr D, von Lewinski D, Wende AR, Zirlik A, Bugger H. Sirtuin 4 accelerates heart failure development by enhancing reactive oxygen species-mediated profibrotic transcriptional signaling. In revision at *Basic Research in Cardiology*.

VI. Table of contents

1. Abbreviations

Abbreviation	Definition
8-iso-PGF2α	8-iso-prostaglandin F2α
ACC	American College of Cardiology
ADP	Adenosine diphosphate
AHA	American Heart Association
ALDH2	Aldehyde dehydrogenase 2
ANF	Natriuretic peptide precursor type A
ANG	Angiotensin
ANOVA	Analysis of variance
ANP	Atrial natriuretic peptide
αTub	Alpha Tubulin
BNP	Brain natriuretic peptide
bp	Base pair
CAD	Coronary artery disease
CaMK II	Calcium/calmodulin- dependent protein kinase type II
cAMP	Cyclic adenosine monophosphate
cDNA	Complementary Deoxyribonucleic acid
cGMP	Cyclic Guanosine Monophosphate
CO_2	Carbon dioxide
CPS1	Carbamoyl Phosphate Synthetase I
CtIP	C-terminal binding protein -interacting protein
CVD	Cardiovascular disease
CYPD	Cyclophilin D
DAG	Diacylglycerol
DAPI	4',6-diamidino-2-phenylindole
DMEM	Dulbecco's Modified Eagle Medium
DNA	Deoxyribonucleic acid
e.g.	Exempli gratia
EF	Ejection fraction
eNOS	Endothelial nitric oxide synthase
FAO	Fatty acid oxidation

FBS	Fetal bovine serum
FOXO1	Forkhead-Box-Protein O1
FOXO3	Forkhead-Box-Protein O3
FOXO3a	Forkhead-Box-Protein O3a
GABP-ß1	GA-binding protein subunit beta-1
GDH	Glutamate dehydrogenase
GPCR	G protein-coupled receptors
Gq11	G protein subunit alpha q11
GSHPx	Glutathione peroxidase
HFmrEF	Heart failure with mildly reduced ejection fraction
HFpEF	Heart failure with preserved ejection fraction
HFrEF	Heart failure with reduced ejection fraction
H1F1a	Hypoxia-Inducible Factor 1-Alpha
H1F2a	Hypoxia-Inducible Factor 2-Alpha
H1K26	Histone 1 lysine residue at position 26
H3K18	Histone 3 lysine residue at position 18
H3K56	Histone 3 lysine residue at position 56
H3K9	Histone 3 lysine residue at position 9
H4K16	Histone 4 lysine residue at position 16
H9c2	Rat cardiomyoblast cell line
HDAC	Histone Deacetylase
HF	Heart failure
HMGCS2	3-hydroxy-3-methylglutaryl-CoA synthase 2
HSF1	Heat Shock Factor 1
Hsp60	Heat Shock Protein 60
IP3	Inositol Trisphosphate
ISO	Isoproterenol
KAP1	Krüppel-associated box (KRAB)-associated protein 1
Ku68	Kurchatov antigen 68
LB	Lysogeny broth
LV	Left ventricle
MCCC	Methylcrotonyl-CoA carboxylase
MCD	Malonyl-CoA decarboxylase

ß-MHC	ß-myosine heavy chain
MI	Myocardial infarction
MnSOD	Manganese Superoxide Dismutase
mRNA	Messenger Ribonucleic acid
mtDNA	Mitochondrial Deoxyribonucleic acid
MYH7	myosin, heavy chain 7, cardiac muscle, β
NADPH	Nicotinamide Adenine Dinucleotide Phosphate
N.D.	Not detectable
NF-kB	Nuclear Factor-kappa B
NFAT	Nuclear Factor of Activated T-cells
Nox	NADPH oxidase
Nox4	NADPH oxidase 4
NP	Natriuretic peptide
NPR	Natriuretic Peptide Receptor
p53	protein 53
PDH	Pyruvate dehydrogenase
PGC1α	Peroxisome Proliferator-Activated Receptor Gamma Coactivator 1-Alpha
PJ	PolyJet™
PKG	Protein Kinase G
PTP	Permeability Transition Pores
RAAS	Renin-Angiotensin-Aldosterone System
PAF53	Polymerase I-associated factor 53
RARP1	Retinoic acid-responsive proline-rich protein 1
rDNA	Recombinant DNA
RHOA-RHO	Ras Homolog Family Member A
RIPA	Radio-Immunoprecipitation Assay
RNA	Ribonucleic acid
ROS	Reactive oxygen species
RV	Right ventricle
S.O.C-media	Super Optimal Broth with Catabolite repression medium
SEM	Standard Error of the Mean
Sirt4	Sirtuin 4

SMAI	Serratia marcescens restriction enzyme I
SNS	Sympathetic Nervous System
SOD	Superoxide Dismutase
TAC	Transverse aortic constriction
TAE	Tris-Acetate-EDTA
TCA	Tricarboxylic acid
TNFα	Tumor Necrosis Factor alpha
TRPC	Transient Receptor Potential Canonical
U3-55k	Uridine 3-55 kilodaltons
UOX	Urate oxidase
WAT	White adipose tissue
WGA	Wheat germ agglutinine
WT	Wild type

2. List of Figures

3. List of Tables

4. Introduction

4.1 Heart failure

4.1.1 Definition, Epidemiology, Etiology

Heart failure (HF) is a major global health problem and is one of the leading causes of mortality worldwide (Ziaeian and Fonarow, 2016, Conrad et al., 2019). Currently, the incidence of HF in Europe is approximately 3/1000 person-years (all ages) and approximately 5/1000 person-years in adults (Meyer et al., 2015, Brouwers et al., 2013, McDonagh et al., 2021). The prevalence can be estimated to be about 1-2% of adults (Conrad et al., 2018, Collaborators, 2020, Roger, 2021, Mosterd and Hoes, 2007, Smeets et al., 2019, Virani et al., 2020), but since these studies include only diagnosed cases of HF, the true prevalence is most likely higher (McDonagh et al., 2021, van Riet et al., 2014).

As defined by the American College of Cardiology (ACC) and the American Heart Association (AHA), HF manifests as a complex clinical syndrome characterized by symptoms and signs resulting from structural or functional impairments in the filling or ejection of blood from the ventricles (Heidenreich et al., 2022). Essentially, due to structural and/or functional abnormalities the heart can no longer generate sufficient cardiac output to provide the body with enough blood and oxygen to meet the needs of peripheral organs (McDonagh et al., 2021), resulting in a constellation of symptoms and adverse outcomes. The most common clinical symptoms include decreased exercise tolerance, fatigue, weakness, shortness of breath and peripheral edema.

The Global Burden of Disease Study identifies 17 primary aetiologies of HF (Collaborators, 2020). Predominant pathologies include ischemic heart disease such as coronary artery disease (CAD), chronic obstructive pulmonary disease, hypertensive heart disease, and rheumatic heart disease, which together account for two-thirds of all cases of HF (Ziaeian and Fonarow, 2016). A list of all common causes is presented in **Table 1**. When diagnosing HF, it is essential to identify the cause of the underlying cardiac dysfunction, as the pathology may dictate the subsequent course of treatment.

Table 1: Causes of HF and their common modes of presentation.

Causes	Examples of presentations
CAD	Myocardial infarction (MI), angina or "angina-equivalent", arrhythmias
Hypertension	HF with preserved systolic function, malignant hypertension/ acute pulmonary oedema
Valve disease	Primary valve disease e.g., aortic stenosis, secondary valve disease e.g., functional regurgitation, congenital valve disease
Arrhythmias	Atrial tachyarrhythmias, ventricular arrhythmias
CMPs	All, dilated, hypertrophic, restrictive, ARVC, peripartum, Takotsubo syndrome, toxins: alcohol, cocaine, iron, copper
Congenital heart disease	Congenitally corrected/repaired transposition of great arteries, shunt lesions, repaired tetralogy of Fallot, Ebstein's anomaly
Infective	Viral myocarditis, Chagas disease, HIV, lyme disease
Drug-induced	Anthracyclines, Trastuzumab, VEGF inhibitors, immune checkpoint inhibitors, proteasome inhibitors, RAF+MEK inhibitors
Infiltrative	Amyloid, sarcoidosis, neoplastic
Storage disorders	Hemochromatosis, Fabry disease, glycogen storage diseases
Endomyocardial disease	Radiotherapy, endomyocardial fibrosis/ eosinophilia, carcinoid
Pericardial disease	Calcification, infiltrative
Metabolic	Endocrine disease, nutritional disease (thiamine, Vitamin B1 and selenium deficiencies), autoimmune disease
Neuromuscular disease	Friedreich's ataxia, muscular dystrophy

*Table based on 20211 ESC Guidelines for the diagnosis and treatment of acute and chronic heart failure, Table 5 (McDonagh et al., 2021).

4.1.2 Classification regarding ventricular function

HF is primarily categorized based on the performance of the left ventricle (LV), which is typically assessed by measuring the LV ejection fraction (EF) using echocardiography (McDonagh et al., 2021). The EF is the percentage of blood ejected during a contraction relative to the total ventricular volume and is therefore calculated as the ratio of stroke volume to end diastolic volume.

A reduced LVEF is defined as <40%, indicating a significant decrease in systolic LV function. This condition is referred to as HF with reduced EF (HFrEF). HFrEF is mainly characterized by an accumulation of myocardial damage often due to myocardial infarction (MI), hypertensive heart disease, or cardiomyopathy. Progressive cardiomyocyte loss associated with increased oxidative stress is one mechanism by which HFrEF develops (Shimizu and Minamino, 2016). This leads to replacement fibrosis (Paulus and Tschope, 2013) and other changes in the extracellular matrix, such as LV dilation and eccentric LV remodeling (Janicki et al., 2004).

Individuals with symptoms and signs of HF, along with evidence of structural and/or functional cardiac abnormalities, elevated natriuretic peptides (NPs, see chapter 7.2.2), and an LVEF >50%, fall into the category of HF with preserved EF (HFpEF) (McDonagh et al., 2021). HFpEF is mainly associated with systemic diseases, such as obesity, hypertension, diabetes mellitus, chronic pulmonary disease, anemia, and chronic kidney disease, which induce a state of systemic inflammation (Shimizu and Minamino, 2016). In contrast to HFrEF, HFpEF does not typically lead to replacement fibrosis, as cell death is not predominant (Shimizu and Minamino, 2016). It is usually associated with cardiomyocyte hypertrophy and stiffness, as well as interstitial fibrosis (Shimizu and Minamino, 2016). In addition, concentric remodeling and diastolic LV dysfunction are typically observed, i.e. the impaired ability of the heart to relax and fill with blood during the diastolic phase, leading among other things to pulmonary hypertension and reduced cardiac output (Shimizu and Minamino, 2016, van Heerebeek et al., 2006, Selby et al., 2011, Kasner et al., 2011, Borbely et al., 2005). Whether HFrEF and HFpEF represent distinct pathological conditions or a syndrome existing along a spectrum is an ongoing subject of exploration (Burchfield et al., 2013). Patients with an LVEF ranging from 41% to 49% exhibit a slightly reduced systolic LV function, termed HF with mildly reduced EF (HFmrEF) (McDonagh et al., 2021).

Dysfunction of the right ventricle (RV) may also be the cause of HF, although less common. This is usually due to an increase in pressure or volume load, e.g., in the case of

arrhythmogenic right ventricular cardiomyopathy, MI or valve disease, resulting in altered mechanics and function of the RV (Arrigo et al., 2019). However, in most cases, the cause of chronic RV failure is pulmonary hypertension induced by LV dysfunction (Arrigo et al., 2019).

4.2 Cardiac Hypertrophy

Cardiomyocytes are specialized muscle cells, that constitute the myocardium, the middle of the three histological layers of the heart. Cardiomyocytes account for about one third of all heart cells (Tirziu et al., 2010). The remaining cells that make up the heart tissue include the smooth muscle and endothelial cells of the coronary vessels, the endocardium, fibroblasts and other connective tissue cells, mast cells and other cells of the immune system as well as stem cells (Tirziu et al., 2010). Unlike other muscle cells, cardiomyocytes have gap junctions that transmit electrical impulses from the pacemaker centers, allowing the heart to function uniformly because all cardiomyocytes are coordinated to contract simultaneously. This serves as the basis for the heart's ability to efficiently circulate the blood. Cardiomyocytes can adapt to environmental conditions by either atrophic or hypertrophic remodeling, depending on the stressor (Shimizu and Minamino, 2016). Hypertrophy is defined by the enlargement of tissue due to the increase of individual cell size. In case of heart tissue pathological and physiological hypertrophy can be differentiated.

Physiological cardiac hypertrophy is an adaptive response to increased cardiac stress, due to, for example, body growth, pregnancy, or exercise (Hill and Olson, 2008, Shimizu and Minamino, 2016, Weeks and McMullen, 2011). Anemia- and thyrotoxicosis-induced cardiac hypertrophy are also considered physiological hypertrophies (De Boer et al., 2003). It is usually associated with normal or improved cardiac function, and is characterized by an increase in cardiac mass of approximately 10-20% normalized to body mass (Maillet et al., 2013) while retaining physiological cardiac architecture (Weeks and McMullen, 2011). Physiological cardiac hypertrophy is not considered a risk factor for HF but is merely adaptive in nature, as it is reversible when the stimulus ceases (De Boer et al., 2003, Shimizu and Minamino, 2016).

Pathological hypertrophy, on the other hand, is associated with cardiac dysfunction, along with cardiomyocyte death and fibrotic remodeling. This can lead to systolic and diastolic dysfunction, and ultimately the development of HF (Shimizu and Minamino, 2016, Rockey et al., 2015). Abnormal coronary vasculature and reduced coronary vasodilatory capacity in pathological hypertrophy are underlining mechanisms driving the progression of HF (Shimamatsu and Toshima, 1987). Physiologic cardiac hypertrophy can transition to pathologic hypertrophy with prolonged pathological stress (Oldfield et al., 2020). Decreases in capillary density, increased oxidative stress, intracellular Ca^{2+} overload, apoptosis of

cardiomyocytes and chronic inflammation have been identified as pathways leading to this shift (Oldfield et al., 2020).

Hypertrophic cardiac growth can be further divided into two main categories depending on the geometry of the heart: eccentric and concentric growth. Eccentric hypertrophy occurs when the ventricles are dilated due to volume overload, thereby resulting in an outward increase in thickness (**Figure 1**) (Shimizu and Minamino, 2016). In physiological eccentric hypertrophy, cardiomyocytes grow in both length and width, resulting in uniform growth of the wall and septal thickness (Shimizu and Minamino, 2016). Pathological eccentric hypertrophy, on the other hand, often occurs in the setting of MI or dilated cardiomyopathy, leading to isolated cardiomyocyte length growth and increased ventricular dilatation (**Figure 1**) (Shimizu and Minamino, 2016).

In contrast, concentric growth is due to chronic pressure overload resulting in an inward increase in wall thickness accompanied by a reduction in ventricular volume. In cases of concentric hypertrophy, cardiomyocytes exhibit primarily growth in thickness (Selby et al., 2011, Heineke and Molkentin, 2006). The most common pathologies leading to concentric hypertrophy are hypertension or valvular disease (Shimizu and Minamino, 2016).

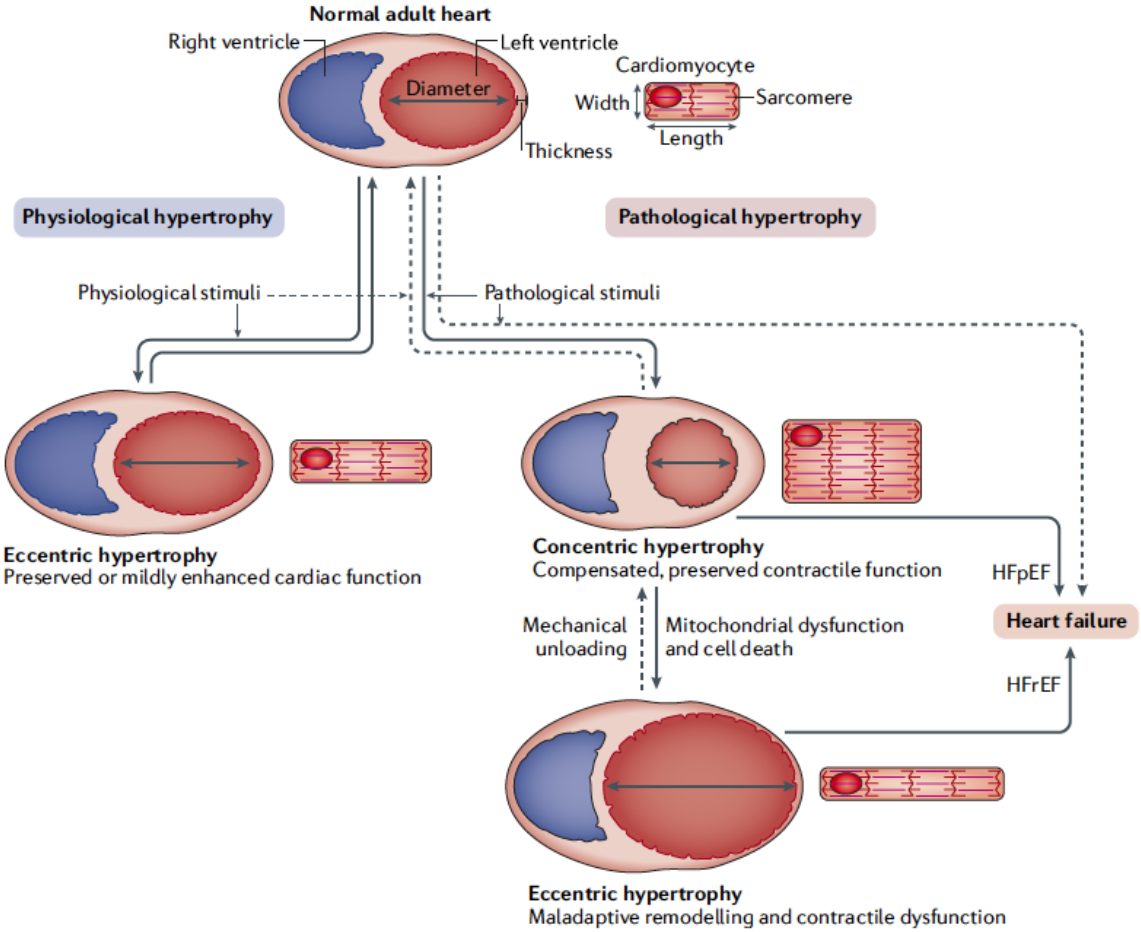

Figure 1: Overview of physiological and pathological hypertrophy.

Cardiac mass can increase both physiologically and pathologically to reduce ventricular wall pressure. Physiological hypertrophy involves increased ventricular volume, coordinated eccentric wall thickening, and cardiomyocyte growth in length and width. It is reversible when the stimulus is removed. Pathological hypertrophy shows reduced ventricular size, thickened walls (concentric), and increased cardiomyocyte thickness. It may result in eccentric myocardial growth and impaired contractile function, often found in HFrEF and HFpEF. Solid arrows denote proven pathways, dashed arrows hypothetical or controversial pathways. Figure adapted from Nakamura et al., 2018.

4.2.1. Angiotensin II and Isoproterenol

Angiotensin II

Angiotensin (ANG) II is an effector hormone of the renin-angiotensin-aldosterone system (RAAS). The RAAS is triggered by decreased cardiac output and blood pressure and serves to upregulate the blood pressure to maintain homeostasis (Kuwahara, 2021). Prolonged activation of the RAAS in HF results in a variety of adverse effects on the heart, kidneys, and peripheral vasculature (Hartupee and Mann, 2017). In the heart, it leads to cardiac remodeling, myocyte hypertrophy and fibrosis, as well as myocyte necrosis and apoptosis, resulting in long-term impairment of diastolic and systolic function (Hartupee and Mann, 2017). The kidneys are affected with a decreased renal blood flow, increased tubular reabsorption of Na^+ and increased renal vascular resistance (Hartupee and Mann, 2017). In the periphery the vessels experience neurogenic vasoconstriction and hypertrophy (Hartupee and Mann, 2017). In a clinical setting, the RAAS is widely targeted to reverse maladaptive cardiac hypertrophy by the drug-induced inhibition of the angiotensin converting enzyme (ACE), which stops the conversion of the inactive form ANG I to the active form ANG II (Klingbeil et al., 2003).

ANG II has been demonstrated to trigger hypertrophy by influencing reactive oxygen species (ROS) production, in addition to other mechanisms. Bendall et al. were able to show that ANG II accumulates ROS in cells by activating nicotinamide adenine dinucleotide phosphate (NADP/NADPH) oxidase (NOX), resulting in oxidative stress (Bendall et al., 2002). It also triggers a 50% increase of total ROS in neonatal cardiomyocytes (Dai et al., 2011). The increase in ROS production has a major influence on the development of pathological hypertrophy (refer to **chapter 7.3**).

In cell culture, ANG II is often used as a stimulant of hypertrophy. ANG II is repeatedly shown to induce cellular changes, such as the enlargement of cells, the accumulation and reorganization of contractile proteins and the upregulation of genes specific to hypertrophy (Watkins et al., 2011, Luo et al., 2017).

Isoproterenol

Isoproterenol (ISO) is a synthetic catecholamine that targets ß-adrenergic receptors (Nichtova et al., 2012) and has effects similar to the neurohumoral factors of the sympathetic nervous system (SNS). The SNS, like the RAAS, is upregulated as a compensatory mechanism when cardiac output is low (Kuwahara, 2021), leading to similar adverse effects

as the RAAS with prolonged stimulation. Myocardial remodeling, ischemia, angina, infarction, cardiac arrhythmias, and sudden cardiac death are some of the pathologies caused by increased supply of endogenous or exogenous catecholamines (Raab, 1960, Rona, 1985). The blood catecholamine levels are inversely correlated with survival in patients and animal models with chronic HF (Brede et al., 2002).

Medicinal blocking of ß-adrenergic receptors is one way to reduce HF-associated pathologic changes in cardiac remodeling, as Beta-Blockers reduce heart rate, reduce risk of arrhythmias, improve coronary blood flow, and protect the heart against cardiotoxic overstimulation by catecholamines (von Lueder et al., 2017, Lymperopoulos et al., 2013). Meta-analyses have suggested that beta-blockers can reduce all-cause mortality to up to 50% in patients with HFrEF and HFmrEF (Cleland et al., 2018).

On a cellular level, catecholamines activate adenylyl cyclase, thereby increasing cyclic adenosine monophosphate (cAMP) levels. cAMP activates protein kinase A (PKA), which leads to an increase in cytosolic Ca^{2+}. This leads via the activation of calcium/calmodulin-dependent protein kinase type II (CaMK II) to an inhibition of Class II histone deacetylase (HDACs), which results in cell growth (Nakamura and Sadoshima, 2018).

Similar to ANG II, ISO is routinely used as a hypertrophic agent in both cell culture and animal models (Muehleman et al., 2022, Yuan et al., 2017, Li et al., 2024).

4.2.2 Natriuretic peptides as markers for HF

The production of NPs that are cardiac specific, such as atrial natriuretic peptide (ANP) and BNP, is induced by mechanical or neuroendocrine stimuli. They are secreted by cardiomyocytes, namely cardiomyocytes in the atria (ANP) or in the LV (BNP). NPs have antihypertrophic and cardioprotective effects (Nakamura and Sadoshima, 2018). Natriuretic peptide receptor (NPR)-A deficient mice, for example, have significantly higher levels of hypertrophic changes in the heart than controls (Knowles et al., 2001). In addition, the cardiac-specific deletion of the ANP receptor 1 (*Npr1*) gene resulted in mild hypertrophy that developed to pathologic hypertrophy and remodeling of the heart upon exposure to pressure overload (Holtwick et al., 2003). An inactivation mutation of *Npr-B* in mice does not cause hypertrophy (Tamura et al., 2004, Tsuji and Kunieda, 2005), but transgenic rats expressing a dominant-negative mutation of *Npr-B* show mild hypertension-independent cardiac hypertrophy and increased heart rate (Langenickel et al., 2006, Potter et al., 2009).

NPs act via the activation of guanylate cyclase after binding to the NPR, which stimulates the production of cyclic guanosine monophosphate (cGMP). cGMP then activates protein kinase G (PKG), which is anti-hypertrophic by inhibiting calcineurin- Nuclear Factor of Activated T-cells (NFAT), the canonical transient receptor potential channels (TRPCs) and the RHOA-RHO kinase pathways (Rainer and Kass, 2016).

Among other things, NPs act on the kidneys by increasing the glomerular filtration rate through vasodilation of afferent arterioles and vasoconstriction of efferent arterioles, as well as through diuretic effects (Volpe et al., 2016). In addition, NPs cause a reduced preload of the heart through peripheral vasodilation and inhibit cardiac remodeling (Volpe et al., 2016). Notably, BNP is used as a biomarker for numerous cardiac diseases, as plasma BNP and serum N-terminal proBNP (a byproduct of BNP production) are significantly elevated in patients with cardiac pathologies (Emdin et al., 2007, Kuwahara, 2021). In HF, it is established as an important diagnostic and prognostic tool (Table 2) (Heidenreich et al., 2022). However, prolonged excessive activation of NP secretion, such as during chronic HF, leads to reduced organ responsiveness, thereby reducing the efficacy of the cardioprotective impact (Diez, 2017).

4.3 Oxidative Stress and cardiac disease

Under healthy conditions, there is a balance between oxidation and reduction reactions in the form of ROS and the antioxidant capacity of the system, called redox homeostasis (Pisoschi and Pop, 2015). If this balance is disturbed by increased ROS production or a compromised antioxidant system, oxidative stress occurs. In oxidative stress, ROS can roam freely, harming cell organelles and leading to tissue damage (Matsushima et al., 2006a, Pisoschi and Pop, 2015). For example, superoxide (O_2^-) is known to oxidize the Fe-S centers of several mitochondrial enzymes, thereby impairing their function (Matsushima et al., 2006a). Hydrogen peroxide (H_2O_2), another ROS, damages cellular macromolecules, including proteins, lipids, and nucleic acids (Matsushima et al., 2006a). The hydroxyl radical (OH) oxidates the nucleoside guanosine and peroxidases unsaturated fatty acids (Pisoschi and Pop, 2015). Antioxidant substances, such as the enzyme catalase, can neutralize ROS and thus delay or prevent the oxidation of the above-mentioned substrates, thereby preventing oxidative stress, cell damage and DNA mutations (Pisoschi and Pop, 2015).

In many cardiac pathologies, an imbalance of the redox homeostasis is present (Sabri et al., 2003, Maulik and Kumar, 2012). It has been well established in the literature, that an excess of ROS plays a major role in the development of HF (Giordano, 2005, Seddon et al., 2007). In patients with HF 8-iso-prostaglandin F2α (8-iso-PGF2α), a specific and quantitative marker of oxidant stress *in vivo*, was significantly increased systemically and in the pericardium (Mallat et al., 1998). Furthermore, the levels of 8-iso-PGF2α were correlated with the functional severity of HF (Mallat et al., 1998). An increase in ROS has also been repeatedly observed in various *in vivo* and *in vitro* models of cardiac hypertrophy, such as for example mice treated with transverse aortic constriction (TAC) (Takimoto et al., 2005, An et al., 2021, Lu et al., 2023b), ANG II- stimulated H9c2 rat cardiomyoblasts (Cheng et al., 2021, Ren et al., 2023, Luo et al., 2024) and ISO treated cardiomyocytes (Liu et al., 2021, Zang et al., 2020), clearly showing a link between increased ROS production and hypertrophy.

Hirotani et al. were the first to show a mechanism by which ROS induced cardiac hypertrophy (Hirotani et al., 2002). They were able to show that hypertrophy agonists such as ANG II, endothelin-1 and phenylephrine stimulate ROS production in primary cultures of rat ventricular cardiomyocytes via the G-protein-coupled receptor (GPCR). These ROS molecules then activated nuclear factor κB (NF-κB), a transcription factor known to regulate the expression of genes involved in various cellular processes, including inflammation and

hypertrophy (Hall et al., 2006). Once NF-κB is activated, it triggers the transcription of various hypertrophic genes, leading to an increase in cell size and ultimately cardiac hypertrophy (Zelarayan et al., 2009). An increase in NF-kB DNA binding activity was also observed in rats stimulated with ISO, but only at high doses (Takemoto et al., 1999), also mediated via GPCR (Maulik and Kumar, 2012). Another pathway by which ROS induce hypertrophy, that has been identified, is via the extracellular receptor kinase 1/2 (Bueno et al., 2000).

A growing body of evidence has shown that an increase in antioxidative systems exerts protective effects against HF (Maulik and Kumar, 2012, Sabri et al., 2003). The major endogenous antioxidants include glutathione, glutathione peroxidase (GSHPx), superoxide dismutase (SOD) and catalase (Maulik and Kumar, 2012). Overexpression of GSHPx was shown to attenuate LV remodeling and myocyte hypertrophy in diabetic mouse heart (Matsushima et al., 2006b), as well as after MI in mice (Shiomi et al., 2004). In addition, ANG II-mediated hypertrophic changes such as ventricular mass, myocyte cross-sectional area, and intraventricular septal thickness were accelerated in GSHPx knockout mice (Ardanaz et al., 2010). Dai et al. were able to show, that mice with an overexpression of a catalase, that was targeted to mitochondria, were resistant to ANG II-induced cardiac remodeling, as supposed to mice with an overexpression of peroxisomal catalase (Dai et al., 2011), emphasizing the importance of mitochondrial oxidative stress in HF.

There are also numerous studies investigating the effect of various exogenous antioxidants on cardiac hypertrophy. For example, Dihydromyricetin is a flavonoid in vine tea, that was shown to ameliorate TAC induced myocardial hypertrophy in mice related to oxidative stress inhibition (Chen et al., 2018). Flavonoids are natural substances, commonly found in vegetables and fruit, that are known for their antioxidant effects (Serafini et al., 2010). Baicalein is another natural flavonoid extracted from the root of Scutellaria baicalensis (Liu et al., 2021). It was shown to have antihypertrophic effects in ISO stimulated *in vivo* and *in vitro* models by decreasing ROS levels (Liu et al., 2021). LCZ696 is a drug combination, containing sacubitril, a neprilysin inhibitor, and valsartan, an angiotensin-receptor blocker (McMurray et al., 2014). In clinical studies, it was shown to have a better effect in reducing mortality and rehospitalization rate in patients with chronic heart failure than angiotensin-converting enzyme inhibitor enalapril (McMurray et al., 2014). This was shown to be due to an increased antioxidant effect of LCZ696, which alleviated the accumulation of ROS (Peng et al., 2020).

Altogether, these studies suggest that increased ROS production with insufficient antioxidant shielding are a main contributor to cardiac hypertrophy and HF.

4.3.1 NAPDH oxidase 4

NADPH oxidases (NOX) are transmembrane enzymes that transfer electrons across membranes, where they reduce oxygen to superoxide, thus producing ROS (Bedard and Krause, 2007). Seven NOXs have been identified to date, NOX1-5 and DUOX1-2 (Ago et al., 2010, Sumimoto, 2008). NOX4 is ubiquitously expressed in the human organism (Krause, 2007), but is primarily localized in mitochondria (Ago et al., 2010).

The NOX family and their influence on the development of heart disease is currently under investigation. For example, in pressure-overload LV hypertrophy models in guinea pig myocardium, NOX derived ROS generation increases significantly, which is at least partly due to an increased expression of oxidase components (Li et al., 2002). This indicates that NOX may be a major source of oxidative stress in hypertrophy. In human end-stage HF, NOX activity was significantly increased compared to non-failing heart (Heymes et al., 2003).

In contrast to the other members of the NOX family, NOX4 is permanently active and does not need cytosolic factors for activation, which is why the extent of expression can be equated with the superoxide production (Ago et al., 2010). Ago et al. were able to show, that when mice were stimulated with ANG II as a hypertrophic agent, *Nox4* is upregulated in the heart (Ago et al., 2010). Additionally, in their study, mice that were overexpressing *Nox4*, showed higher levels of oxidative stress, including oxidative DNA damage and O_2^-, as well as mitochondrial dysfunction (Ago et al., 2010). An overexpression of *Nox4* did not, however, lead to hypertrophy, only fibrotic remodeling and reduced LVEF was observed (Ago et al., 2010). Kuroda et al. showed that endogenous NOX4 plays an essential role in mediating oxidative stress and pathological hypertrophy, as *Nox4* knockout mice exhibited attenuated cardiac hypertrophy and increased cardiac function compared to wild type (WT) (Kuroda et al., 2010).

4.4 Sirtuins

4.4.1 History and overview

Epigenetic modifications have been associated with promoting or suppressing disease development by affecting protein functionality (Raghubeer, 2024). In particular, lysine residue acetylation is an important form of epigenetic modification. It involves the addition of an acetyl group to a lysine residue by an acetyltransferase, which alters the electrostatic properties of the protein (**Figure 2**) (Glozak et al., 2005). Especially the NAD^+-dependent deacetylases of the sirtuin (SIRT) family regulate lysine residue acetylation in eukaryotes (**Figure 2**) (North and Verdin, 2004). Specifically, sirtuins belong to the class III of HDACs. Among other, they enable the deoxyribonucleic acid (DNA) to wrap itself more tightly around the histones by removing an acetyl group from the ε-N-acetyl lysine amino acids on the histones (Matsushima and Sadoshima, 2015). Other specific post-translational protein modifications such as adenosine diphosphate (ADP)-ribosylation, desuccinylation, demalonylation, deglutarylation, delipolylation and decrotonylation are also part of the enzymatic activities of sirtuins (Wang et al., 2023, Nakagawa et al., 2009, Ahuja et al., 2007, Du et al., 2011, Pan et al., 2011).

Sirtuins are orthologs from the silent information regulator 2 (SIR2) protein, which was identified in 1979 from the budding yeast *Saccharomyces cerevisiae* (Rine et al., 1979, Kaeberlein et al., 1999). The gene corresponding to the SIR2 protein, *Sir2*, has been linked in later research to the silencing of gene activity at mating-type loci in yeast cells, as well as silencing at the ends of yeast telomeres and recombinant DNA (rDNA) (Smith and Boeke, 1997, Bryk et al., 1997). It was also found that this gene plays a role in the distribution of carbonylated proteins between mother and daughter cells (Aguilaniu et al., 2003, Haigis and Sinclair, 2010). NAD^+-dependent deacetylation of proteins was eventually identified as the major enzymatic activity of SIR2 (Imai et al., 2000). Finally, *Sir2* was also associated with lifespan extension in *Saccharomyces cerevisiae* exposed to calorie restriction (Lin et al., 2000). The same results were later replicated in the fly genus *Drosophilia melanogaster* (Rogina and Helfand, 2004) and the nematode genus *Caenorhabditis elegans* (Wood et al., 2004).

Recently, the sirtuin family has been implicated in several physiological and pathological mechanisms, such as aging, stress resistance, apoptosis, and inflammation (Matsushima and

Sadoshima, 2015). They are currently at the forefront of extensive research, and their exploration continues to advance.

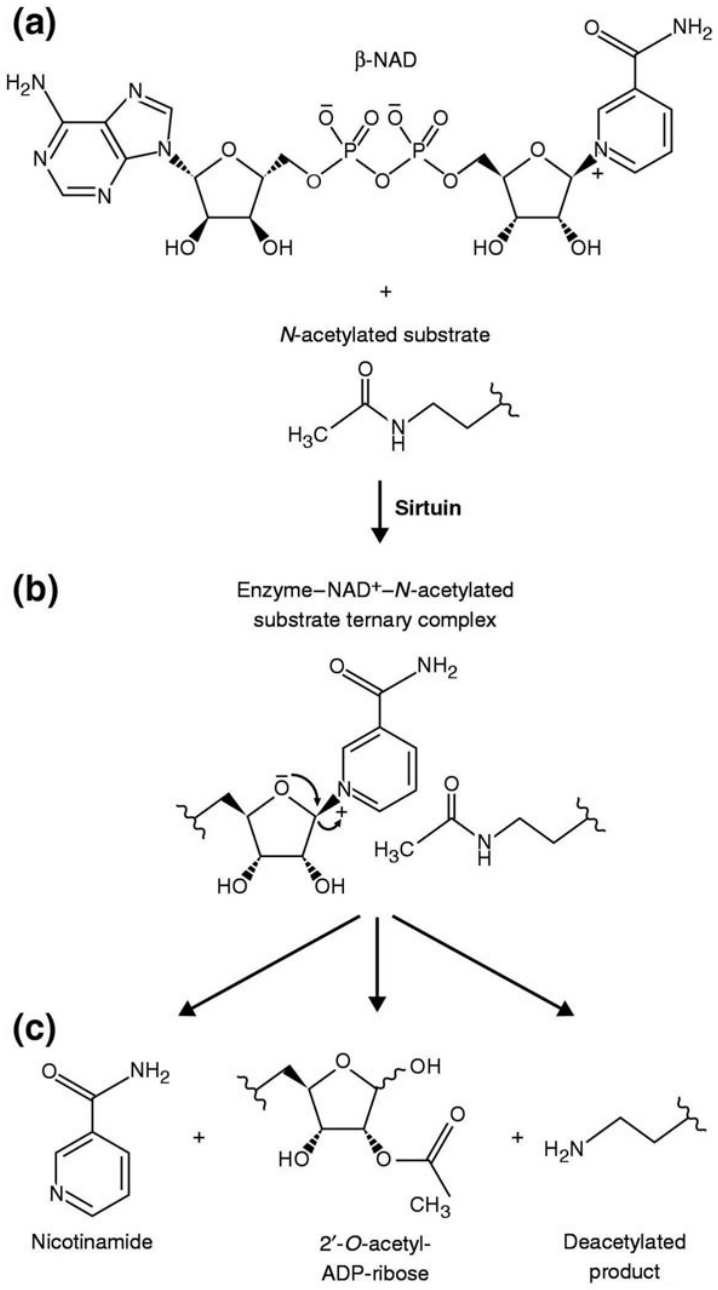

Figure 2: Enzymatic deacetylation by sirtuins.

(a) ß-NAD, an N-acytelated substrate and a sirtuin are needed for the deacetylation. (b) An enzyme-NAD+-N-acetylated substrate tertiary complex is formed. (c) The products are the deacetylated protein, 2'-O-acetyl-ADP-ribose and nicotinamide. Figure adapted from North and Verdin, 2004.

4.4.2 Classification, localization, and functions

Sirtuins are highly conserved, as they are found in a wide variety of living organisms, from viruses and bacteria to lower multicellular organisms such as flies and worms, up to humans (Imai et al., 2000, Kaeberlein et al., 1999, Tissenbaum and Guarente, 2001, Rogina and Helfand, 2004, Nakagawa and Guarente, 2011).

Seven sirtuins have been identified in mammals, which can be assigned to four distinct phylogenetic classes based on their amino acid sequence (**Figure 3**). Class I is subdivided into groups Ia, Ib and Ic and includes SIR2 (Ia), SIRT1 (Ia), SIRT2 (Ib) and SIRT3 (Ib). Class I sirtuins are not found in prokaryotes and class Ic sirtuins are only found in yeast. Human SIRT4 belongs to class II, whereas SIRT5 is a class III sirtuin. Class IV sirtuins are further subdivided into class IVa, which includes SIRT6, and class IVb, including SIRT7. Class IV Sirtuins are again not found in prokaryotes. Class U includes Sirtuins that appear to be intermediate between classes I and IV or II and III. They can be found in some gram-positive bacteria and are considered undifferentiated (**Figure 3**) (Frye, 2000).

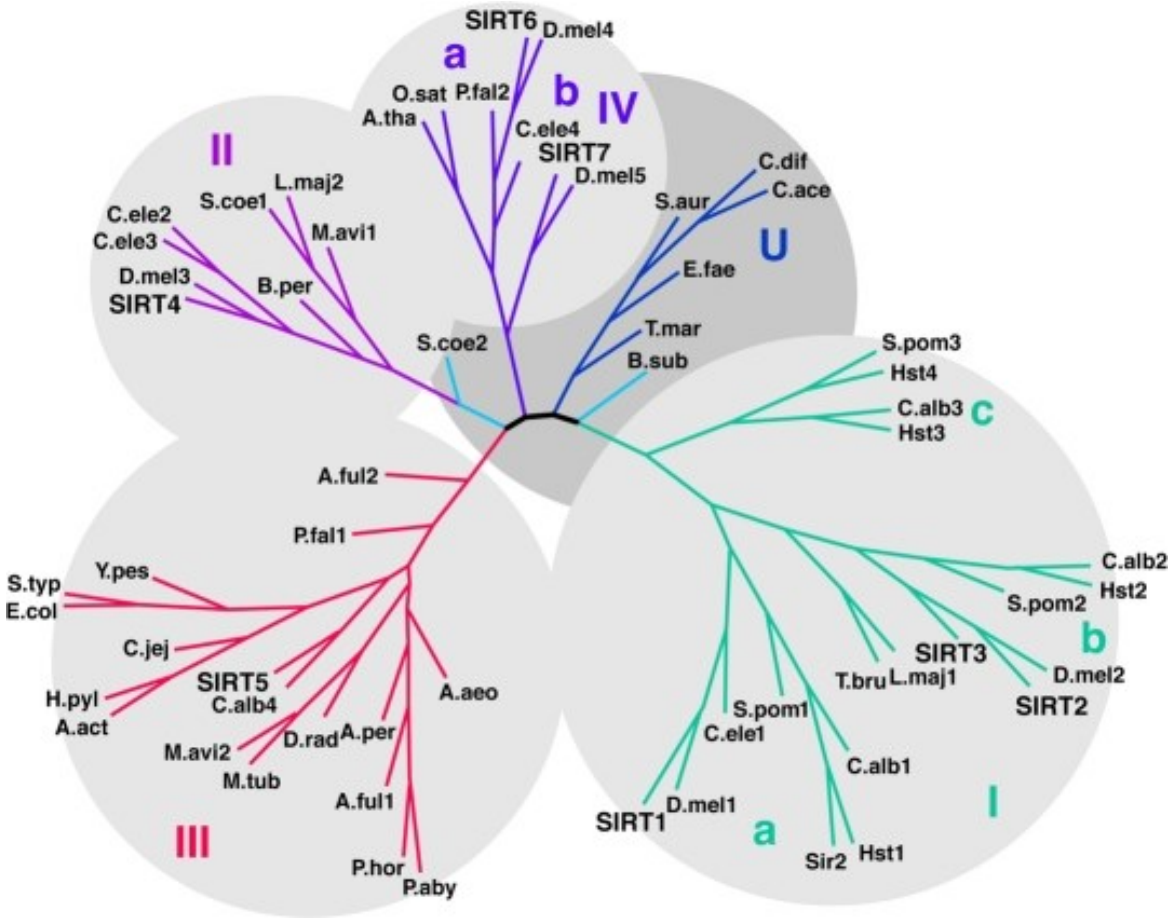

Figure 3: Phylogenetic classes of sirtuins. *Figure adapted from Frye, 2000.*

The Sirtuin family are ubiquitous in the human organism, but each sirtuin has a unique expression profile (Michishita et al., 2005). Many substrates and functions have been identified for this family (**Table 2**). Key localizations, targets, and functions, especially regarding cardiovascular disease, are outlined below.

SIRT1 is primarily found in the cytosol and nucleus (Finkel et al., 2009). It is structurally closest to SIR2 and has been the most intensively studied of all sirtuins. SIRT1 plays a critical role in the regulation of cell death and survival through the regulation of protein 53 (Yin et al., 2023). Knockout of SIRT1 results in perinatal death and defects in the retina, bone and heart (Cheng et al., 2003, Finkel et al., 2009). In addition, SIRT1 has been implicated in the development of neurodegenerative, neoplastic, and cardiovascular diseases (Potente et al., 2007, Firestein et al., 2008, Gan and Mucke, 2008) and is particularly involved in the pathogenesis of HF. Inhibition of SIRT1 through nicotinamide mononucleotide or sirtinol has been shown to attenuate cardiomyocyte hypertrophy (Alcendor et al., 2004, Matsushima and Sadoshima, 2015). Additionally, studies using SIRT1 knockout mice have demonstrated that these animals exhibit smaller hearts compared

to wild-type counterparts and are resistant to the development of cardiac hypertrophy in response to hypertrophic stimuli (Matsushima and Sadoshima, 2015). However, the effect of increased SIRT1 seems to depend on the overexpression level (Alcendor et al., 2007). Low (2.5-fold) to moderate (7.5-fold) overexpression of SIRT1 attenuated age-dependent increases in cardiac hypertrophy, while high levels (12.5-fold) exacerbated hypertrophy (Alcendor et al., 2007).

SIRT2 is also mainly localized in the cytoplasm and in the nucleus (Finkel et al., 2009). Like SIRT1, it can deacetylate p53, whereby it influences the cell cycle, among other things (Zavileyskiy and Bunik, 2022). In the heart, SIRT2 protects against ischemia-reperfusion injury (Lynn et al., 2008) and pathological hypertrophy (Tang et al., 2017), but it appears to first and foremost play a role in neurogenerative diseases, such as Alzheimer's (Biella et al., 2016, Wang et al., 2019). It also has an influence on oxidative stress by reducing the acetylation level of Forkhead-Box-Protein O3a (FOXO3a) (Wang et al., 2007).

SIRT3 is primarily a mitochondrial enzyme (Finkel et al., 2009), but can also be found in the nucleus and cytoplasm (Scher et al., 2007). It has a positive effect on oxidative stress and cardiac hypertrophy by activating antioxidant enzymes such as catalase or Manganese SOD (MnSOD) via FOXO3a (Sundaresan et al., 2009). In HF, SIRT3 can delay the progression of the disease by improving mitochondrial function (Grillon et al., 2012, Wang et al., 2021). In addition, decreased SIRT3 expression, as well as increased global mitochondrial protein lysine acetylation, indicating impaired SIRT3 activity, can be observed in rats with HF (Grillon et al., 2012). This indicates, that pharmacological activation or induction of SIRT3 has therapeutic potential against cardiac hypertrophy and HF (Koentges et al., 2016).

Another mitochondrial based enzyme is SIRT5 (Finkel et al., 2009). Similar to other mitochondrial sirtuins, it is highly involved in mitochondrial energy pathways, especially in the heart (Koentges et al., 2016). SIRT5 knockout mice have been shown to develop hypertrophic cardiomyopathy and reduced cardiac function, as the lack of SIRT5 leads to reduced fatty acid oxidation (FAO), decreasing cardiac ATP levels (Sadhukhan et al., 2016).

SIRT6 is mainly found in the nuclei (Finkel et al., 2009). It deacetylates lysine 9 of histone H3 at the telomeric chromatin, preventing replication-associated telomere defects, which is an important feature of human HF (Michishita et al., 2008, Wu et al., 2023). SIRT6 is also known to stimulate DNA repair after oxidative stress by interacting with Poly (ADP-ribose) Polymerase 1 (Mao et al., 2011). This results in the important role of SIRT6 in cardiac hypertrophy and degenerative changes in the heart. *Sirt6* deficiency aggravates cardiac

hypertrophy and fibrosis in mice, whereas the overexpression of *Sirt6* blocks the cardiac hypertrophic response (Sundaresan et al., 2012).

SIRT7 is mainly localized in the nucleolus (Finkel et al., 2009) and its main function includes the regulation of responses to endogenous and exogenous stresses (Raza et al., 2024). Cardiomyocytes that are deficient in SIRT7 exhibit increases in inflammatory changes and sensitivity to oxidative stress, as well as apoptosis (Vakhrusheva et al., 2008). On the other hand, several studies have suggested that SIRT7 has oncogenic potential (Blank and Grummt, 2017), by promoting cancer cell migration and invasiveness (Malik et al., 2015).

Table 2: Overview of sirtuins and their substrates and functions

Isoforms	Localization	Substrates	Enzymatic activity	Function
SIRT1	Nuclear, cytoplasmatic	p53, NF-kB, FOXO1, FOXO3, PGC1α, H1F1a, H1F2a, eNOS, H1K26, H3K9, H4K16, Ku68, KAP1, HSF1	Deacetylase	Stress response, metabolic problem, genome stability, apoptosis, cancer, neurodegeneration, lifespan, cardiovascular disorders
SIRT2	Nuclear, cytoplasmatic	H4K16, FOXO1, FOXO3a, NF-kB, p53, a-TUB	Deacetylase	Cell cycle, cell differentiation, genome stability, stress response, neurode generation, energy metabolism
SIRT3	Mitochondrial, (nuclear, cytoplasmatic)	FOXO3a, H1F1a, CYPD, MnSOD; SOD2	Deacetylase	Lifespan, oxidative stress, cell apoptosis
SIRT4	Mitochondrial, (nuclear, cytoplasmatic)	GDH, MCD, PDH, Hsp60	ADP-ribosylation, deacylation, delipolation, deacetylation	TCA cycle, insulin secretion, FAO, tumor, genome stability
SIRT5	Mitochondrial	CPS1, HMGCS2, SOD1, UOX	Malonyl, succinyl, glutaryl deacerylase	Urea cycle, ketone body synthesis, oxidative stress, cellular respiration
SIRT6	Nuclear	TNFα, H3K9, H3K56, RARP1, CtIP	Deacetylase, ADP-ribosyl-transferase, long-chain fatty acyl deacylase	Genome stability, metabolism, inflammation, cancer, cardiovascular disease
SIRT7	Nuclear	H3K18, PAF53, GABP-ß1, U3-55k	Deacetylase	Transcriptional regulation, genome stability, oxidative stress

*Table adapted from Wang et al., 2019 and (Carafa et al., 2016).

4.4.3 SIRT4

Along with SIRT3 and SIRT5, SIRT4 is an enzyme primarily found in mitochondria (Finkel et al., 2009). However, in many cells SIRT4 has also been found to be present in the cytosol and nucleus (Ramadani-Muja et al., 2019) as well as in the centrosomes with an intensity peak in G_2 and early mitosis, suggesting a functional role in cell cycle regulation (Bergmann et al., 2020). Among the most important enzymatic functions of SIRT4 are ADP-ribosylation, deacylation, and delipolation, whereas NAD^+-dependent deacetylation seems to only play a minor role *in vitro* (Koentges et al., 2016, Min et al., 2018).

Like all sirtuins, SIRT4 is expressed ubiquitously, but at particularly high levels in the heart, kidney, brain, and liver (Haigis et al., 2006). The metabolic roles, as well as the enzymatic function and substrates of SIRT4, differ in different organs. In the liver and skeletal muscle, it inhibits FAO, an important source of ROS production, through two different mechanisms (Nasrin et al., 2010). In muscle, as well as in white adipose tissue (WAT), SIRT4 deactivates mitochondrial malonyl-CoA decarboxylase (MCD), whereas in liver cells it blocks the interaction between SIRT1 and PPARα (Nasrin et al., 2010). Instead, SIRT4 leads to increased lipogenesis in WAT (Laurent et al., 2013). Therefore, SIRT4 deletion has been shown to protect against diet-induced obesity by displaying increased FAO and decreased lipogenesis (Laurent et al., 2013).

In pancreatic cells SIRT4 has been shown to reduce glutamate dehydrogenase (GDH) activity through ADP-ribosylation, thereby inhibiting insulin secretion (Haigis et al., 2006). In addition, SIRT4 regulates leucine-stimulated insulin secretion by inhibiting the methylcrotonyl-CoA carboxylase (MCCC), which in turn decreases lysine degradation (Anderson et al., 2017). In SIRT4 knockout mice, the absence of SIRT4 increased the circulating insulin levels by up to 30%, suggesting a possible role in the pathogenesis of diabetes (Haigis et al., 2006).

SIRT4 also plays an important role in mitochondrial energy metabolism. It has been shown to inhibit pyruvate dehydrogenase (PDH) by enzymatic hydrolysis of the lipoamide cofactor, thereby impairing intracellular glucose oxidation (Mathias et al., 2014, Bugger et al., 2016). Additionally, Jeong et al. were able to show, that that genotoxic stress limits glutamine entry into the central mitochondrial metabolism of the tricarboxylic acid (TCA) cycle via induction of SIRT4 (Jeong et al., 2013). This impaired TCA cycle anaplerosis, in turn, is likely to lead to impaired ATP synthesis and energy deficiency (Bugger et al., 2016).

SIRT4 has also been suggested to possess tumor suppressive effects, as it inhibits proliferation and/or migration of tumor in acute myeloid leukemia, Burkitt lymphoma, as well as colorectal, gastric and lung cancer (Bradbury et al., 2005, Jeong et al., 2014, Miyo et al., 2015, Huang et al., 2015, Fu et al., 2017, Min et al., 2018). Additionally, in colon, breast, endometrial and esophageal cancer tissues, messenger Ribonucleic acid (mRNA) levels of *Sirt4* were reduced (Huang and Zhu, 2018, Huang et al., 2016, Nakahara et al., 2016, Igci et al., 2016, Bartosch et al., 2016). The tumor suppressive effect is attributed to the suppressive effect of SIRT4 on glucose metabolism via inhibition of PDH, as well as on reduced mitochondrial glutamine metabolism via inhibition of GDH (Huang and Zhu, 2018). Tumor cells require additional energy for pathological tissue growth, which they obtain via increased glucose and glutamine metabolism. (Daye and Wellen, 2012). In addition, glutamine is an important amino acid in the cell cycle, especially during the transition from G1 to S phase (Colombo et al., 2011). When glutamine metabolism is inhibited, e.g. by the influence of SIRT4, the cell cycle comes to a standstill, which reduces the accumulation of DNA damage (Jeong et al., 2013).

Hypoxia-induced apoptosis is an important feature of many cardiac pathologies, such as ischemic cardiomyopathy, MI, and CAD. In H9c2 cardiomyoblast cells, *Sirt4* knockdown decreases cell viability and increases apoptotic cells, while overexpression has the opposite effect (Liu et al., 2013). Additionally, SIRT4 expression is markedly reduced in hypoxia-induced apoptosis in H9c2 cells, indicating that SIRT4 is an important regulator of H9c2 cell apoptosis (Liu et al., 2013). SIRT4 also effects mitochondrial permeability transition pores (PTP), who play a crucial role in ischemia-reperfusion injury-induced development of mitochondrial damage and necrotic cell death (Halestrap et al., 1997). Ischemia-reperfusion injury, such as in MI, leads to oxidative stress and inflammation, causing cellular damage. Increased oxidative stress heightens PTP susceptibility and ROS production, inducing PTP opening (Bernardi et al., 1992). Verma et al. demonstrated that SIRT4 modulates PTP sensitivity in HeLa cells, a human cancer cell line taken from a cervical cancer patient, Henrietta Lanks, in 1951 (Beskow, 2016), primarily via the regulation of GDH-1 (Verma et al., 2013). SIRT4 depletion prevents the induction of PTP and protects the cell from PTP-dependent cell death (Verma et al., 2013).

SIRT4 has also been recently associated with pathological cardiac hypertrophy. In their 2017 paper, Luo et al. investigated the role of SIRT4 in pathological cardiac hypertrophy in H9c2 cells. They found that SIRT4 deficiency impeded ANG II-induced cardiac hypertrophic growth, while myocardial SIRT4 overexpression accelerated it, suggesting that SIRT4 is a

regulator of the hypertrophic response to ANG II in cardiomyocytes. The effect of SIRT4 is thought to occur upon the deactivation of MnSOD as the underlying mechanism (Luo et al., 2017).

MnSOD is an antioxidant enzyme, which protects cells against oxidative damage from ROS, helping to maintain cardiac function (Munzel et al., 2015). SIRT4 knockout inhibits the ANG II-induced decrease in MnSOD activity, while SIRT4 overexpression has the opposite effect (Luo et al., 2017). Luo et al. have shown that SIRT4 inhibits SIRT3-mediated MnSOD deacetylation, maintaining higher MnSOD acetylation, thereby decreasing MnSOD activity upon ANG II stimulation, leading to an impaired antioxidant activity and increased oxidative stress. They were able to substantiate this by showing that the inhibition of ROS by manganese-5,10,15,20-tetrakis-(4-benzoic acid) porphyrin counteracted the hypertrophic effect of SIRT4 (Luo et al., 2017).

Ji et al. also showed, that SIRT4 overexpression markedly promoted hypertrophy in ANG II induced cardiomyocytes, apparent through an increase in ANP, BNP and ß-MHC (Ji et al., 2022). Although SIRT4 is highly expressed in the heart and recent studies have implicated SIRT4 in cardiac hypertrophy, research on the role of SIRT4 in cardiac hypertrophy remains limited, particularly in the context of oxidative stress.

4.5 Aims of the project.

Pathological hypertrophy is a significant contributor to ventricular dysfunction and HF (Shimizu and Minamino, 2016). Oxidative stress, recognized as a major driver of cardiac remodeling (Shiomi et al., 2004), is closely linked to the hypertrophic process. The mitochondrial sirtuin, SIRT4, has been shown in animal studies to drive pathological hypertrophy, potentially by impairing the myocardial antioxidative capacity resulting in oxidative stress (Luo et al., 2017). In addition, NOX4, an enzyme that is predominantly found in the mitochondria with an important role in the formation of ROS (Ago et al., 2010), has been identified as a potential player in this complex pathway. Preliminary data from our group suggests that the expression of NOX4 is increased in SIRT4 overexpressing mice following pressure-overload, which is associated with aggravated cardiac hypertrophy and dysfunction. Therefore, the aim of the present study was to investigate NOX4 as a possible mediator via which overexpression of SIRT4 exacerbates cardiac hypertrophy. Understanding the relationship between these proteins could provide valuable insights into the pathophysiology of cardiac remodeling and may reveal potential therapeutic targets for cardiovascular diseases.

5. Material and Methods

5.1 Material

5.1.1 Lab equipment

Table 3: Lab equipment

Equipment	Manufacturer
Autoclave NB100ABE	Fedegari Group, Albuzzano, Italy
Centrifuge Multifuge 3	Thermo Fisher Scientific, Waltham, MA, USA
CO_2 Incubator	Binder GmbH, Tuttlingen, Germany
Electronic Scale CPA64	Sartorius, Göttingen, Germany
Heraeus Fresco 21 Centrifuge	Thermo Fisher Scientific, Waltham, MA, USA
Heraeus Multifuge 1 L-R	Thermo Fisher Scientific, Waltham, MA, USA
IX51 Inverted Fluorescence Microscope	Olympus, Tokyo, Japan
Laminar Flow Hood HERAsafe KS	Kendro Laboratory Products GmbH, Langenselbold, Germany
Multipete plus	Eppendorf SE, Hamburg, Germany
Multitron Incubator Shaker	Infors HAT, Bottmingen, Switzerland
MyFuge mini Centrifuge	Benchmark Scientific, Sayreville, MA, USA
NanoDrop 2000c Spectrophotometer	Thermo Fisher Scientific, Waltham, MA, USA
PowerPac™ Basic Electrophoresis Power Supply	Bio-Rad, Hercules, CA, USA
ProteinSimple Jess	Bio-Techne, Minneapolis, MN, USA
Shaking Precision Water Bath with electronic regulation	J.P. Selecta, Barcelona, Spain
Spectrometer Spectra Max Plus 384	Molecular Devices, LLC, San José, CA, USA

TC20 Automated Cell Counter	Bio-Rad, Hercules, CA, USA
Thermal Cycler T100	Bio-Rad, Hercules, CA, USA
Thermomixer comfort	Eppendorf SE, Hamburg, Germany
Therocycler CFX96	Bio-Rad, Hercules, CA, USA
Ultra-Turrax T10 Basic	IKA-Werke GmbH & Co. KG, Staufen, Germany
UP50H Ultrasonic Processor	Hielscher Ultrasonics, Teltow, Germany

5.1.2 Consumables

Table 4: Consumables

Consumables	Manufacturer
Amico Ultra Centrifugal Filters	Merck KGaA, Darmstadt, Germany
Cell Culture Flasks	SPL Life Sciences, Poncheon-si, South Korea
Corning® Costar® Stripette® Disposable Serological Pipette	Corning Inc., New York, USA
Coverslips 24x50mm	Carl Roth GmbH & Co. KG, Karlsruhe, Germany
Culture Tubes	STARLAB International GmbH, Hamburg, Germany
Dual Chamber Couting Slides	Bio-Rad, Hercules, CA, USA
Falcon™ Aspiration Pipette	Thermo Fisher Scientific, Waltham, MA, USA
Falcon™ Petri Dish	Corning Inc., New York, USA
Falcon™ Polypropylene Conical Tube	Thermo Fisher Scientific, Waltham, MA, USA
Lab-Tek II CC2 Chamber Slide System	Thermo Fisher Scientific, Waltham, MA, USA
PCR SingleCap 8er-SoftStrips	Biozym Scientific GmbH, Oldendorf, Germany
Pipet Tips	Eppendorf SE, Hamburg, Germany
Safe-lock Centrifugation Tubes	Eppendorf SE, Hamburg, Germany

Weighing Paper	Macherey-Nagel GmbH & Co. KG, Düren, Germany

5.1.3 Kit-Systems

Table 5: Kit-Systems

Kits	Manufacturer
12-230kDa Fluorescence Separation Module for JESS	Bio-Techne, Minneapolis, MN, USA
QIAprep Spin Miniprep Kit #27104	QIAGEN GmbH, Hilden, Germany
QuantiTect RT Kit #205313	QIAGEN GmbH, Hilden, Germany
RePlex Module for JESS	Bio-Techne, Minneapolis, MN, USA
RNAse-Free DNase Set #79254	QIAGEN GmbH, Hilden, Germany
RNeasy Micro Kit #74004	QIAGEN GmbH, Hilden, Germany

5.1.4 Chemicals and Reagents

Table 6: Chemicals and Reagents

Chemicals/ Reagents	Manufacturer
iQ SYBR Green Supermix	Bio-Rad, Hercules, CA, USA
10X FastDigest Buffer	Thermo Fisher Scientific, Waltham, MA, USA
6X DNA Loading Dye	Thermo Fisher Scientific, Waltham, MA, USA
4',6-Diamidino-2-phenylindol Dihydrochlorid (DAPI)	Carl Roth GmbH & Co. KG, Karlsruhe, Germany
Agar granulated	Fisher BioReagents, Thermo Fisher Scientific, Waltham, USA
Ambion Nuclease-Free Water	Life Technologies Corp., Austin, TX, USA
Angiotensin II, human	Sigma-Aldrich, St. Louis, MO, USA
Bovine Serum Albumine	Sigma-Aldrich, St. Louis, MO, USA

cOmpleteTM, EDTA-free Protease Inhibitor Cocktail	Sigma-Aldrich, St. Louis, MO, USA
D5α-competent cells	Thermo Fisher Scientific, Waltham, MA, USA
Dako Fluorescence Mounting Medium	Agilent Technologies Inc., Santa Clara, CA, USA
EMSURE® Ethanol absolute for analysis	Merck KGaA, Darmstadt, Germany
Ethylenediaminetetracetic acid disodium salt dihydrate	Sigma-Aldrich, St. Louis, MO, USA
FastDigest SmaI	Thermo Fisher Scientific, Waltham, MA, USA
Gelred® Nucleic Acid Gel Stain	Biotium, Fremont, CA, USA
gibco 0,25% Trypsin-EDTA	Life Technologies Limited, Paisley, UK
gibco DPBS (1X) [+] CaCl2 [+] MgCl2	Life Technologies Limited, Paisley, UK
gibco Dulbecco's Modified Eagle Medium [+] 4.5g/L D-Glucose, L-Glutamine [+] Pyruvate	Life Technologies Limited, Paisley, UK
gibco Fetal Bovine Serum Performance Plus	Life Technologies Limited, Paisley, UK
gibco PBS pH 7,2 (1X) [-] $CaCl_2$ [-] $MgCl_2$	Life Technologies Limited, Paisley, UK
Invitrogen Wheat Germ Agglutinin (WGA)	Thermo Fisher Scientific, Waltham, MA, USA
Isoprenaline hydrochloride	Sigma-Aldrich, St. Louis, MO, USA
Kanamycin solution from Streptomyces kanamyceticus 10mg/ml in 0.9% NaCl	Sigma-Aldrich, St. Louis, MO, USA
Paraformaldehyd 4% in PBS	MORPHISTO GmbH, Offenbach am Main, Germany
Phosphate Inhibitor Cocktail 2	Sigma-Aldrich, St. Louis, MO, USA
Phosphate Inhibitor Cocktail 3	Sigma-Aldrich, St. Louis, MO, USA
Pierce™ BCA Protein Assay Reagent A	Thermo Fisher Scientific, Waltham, MA, USA

Pierce™ BCA Protein Assay Reagent B	Thermo Fisher Scientific, Waltham, MA, USA
PolyJet™ In Vitro DNA Transfection Reagent	SignaGen Laboratories, Rockville, MD, USA
Quick Load Purple 1kb DNA Ladder	New England BioLabs, Frankfurt am Main, Germany
SIRT4 Human Tagged ORF Clone RC212226	OriGene Technologies, Inc., Rockville, MD, USA
S.O.C Medium	Thermo Fisher Scientific, Waltham, MA, USA
SDS-Pellets	Carl Roth GmbH & Co. KG, Karlsruhe, Germany
Sodium Chloride	Carl Roth GmbH & Co. KG, Karlsruhe, Germany
Sodium deoxycholate	Sigma-Aldrich, St. Louis, MO, USA
Tris-acetate-EDTA 50X (TAE) electrophoresis buffer	Thermo Fisher Scientific, Waltham, MA, USA
Transfection Reagent PolyJet	SignaGen Laboratories, Frederick, MA, USA
Tris-Pufferan® ≥ 99,9%, p.a.	Carl Roth GmbH & Co. KG, Karlsruhe, Germany
Triton™ X	Sigma-Aldrich, St. Louis, MO, USA
Trypan Blue Solution	Sigma-Aldrich, St. Louis, MO, USA
Tryptone	Sigma-Aldrich, St. Louis, MO, USA
Yeast Extract	Sigma-Aldrich, St. Louis, MO, USA

5.1.5 Oligonucleotides

Table 7: Primer

Target Gene	Primer	Sequence (5' → 3')
Tuba1a	Forward	GACAAGACCATTGGGGGAGG

	Reverse	GGAAGAGCTGGCGGTAGGTG
***Sirt4* (rat)**	Forward	CAGCGTGTGAAAGAAGCTGA
	Reverse	CAAGCCAAATCGTCAGACCT
***SIRT4* (human)**	Forward	TGGATGCTTTGCACACCAAG
	Reverse	GGACTTGGAAACGCTCTTGC
Nox4	Forward	CTGGTGAAGATTTGCCTGGAAG
	Reverse	GTGACAGGTTTGTTGCTCCG
NppB	Forward	TTAGGTCTCAAGACAGCGCC
	Reverse	CGCCGATCCGGTCTATCTTC

5.1.6 Antibodies

Table 8: Antibodies

Antibody	**Manufacturer**
Anti-SIRT4 bs-7537R	Bioss Inc., Woburn, MA, USA
Anti-NOX4 #14347-1-AP	Proteintech® Group Inc., Los Angeles, CA, USA

5.2 Methods

5.2.1 *SIRT4* overexpression Plasmid Production

To multiply *SIRT4* overexpression human sourced Plasmid DNA (RC212226, OriGene), DH5-α competent cells (Escherichia coli, Thermo Fisher Scientific) were used. The transformation of DH5-α competent cells involves making these bacterial cells capable to accept and express the foreign DNA plasmids. The key lies in making the cell membranes permeable to the introduced DNA. To achieve this, competent cells are first prepared by subjecting them to a cold shock and incubating them with specialized solutions, making their membranes more receptive to foreign DNA. Once the cells become competent, the target plasmid is introduced into the cell suspension. The cells uptake this DNA during a brief heat shock, allowing it to enter the bacterial cell. This process results in the transformation of the bacterial cells, incorporating the foreign DNA. These transformed cells are then selected and grown on culture plates containing an antibiotic, in this case kanamycin (Sigma Aldrich), which only the transformed cells are able to survive, as the target plasmid contains a region which expressed a resistance against kanamycin (**Figure 6**). The introduced DNA is replicated as the cells multiply, making it possible to produce large quantities of the desired DNA.

The transformation was performed by following the manufacturer's instructions with minor changes (**Figure 4**). The cells, which were stored at -80°C, were thawed on wet ice. 500-1,000 ng of desired plasmid was pipetted into a 1.5 ml microcentrifuge tube, 50 µl of cells were added and mixed by pipetting up and down and then incubated on ice for 30 minutes. Next, cells were heat shocked in a water bath at 42°C for 45 seconds and put back on ice for 2 minutes. To the cell-mixture, 950 µl of room temperature Super Optimal Broth with Catabolite repression medium (S.O.C-media, Thermo Scientific) was added and then incubated in the Multitron Incubator Shaker at 155 rpm and 37°C for 50 minutes. 150 µl of the cell suspension were then plated on 37°C pre-heated, 90 mm lysogeny broth (LB) plates, which were prepared beforehand (**Table 9**, **Figure 4B**). The inoculated plates were then incubated at 37°C for 2-3 days until sufficient amounts of bacterial colonies had been formed.

Table 9: LB plate preparation

1.25 g	Tryptone
0.624 g	Yeast
1.25 g	Sodium Chloride
1.875 g	Agar
Filled up to 250 ml with distilled water and autoclaved.	
2.5 ml	Kanamycin

The colonies were sub-cultured into 5 ml of LB liquid media (one 10 ml test tube per colony) supplemented with 1% kanamycin (Sigma Aldrich) and incubated at 37°C overnight in a shaker at 155 rpm to multiply the bacteria (**Figure 4C**).

The Plasmid DNA was then extracted using a QIAprep Spin Miniprep Kit (QIAgen) according to the manufacturer's instructions (**Figure 4D**). The bacterial overnight culture was centrifuged at 6.800 x g for 3 minutes at room temperature. The pellet was then resuspended in 250 µl Buffer P1 (QIAprep Spin Miniprep Kit, QIAgen) and transferred to a microcentrifuge tube. After adding 250 µl of Puffer P2 (QIAprep Spin Miniprep Kit, QIAgen) the mixture was thoroughly mixed by inverting the tube.

The following centrifugations steps were all performed at 17.900 x g and room temperature. First, 350 µl of Buffer N3 (QIAprep Spin Miniprep Kit, QIAgen) was mixed and centrifuged for 10 minutes. 800 µl of the supernatant was then applied on to the QIAprep 2.0 spin column. Thereafter the spin column was centrifuged for 30-60 seconds and the flow-through discarded. The QIAprep 2.0 spin column was then washed by adding 750 µl Buffer PE (QIAprep Spin Miniprep Kit, QIAgen) and centrifuged, discarding the flow-through. The Spin-column was then centrifuged again for 1 minute to remove residual wash buffer. To elude the DNA 30 µl of H_2O was added to the center of the QIAprep 2.0 spin column, incubated for 1 minute at room temperature and then centrifuged for another 1 minute. The DNA concentration was measured using a NanoDrop 2000 (Thermo Fisher Scientific).

To test if the transformation was successful, a restriction enzyme digest was performed (**Figure 4E**). For this, approximately 1000 ng of DNA was incubated with a digestion master mix (**Table 10**).

Table 10: Restriction Enzyme Digest

	<500 ng/µl	*>500 ng/µl*
1. H_2O	15 µl	16 µl
2. FastDigest Buffer	2 µl	2 µl
3. DNA	2 µl	1 µl
4. FastDigest SMAI restriction enzyme	1 µl	1 µl
Total	20 µl	20 µl

The mixture was then incubated for 5 minutes at 37°C. During incubation the SMAI restriction enzyme cleaves the DNA in specific areas (CCCGGG) and created fragments with the length of 546 base pairs (bp) and 5277 bp. The subsequent incubation at 65°C for 5 minutes stopped and denatured the restriction enzyme.

The DNA fragments were separated and detected via agarose gel electrophoresis. For gel electrophoresis 4 µl of a 6x Loading Dye (Thermo Scientific) was added to the restricted DNA mix. 2 g of Agarose was dissolved in 250 ml Tris-Acetate-EDTA (TAE) electrophoresis buffer (Thermo Fisher Scientific) to generate a 0.8 % Agarose-gel. 25 µl of Gelred (Biotium Inc.) was added to the liquid gel and mixed until distributed evenly. Next, the mixture was poured into a rack and left at room temperature until solid. The gel was then put into the electrophoresis chamber and covered with electrophoresis buffer. The samples and the Quick Load Purple 1 kb DNA Ladder (New England BioLabs) were pipetted into the gel. The electrophoresis ran with a voltage of 5 Volt/cm for approximately 1 hour.

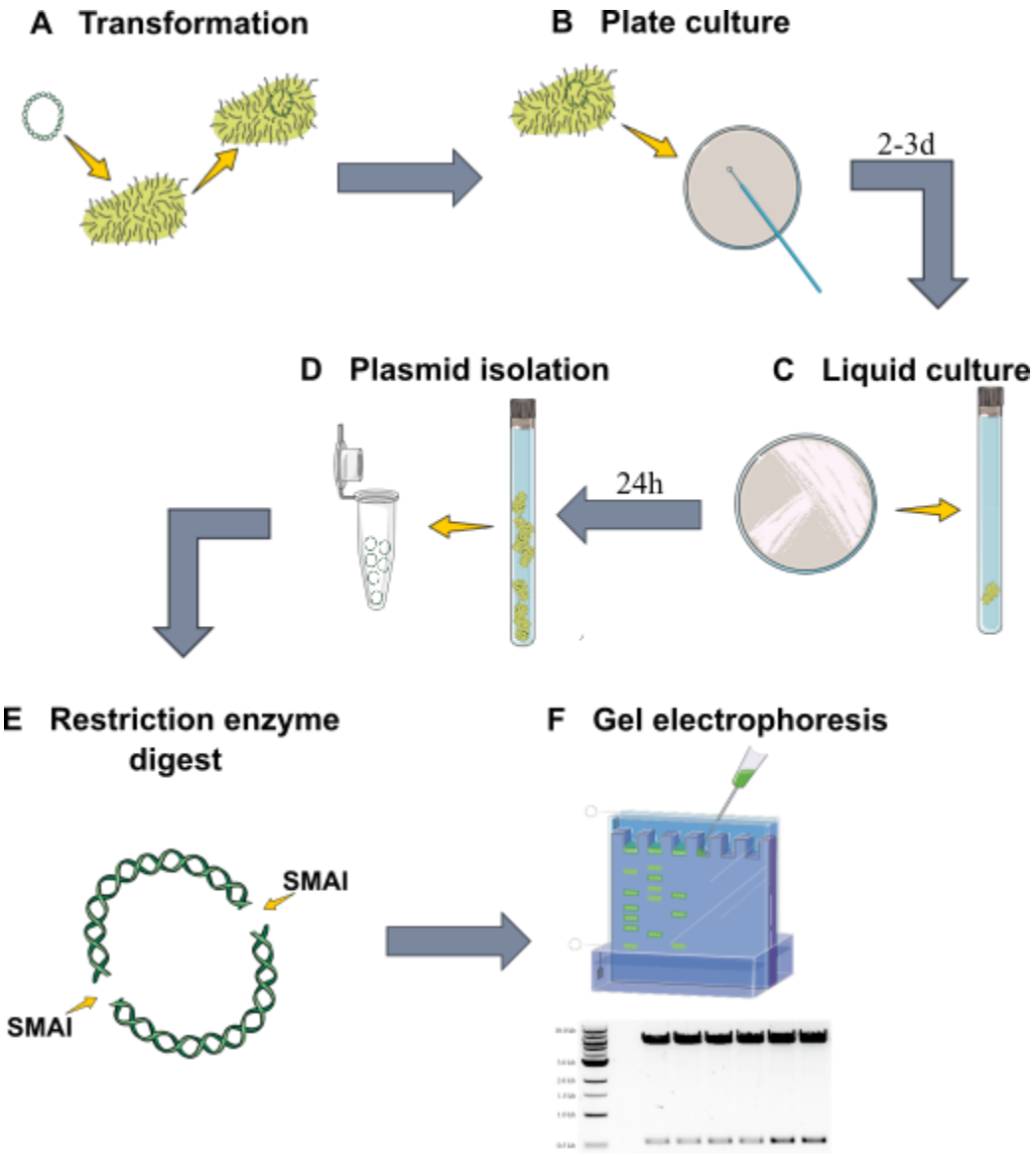

Figure 4: Schematic representation of plasmid production.

A) Day 1: Transforming DH5-α competent cells by making their membrane permeable through a cold shock and adding the desired plasmid. B) Day 2: Plating the transformed bacteria on LB-plates with kanamycin. C) Day 3: Transferring individual colonies from the plate to liquid medium. D) Day 4: Isolating the newly produced plasmids with QIAprep Spin Miniprep Kit. E)/F) Day 5: Testing the efficiency of the transformation using restriction enzymes and gel electrophoresis. Parts of the figure were drawn by using pictures from Servier Medical Art. Servier Medical Art by Servier is licensed under a Creative Commons Attribution 3.0 Unported License (https://creativecommons.org/licenses/by/3.0/).

5.2.2 Cell Culture, Transfection and Drug Treatment

Rat cardiomyoblasts (H9c2 cell line) were cultured at 37°C in 5% carbon dioxide (CO_2) atmosphere in Dulbecco's Modified Eagle Medium (DMEM; Gibco) supplemented with 10 % non-heat inactivated Fetal Bovine Serum (FBS; Gibco). To achieve human SIRT4 overexpression in H9c2 cells, transfection of the plasmid containing *SIRT4* of human origin was performed using the PolyJet *in vitro* DNA Transfection Reagent (PJ), according to the manufacturer's instructions (SignaGen® Laboratories; **Figure 5**). The underlying mechanism of PJ-induced separation depends on lipid-based nanoparticles. In a first step, these lipids form a complex with the negatively charged genetic material due to their cationic properties. When this complex is added to the cells, the lipophilic PJ reagent enables cellular uptake by endocytosis. After a maturation process of the endosomes, the plasmid is released into the cytoplasm where it can unfold its biological effect. Two extra control groups were used, a control group without PJ and vector and a PJ-control group, where PJ was added only, but without vector. Depending on the protein and ribonucleic acid (RNA) based experiments as well as the histological cell staining, cells had to be seeded in different densities in all groups.

In the first trials seeding densities were adjusted to achieve approximately 80% confluency at the final time point of harvest or experiment, respectively. 2,000, 2,500, 2,700, 2,900 and 3,000 cells/cm^2 in T25 cell culture flasks (surface area 25 cm^2) had been tested. Consequently, seeding densities of 1,400 cells/cm^2 for the control, 1,600 cells/cm^2 for the PJ-Control and 3,000 cells/cm^2 for the transfected group were chosen (**Figure 5A**). For the fluorescent staining, the cells were seeded in an 8-well chamber slide system (Lab-Tek II CC2, Thermo Fisher) with 5,000 cells/cm^2 (negative control), 5,500 cells/cm^2 (PJ-control) and 10,000 cells/cm^2 (transfected group), respectively.

First of all, the old medium was replaced by fresh medium completed with 10 % FBS 30 - 60 minutes prior transfection. For each T25 flask, 2.5 µg of plasmid DNA was diluted in 125 µl DMEM and for each well in the 8-well chamber slide system, 0.25 µg of plasmid DNA in 15 µl DMEM. Secondly, 7.5 µl per T25 flask and 0.75 µl per 8-well chamber slide well of PJ-Reagent was diluted in the same volume of diluent (DMEM) as the plasmid DNA. Finally, the PJ-solution was added in a 1:1 ratio to the Plasmid-DNA-solution and incubated at room temperature for 10-15 minutes to allow the PJ/DNA-complexes to form. 250 µl of the solution was added dropwise to the T25 cell culture flask and 30 µl was added to each well of the 8-well chamber slide system. In preliminary experiments, transfection times of 6

and 12 hours were tested for H9c2 cells to determine the optimal duration. The 12 hour transfection resulted in increased cell toxicity, leading to reduced cell numbers and insufficient RNA extraction. Thus, a transfection time of 6 hours was chosen for subsequent experiments due to lower toxicity and satisfactory transfection efficiency. After 6 hours transfection time the transfection media was replaced by complete DMEM. Furthermore, a regeneration period was implemented post-transfection to allow recovery. After microscopic examination at 18, 42, and 64 hours after transfection, 42 hours of regeneration was chosen, with another medium change with complete DMEM after 18 hours.

To induce hypertrophy, sterile filtered ISO solutions of final concentrations of 10 µM, 30 µM and 50 µM were prepared in complete medium (DMEM + 10% FBS) and added to the cells 42 hours after the removal of transfection reagent (**Figure 5C**). After an incubation period of 24 h, the cells were harvested (**Figure 5D**). For harvesting, cells were first washed with phosphate-buffered saline (PBS) and detached from the culture flask using 0.25% Na-trypsin. The detached cells were then centrifuged at 4°C and 500 x g for 3 minutes, washed with PBS to remove residual trypsin and growth medium and centrifuged again at 4°C and 500 x g for 5 minutes. The cell pellet was snap frozen in liquid nitrogen for later processing, such as RNA or protein isolation (**Figure 5E**).

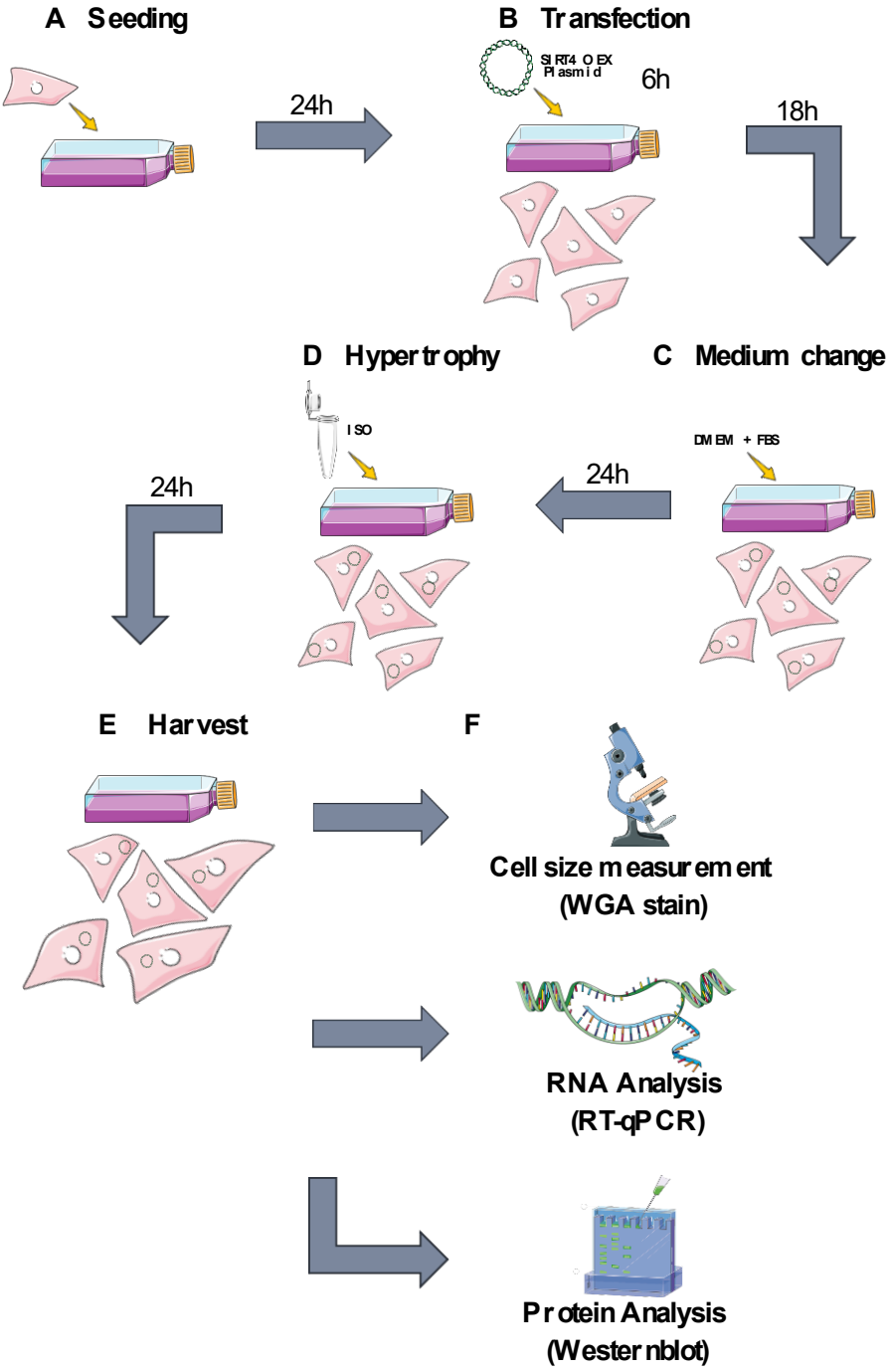

Figure 5: Schematic representation of the experiment procedure.

A) Day 0: Seeding cells in T25 cell culture flask. B) Day 1: Transfection of the cells with PJ-Reagent. C) Day 2: Inducing Hypertrophy in the cells by adding 30 µM of ISO. D) Day 3: Medium change. E) Harvest the cells. F)) Downstream experiments, such as WGA staining, RNA-analysis, and protein analysis. Parts of the figure were drawn by using pictures from Servier Medical Art. Servier Medical Art by Servier is licensed under a Creative Commons Attribution 3.0 Unported License (https://creativecommons.org/licenses/by/3.0/).

5.2.3 RNA-Isolation, cDNA-synthesis, RT-qPCR

RNA Isolation

The RNA purification was performed using the RNeasy MICRO KIT (#74004, Qiagen) suitable for cells, based on the principle of selectively capturing RNA molecules while excluding contaminants like DNA, proteins, and cell debris. After lysing the sample and adding ethanol to create suitable binding conditions, the RNA molecules selectively bind to the silica membrane in a spin column, thus isolating them from other cell components.

The following steps were performed: 350 µl of Buffer RLT (RNeasy Micro KIT #74004, Qiagen) was added to the 2 ml tube containing the snap frozen cells and the cells were homogenized for 40 seconds on ice using an Ultra-Turrax T10 Basic (IKA) at Speed 3. The homogenizer was cleaned with three rinses in water. All samples were kept on ice until the homogenization was completed.

To each tube, 350 µl 70% ethanol was added, followed by vortexing. A maximum of 700 µl of the sample was pipetted onto the RNeasy spin column. The spin columns were then centrifuged at 8,000 x g for 15 seconds at room temperature and the flow-through was discarded. Next, 700 µl of RW1 buffer was added, and the lid was closed before centrifugation at 8,000 x g for 15 seconds. The column was transferred to a fresh collection tube. Any remaining buffer on the inner rim of the column was removed using a pipette. The membrane of the RNeasy column received 80 µl of DNase mix (#79254, Qiagen) directly, and the mixture was incubated for 15 minutes at room temperature using a heatblock at 25°C. Subsequently, 350 µl of Buffer RW1 was added to the RNeasy column, the lid was closed, and centrifugation was carried out for 15 seconds at 8,000 x g. The flow-through was discarded. A total of 700 µl of Buffer RPE was added to the column, followed by centrifugation at 8,000 x g for 15 seconds at room temperature. The flow-through was discarded, and the column was tapped on fresh paper. 500 µl Buffer RPE (RNeasy Micro KIT, Qiagen) was added to the column, and centrifugation was performed at 8,000 x g for 15 seconds at room temperature. Subsequently, 500 µl of 80 % ethanol was added to the spin columns. The lid was closed, and centrifugation was carried out for 2 minutes at 8,000 x g at room temperature.

To remove any remaining buffer, the column was placed into a fresh 2 ml tube (not the collection tube) and remaining buffer and ethanol was removed by pipetting the inner rim of the column. Centrifugation was performed at 8,000 x g for 5 minutes to dry the membrane. The column was then placed in a fresh 1.5 ml tube and 30 µl of RNase-free water was added.

Incubation was carried out for 5 minutes, followed by centrifugation at 8,000 x g for 2-3 minutes at room temperature. The eluate was transferred to a pre-labeled 0.6 ml tube. RNA was measured using a Nanodrop 2000 (ThermoFisher) and the samples were immediately frozen in liquid nitrogen for storage.

The RNA concentration and sample purity were determined using a NanoDrop full-spectrum spectrophotometer. The concentration of RNA was measured by quantifying the absorption of light at a wavelength of 260 nm. Additionally, two ratios were calculated to assess purity: The 260/280 nm ratio, obtained by dividing the absorbance at 260 nm by that at 280 nm, indicates the ratio of nucleic acid to protein, phenol or other contaminants, that absorb strongly near 280 nm. A ratio close to 2.0 signifies a relatively pure sample. The 260/230 nm ratio, calculated by dividing the absorbance at 260 nm by that at 230 nm, was used to evaluate purity with respect to contaminants such as organic solvents. A higher ratio at 2.0 to 2.2 suggests better RNA purity, lower values indicate a higher presence of contaminants. Higher can also indicate that the blank measurement was made on a dirty pedestal, or an inappropriate blank was used.

cDNA Synthesis

The complementary DNA (cDNA) synthesis process using the QuantiTect RT Kit by Qiagen involves converting RNA into cDNA. The key principle behind this process is the use of reverse transcriptase enzymes, which are capable of synthesizing cDNA from RNA templates. In this kit, a reverse transcriptase enzyme is combined with primers and other reagents to initiate the synthesis of cDNA. The primers anneal to the RNA, allowing the reverse transcriptase to create complementary DNA strands. This resulting cDNA molecule can then be used for various downstream applications.

The following steps were performed, according to the company's instruction. Wipeout Buffer (QuantiTect RT Kit, Qiagen), RT Buffer 5x (QuantiTect RT Kit, Qiagen), RT Primer Mix (QuantiTect RT Kit, Qiagen), and H_2O were thawed at room temperature, while sample RNA and Reverse Transcriptase (QuantiTect RT Kit, Qiagen) were kept on ice. H_2O and sample were pipetted into 8-well PCR strips as to achieve the desired concentration of 500 ng RNA per 12 µl per well. 2 µl of Wipeout Buffer was added and the mixture was spun down, mixed well by tapping, and then spun down again. The PCR strips were placed into the thermocycler and run for 2 minutes at 42°C with a Lid temperature of 45°C.

Then, the Mastermix and RT Minus Mix (negative control) were prepared (**Table 11**). The RT-Minus is the negative control where water was added instead of reverse transcriptase.

This ensures that the cDNA detected in the PCR originates from the reverse transcription of the RNA. If a signal is detected in the RT minus control during RT-qPCR, it indicates that contamination with DNA has occurred and that the result of the RT-qPCR may not be reliable.

Table 11: Master Mix for cDNA-Synthesis

Master Mix	*Volume per well*
RT Buffer 5x	4 µl
RT Primer Mix	1 µl
Reverse Transcriptase or H_2O (RT Minus Mix)	1 µl
Total	6 µl

6 µl of the Master Mix was pipetted into the 14 µl RNA-Mix and the mixture was spun down, mixed well by tapping, and then spun down again. The PCR strips were placed into a thermocycler using the following program: 30 minutes at 42°C, 3 minutes at 95°C, Lid temperature 4°C, end at 4°C. Finally, the synthesized cDNA was diluted for the PCR to a concentration of 1 ng/µl.

Quantitative Reverse-Transcriptase-PCR (RT-qPCR)

The qPCR was performed using the SYBR Green method. This method enables the quantitative determination of the expression of a specific gene in a sample. SYBR Green is a DNA-specific fluorescent dye which binds to DNA and only emits light when it is bound to double-strand DNA. Before the amplification starts, samples are first heated up to 95°C, which activates the heat stable DNA-Polymerase. The amplification cycle starts with denaturing double strand PCR products at 95°C, followed by an annealing phase, as the temperature cools down to 59°C, where the primers bind to the complementary sequences on the DNA. During the subsequent extension phase at 72°C, the DNA polymerase synthesizes the complementary DNA segment starting from the primers. The amount of target sequence in the sample therefore doubles with each cycle. After each elongation step, the fluorescent signal is measured. With each cycle, the fluorescence intensity increases in proportion to the amount of PCR product. The threshold cycle count (Ct value), where the fluorescence reaches a predefined threshold, can be used to quantify the initial amount of target gene in the sample.

For this, the following steps were undertaken. Samples, primers (reverse and forward), and the iQ SYBR Green Supermix were thawed on ice. Stock primers (100 µM) were diluted 1:50 to achieve a final primer concentration of 0.1 µM per well. A mastermix was prepared for each target gene as follows (**Table 12**):

Table 12: Master Mix for qPCR

Master Mix	*Volume per well*
iQ SYBR Green Supermix	12.5 µl
1:50 primer forward	1.25 µl
1:50 primer forward	1.25 µl
Total	15 µl

10 µl of each sample with a concentration of 1 ng/µl was pipetted into a 96-well plate in duplicates. Ensuring proper mixing, the contents were tapped and then spun down. Next, 15 µl of Mastermix was added to each well. The 96-well plate was sealed with an adhesive Microseal foil and pressed down with a roller to ensure proper sealing. The plate was then spun down. qPCR settings can be viewed in **Table 13**.

Table 13: qPCR Thermocycler Protocol

1)	95°C	10 min
2)	95°C	15 sec
3)	59°C	30 sec
	+ Plate read	
4)	72°C	45 sec
5)	Go to 2) 39 more times.	
6)	95°C	10 sec
7)	Melt curve 60°C to 90°C increment 0,5°C for 5 sec. + Plate read	

The Ct number at which the curve of the PCR products showed exponential slope was evaluated. The analysis comprised several steps. The mean of the duplicate values were calculated. The calculated mean values were then used in a regression equation of a standard curve to determine the mRNA levels. The results obtained were normalized to the reference gene alpha Tubulin (*αTub*) to compensate for possible variations in RNA extraction or PCR

efficiency. Finally, the gene expressions of the different groups were compared relative to each other, whereby the values were always normalized to a control group.

5.2.4 Protein Isolation, BCA Assay, Jess Automated Western Blot

Protein Isolation

Protein isolation was performed using radioimmunoprecipitation assay buffer (RIPA), which allows the extraction of proteins from biological material such as cells or tissues without denaturing the proteins themselves. The RIPA buffer contains a combination of chemical components, including detergents, salts, and buffering reagents, that collectively dissolve cell membranes, lysed cell organelles, and stabilized proteins (**Table 14**).

Table 14: RIPA Lysis-Buffer

	Volume	*Final Concentration*
Tris-HCL (pH 8) 1.0 M	0.5 ml	50 mM
EDTA (pH 8) 0.1 M	0.1 ml	1 mM
NaCl (5 M)	0.3 ml	150 mM
Triton X-100	1 ml	10 %
Na-deoxycholate 10%	0.5 ml	0.5 %
SDS 10%	0.1 ml	0.1 %
ddH_2O	Up to 10 ml	

For the protein isolation, RIPA-Buffer was prepared as shown in **Table 14**. To this, a Protease/ Phosphatase Inhibitor Cocktail was added in a 100-fold dilution, consisting of 100 µl Phosphatase Inhibitor Cocktail 3 (Sigma), 100 µl Phosphatase Inhibitor Cocktail 2 (Sigma) and 1 pill Protease Inhibitor-Cocktail (Roche) per 10 ml RIPA buffer.

Frozen cells were then resuspended in 300 µl of ice-cold RIPA buffer and incubated for 20 minutes on ice (shaking at 20 rpm). This was followed by sonication (UltraSonic Processor UP50H) at 80% amplitude for 3 seconds on ice.

After centrifugation at 16,000 x g for 20-30 minutes at 4°C, the supernatant was transferred to a fresh 1.5 ml tube and stored on ice. The protein lysate was then transferred to a labeled Amicon Filter Spin Column (AMICONULTRA) and centrifuged at 8,000 x g for 5 minutes at 4°C until the volume was reduced to 100-200 µl. Finally, the protein lysates were aliquoted and stored at -80°C in liquid nitrogen.

BCA Assay

The BCA assay (Bicinchoninic Acid Assay) is a common method for determining protein concentration in solutions. It is based on the reaction of bicinchoninic acid with copper ions in an alkaline environment to form a violet color complex. The intensity of this color correlates directly with the protein concentration in the sample.

Samples were diluted according to the desired dilution (1:2 in this case) by mixing the specified amount of sample with water. Then, 10 µl of the standards, water, and diluted samples were pipetted in duplicates into a clear 96-well plate. Immediately prior to pipetting, a Micro BCA mixture was prepared containing Reagent A and Reagent B in a 50:1 mixing ratio. 190 µl of this mixture were added to each well of the plate. The plate was incubated at room temperature for 15 minutes to allow the reaction to proceed. A SpectroMax Plus 384 from Molecular Devices with a wavelength of 562 nm was used to measure the absorbance. The absorption values of the standards were used to generate a standard curve. The measured absorbance values of the samples were entered into the standard curve to determine the corresponding protein concentrations using linear regression.

JESS Automated Western blot

In the JESS Automated Western Blot System instrument (Protein Simple), capillaries replace both the acrylamide gel and the transfer membrane of the conventional Western blot. Samples are placed in capillaries where both size separation and immunoblot analysis are performed. The proteins contained in the samples are separated in the capillaries by passing through stacking and separation matrices and then immobilized on the capillary walls. Immunoblotting is then performed using primary and (labeled) secondary antibodies (Rustandi et al., 2012, Sormunen et al., 2023).

The JESS capillary-based protein separation and immunodetection was performed according to the company's instructions. The antibodies were diluted with milk-free antibody diluent according to a dilution factor determined experimentally in advance for each antibody. The following primary antibodies were used: SIRT4 (Bioss, bs-7537R) and NOX4 (Proteintech ®, #14347-1-AP). Luminol-S and Peroxide were combined in a 1:1 ratio and the RePlex Reagent was generated by mixing four parts of Reagent 1 and one part of Reagent 2. The protein lysates were diluted to a concentration of 0.6 mg/ml with 0.1X sample buffer and Master Mix included in the kit was added at a dilution factor of 1:5. The samples were then vortexed and boiled at 95°C for 5 minutes.

Prepared samples and other reagents were pipetted into the Jess's pre-filled plate using the company's template. The plate was centrifuged at 900 x g at room temperature for 5 minutes. The Western blot was then started using the Jess protein analyzer. Further analysis of the data was performed using the Compass for SW software.

5.2.5 Fluorescent staining and cell size measurement

The size of cardiomyocytes is a crucial parameter in assessing hypertrophy. To measure this size, Wheat Germ Agglutinin (WGA) staining, as well as a nucleus staining with 4',6-diamidino-2-phenylindole (DAPI)-solution was performed. The WGA staining protocol was carried out as follows: First, the necessary solutions were prepared, including 40 ml of PBS, 1760 µl of PFA 4%, 2.000 µl of 5 µl/ml WGA-solution in PBS and 2.000 µl of 5 µl/ml DAPI-solution in PBS. The WGA and DAPI solutions were stored in the dark (in Eppendorf tubes wrapped in tinfoil) and centrifuged for 15 seconds. 1,760 µl of the supernatant was transferred to a new Eppendorf tube to eliminate any potential protein aggregates and reduce nonspecific background staining.

All following volumes refers per well. After cell seeding and treatment in cell culture 8-well chamber slides with a surface area of 0.8 cm^2 per well, cells were washed twice with 400 µl of PBS. Subsequently, cells were fixed with 200 µl of 4 % PFA for 20 minutes at room temperature with constant agitation on a shaker at 20 rpm. Following fixation, cells were washed three times with 300 µl of PBS for 5 minutes each at room temperature on a shaker at 20 rpm. Next, cells were incubated with 200 µl of 5 µl/ml WGA-solution for 40 minutes at room temperature on a shaker at 20 rpm, in the dark (using a black box). After this incubation, cells were washed three times with 300 µl of PBS for 5 minutes each at room temperature on a shaker. Subsequently, cells were incubated with 200 µl of 5 µl/ml DAPI-solution for 20 minutes on a shaker. Following the DAPI incubation, cells were washed three times with 300 µl of PBS for 5 minutes each at room temperature on a shaker. The chamber grid were then removed from the slides using an applicator and one drop of mounting medium was applied to the cells. The slides were covered with clean coverslips and gently pressed down. Finally, the slides were sealed with nail polish and stored at 4°C in the dark.

The cells were then imaged using an inverted Fluorescence Microscope (IX51, Olympus), with a lens size of 20X magnification. The FITC and DAPI filter sets were used for WGA and DAPI respectively. The cell size in μm^2 was then measured using ImageJ.

5.2.6 Statistics

Data are presented as means with standard error of mean (SEM). The statistical analysis was performed using GraphPad Prism 9 software. The means of three or more unmatched groups were compared using a one-way analysis of variance (ANOVA). When comparing four groups on two variables, a two-factor ANOVA was performed (2-way ANOVA). In the figures, statistically significant transfection effects were marked with a dollar sign ($) and statistically significant hypertrophy effects with a hash symbol (#). A $p<0.05$ was considered a statistically significant result and was marked with an asterisk (*).

6. Results

6.1 Inducing SIRT4 overexpression in H9c2 cells

To induce SIRT4 overexpression, H9c2 cardiomyoblasts were transfected with the human SIRT4 overexpression plasmid, RC212226 (**Figure 6**).

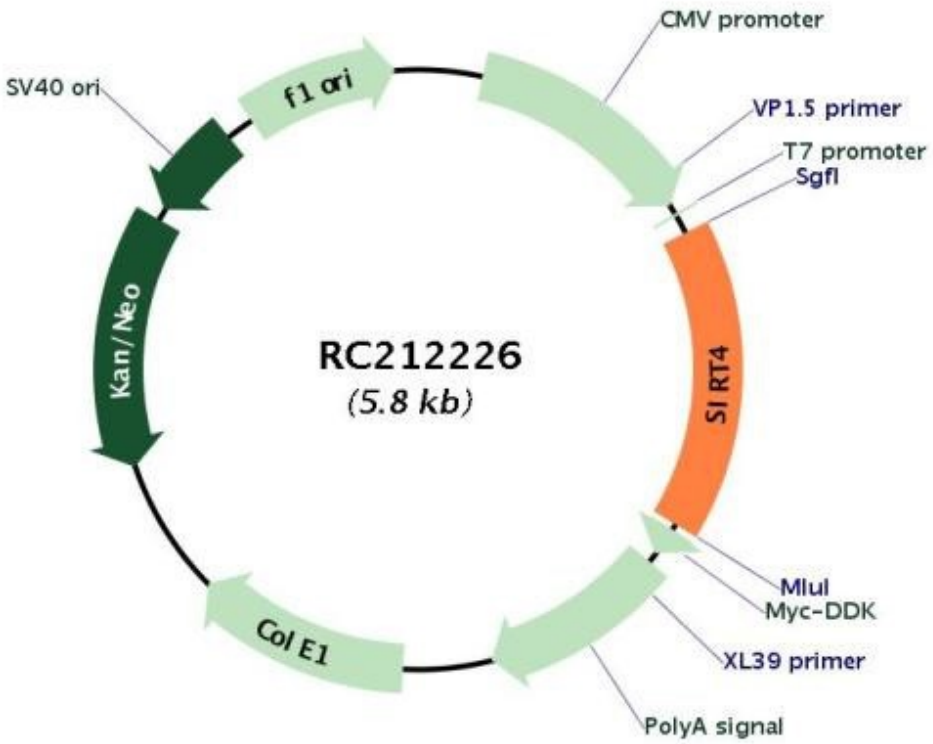

Figure 6: *Schematic of the human SIRT4 plasmid RC212226.*

The vector was multiplied using DH5-α-competent cells selected for kanamycin resistance. We validated successful transformation via SMAl digestion, resulting in distinct DNA fragments of 546 bp and 5277 bp (**Figure 7**).

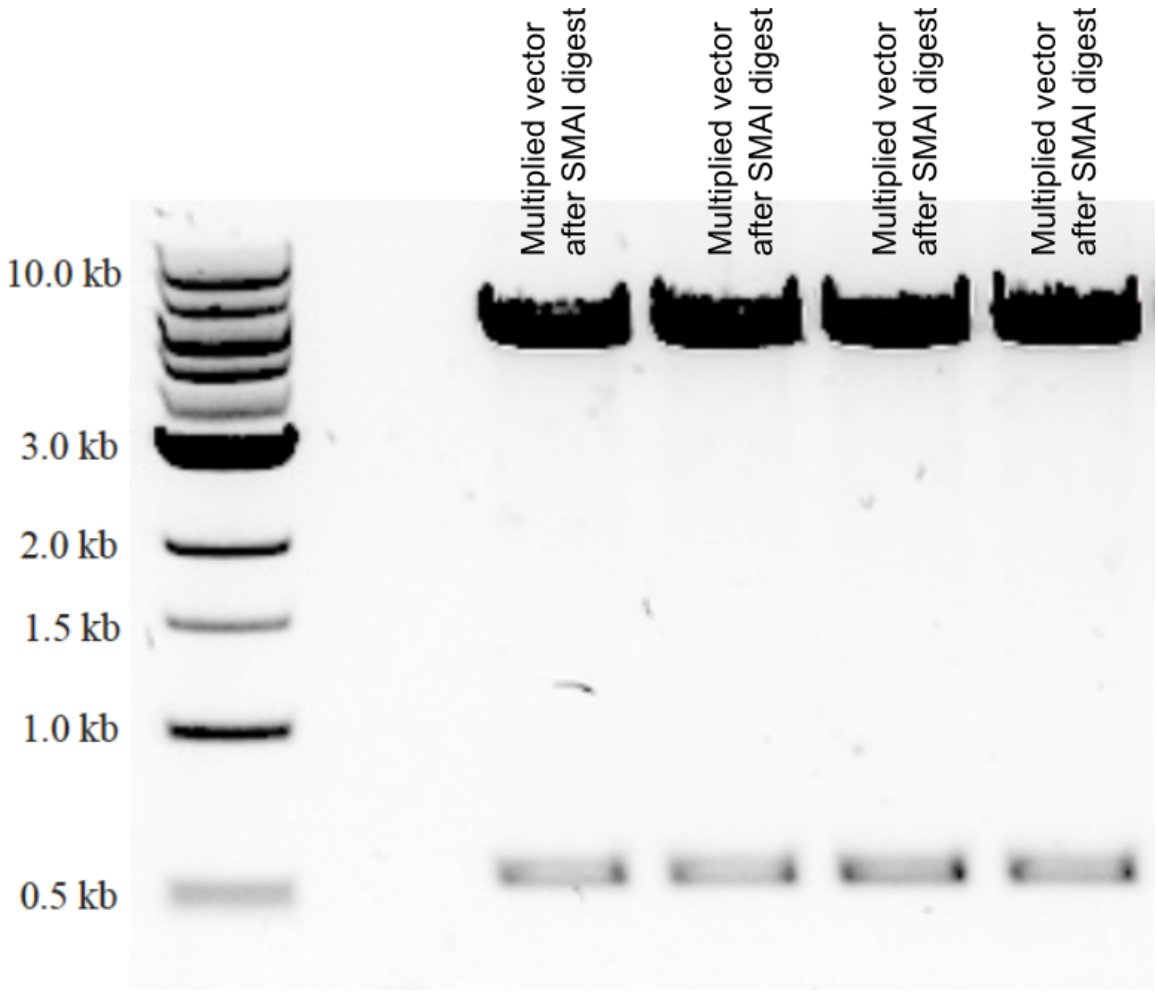

Figure 7: Representative image of PCR products after restriction enzyme digest.

Separation of PCR products on agarose gel according to molecular weight after multiplication of the vector and restriction enzyme digest using SMA1, creating two fragments with the size of 546 bp and 5277 bp.

The expression of *SIRT4* mRNA in H9c2 cells after transfection was confirmed by RT-qPCR analysis. The Control and PJ-Control had no detectable level of *hSIRT4* mRNA, whereas the Transfection group showed a clear expression of *hSIRT4* mRNA levels following transfection with human *SIRT4* (*hSIRT4*) vector (**Figure 8**).

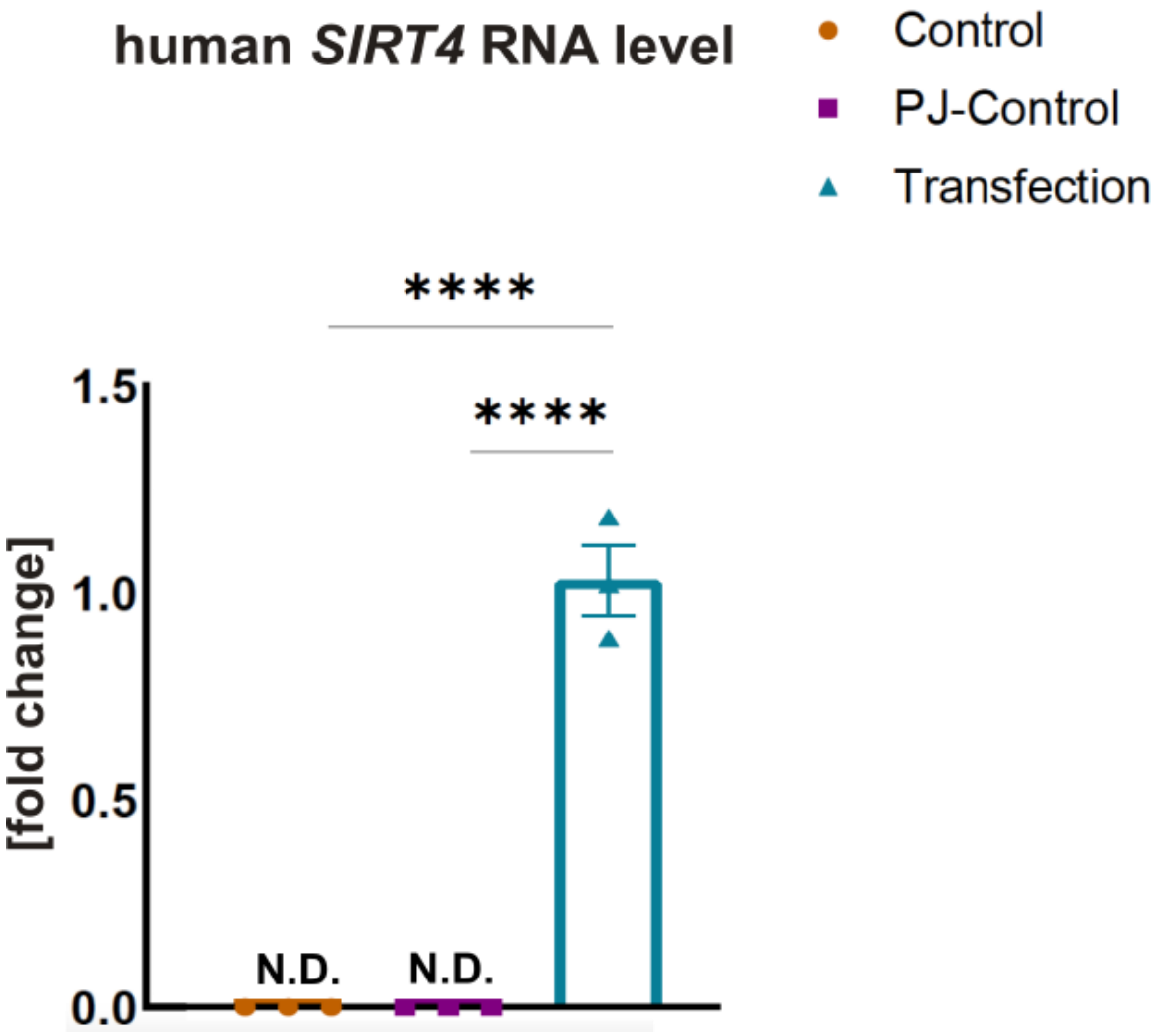

Figure 8: hSIRT4 mRNA level in H9c2 cells after hSIRT4 plasmid transfection.

*hSIRT4 mRNA was not detectable (N.D.) in Control and PJ-Control groups. mRNA levels were normalized to αTub as reference gene. mRNA levels in Transfection group were arbitrarily represented as 1. n=3 in all groups. *p<0.05 versus Control or PJ-Control group.*

Additionally, the measurement of rat *Sirt4* (*rSirt4*) mRNA revealed no discernable difference between the control and PJ-Control groups (**Figure 9**); however, there was a

borderline significant 0.64-fold reduction of *rSirt4* mRNA expression in the Transfection group compared to Control and PJ-Control groups (p=0.0517) (**Figure 9**).

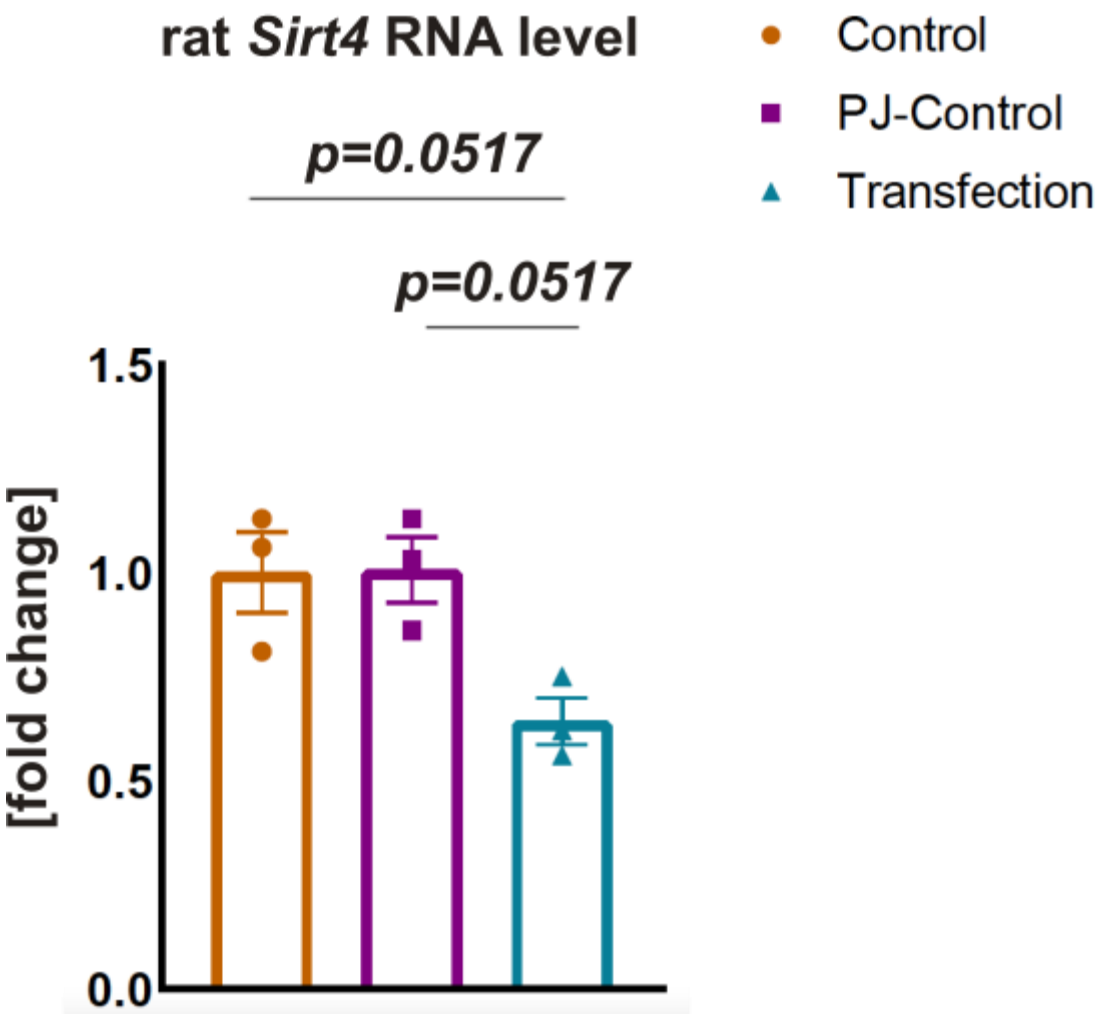

Figure 9: rSirt4 mRNA level in H9c2 cells after hSIRT4 transfection.

*mRNA levels were normalized to αTub as reference gene. mRNA levels in Control group were arbitrarily represented as 1. n=3 in all groups. *p<0.05 versus Control or PJ-Control group.*

6.2 Hypertrophic stimulation of H9c2 cells

To induce cardiomyocyte hypertrophy, H9c2 cardiomyoblasts were treated with ANG II at three different concentrations (5 µM, 10 µM, and 20 µM) followed by mRNA quantification of the hypertrophy marker, *Bnp*. Treatment with ANG II revealed no significant increase in *Bnp* expression in H9c2 cardiomyoblasts compared to 0 µM ISO (**Figure 10**).

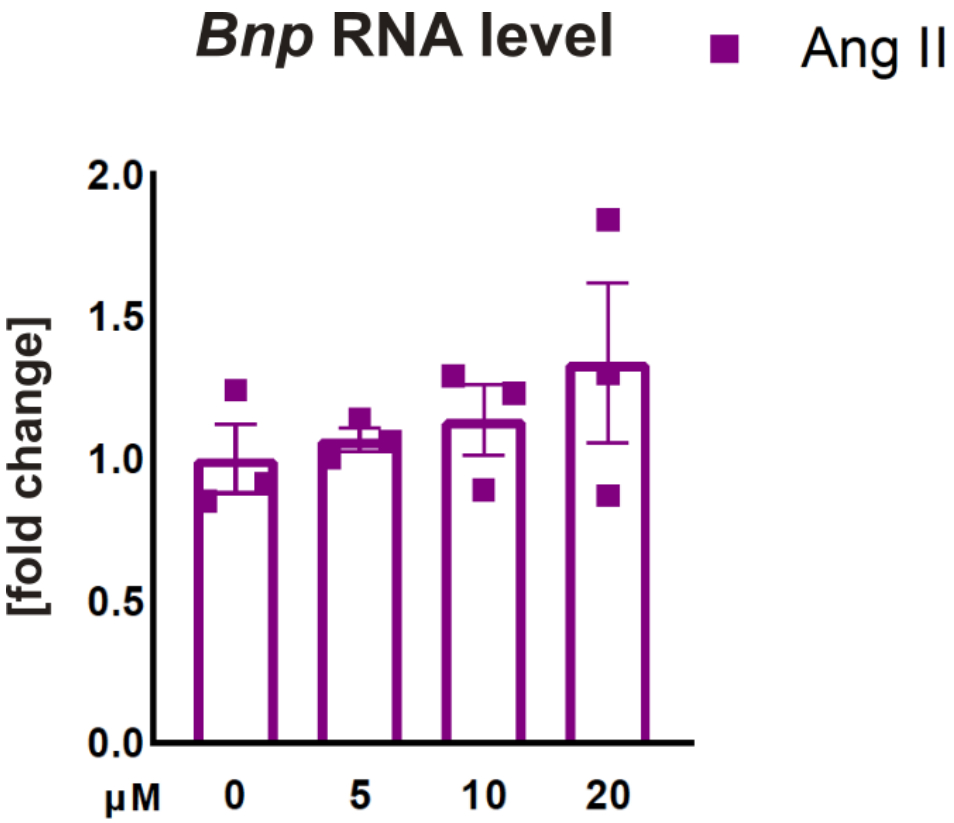

Figure 10: Bnp mRNA level in H9c2 cells treated with ANG II.

*0 µM, 5 µM, 10 µM or 20 µM of ISO were used. mRNA levels were normalized to αTub as reference gene. mRNA levels in Control group were arbitrarily represented as 1. n=3 in all groups. *p<0.05 versus Control or PJ-Control group.*

To corroborate these findings, a subsequent trial was conducted, employing WGA staining for cell size measurement. Again, we showed no significant change in cell size upon ANG II (5-20 µM) stimulation as compared to 0 µM (**Figure 11**). To test alternative hypertrophic agents, H9c2 cardiomyoblasts were treated with ISO at three different concentrations (10 µM, 30 µM, and 50 µM). A significant increase in cell size was evident in cells treated

with 30 µM ISO when compared to 0 µM ISO (**Figure 11**). Representative images of the staining of H9c2 cells treated with 0 µM (**Figure 12A**) or 30 µM (**Figure 12B**) ISO are shown below.

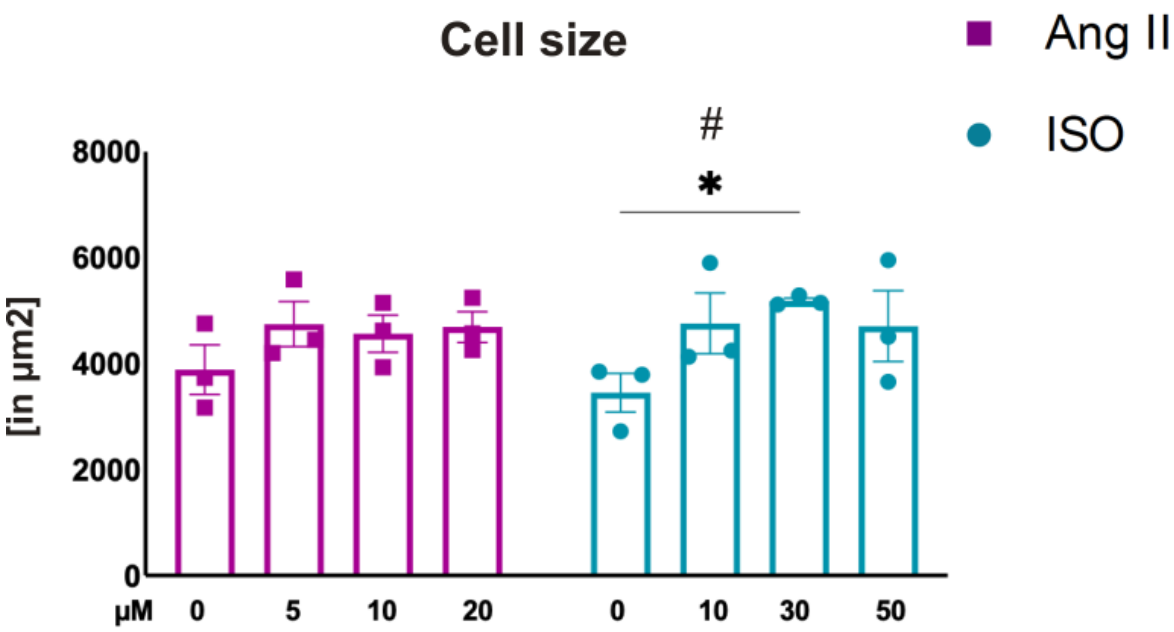

***Figure 11: Cell size of H9c2 cells treated with* ANG II or ISO.**

0 µM, 5 µM, 10 µM or 20 µM or 0 µM, 10 µM, 30 µM or 50 µM of ANG II *and* ISO *were used respectively. 50 cells were measured per sample.*

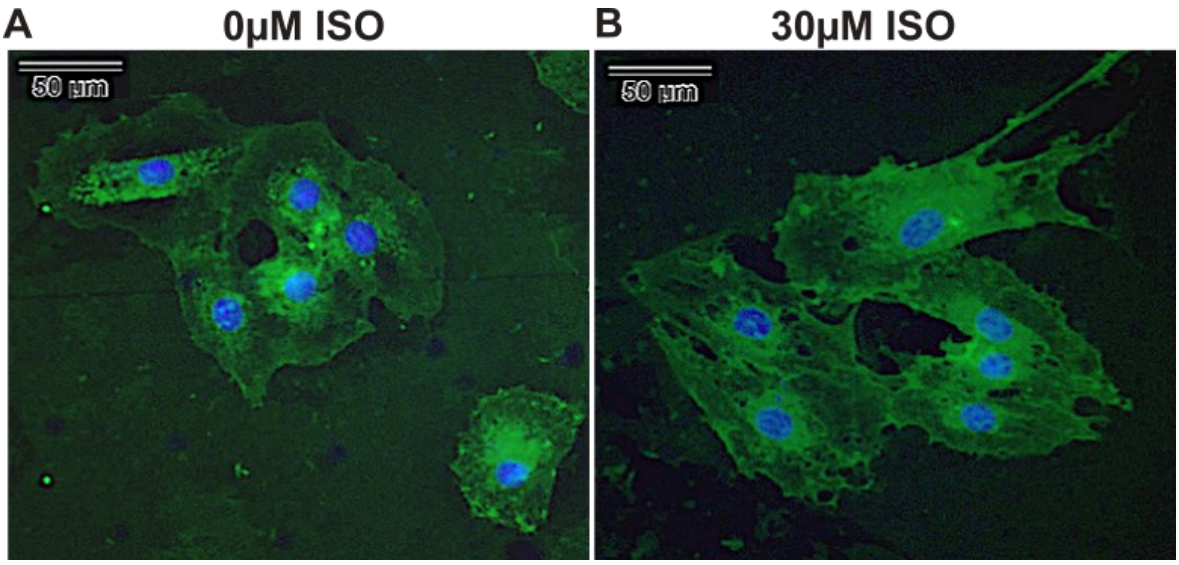

Figure 12: Representative image of H9c2 cells stained with WGA and DAPI upon treatment with 0 µM or 30 µM of ISO.

To corroborate these findings, *Bnp* mRNA levels were assessed at 10µM and 30µM ISO. These results demonstrated a significant elevation in *Bnp* mRNA levels with 30 µM ISO compared to 0 µM ISO (**Figure 13**). Given the inability of ANG II to induce hypertrophy in these trials, we exclusively employed 30 µM ISO for subsequent experiments.

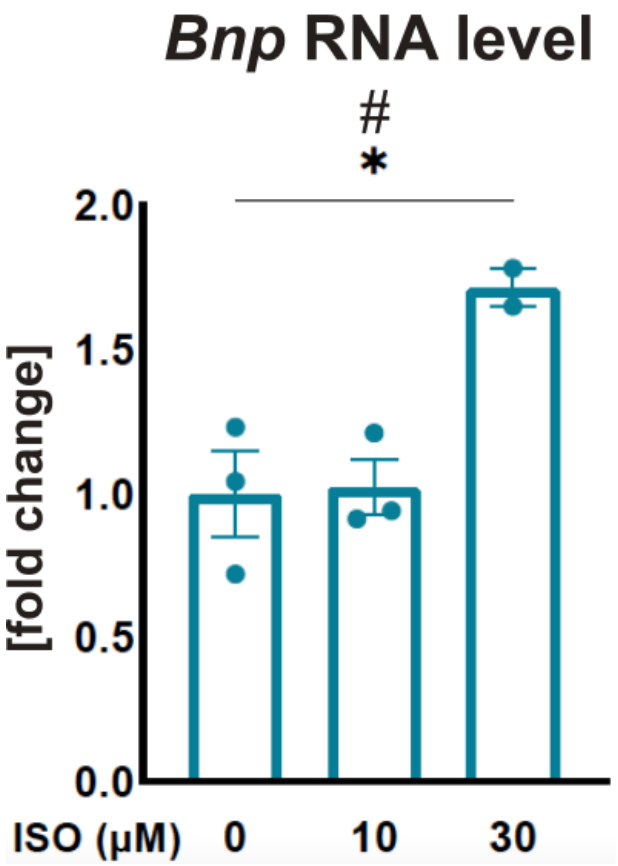

***Figure 13: Bnp mRNA levels in H9c2 cell treated with 0 µM, 10 µM or 30 µM of* ISO.**

*The qPCR results are normalized to the reference gene αTub. mRNA levels in control group were arbitrarily represented as 1; n=3 in all groups. * p<0.05 versus control groups.*

6.3 Expression of NOX4 in SIRT4 amplified hypertrophy.

To assess the role of NOX4 in SIRT4-induced worsening of hypertrophy, H9c2 cardiomyoblast were treated without or with ISO (30 µM) and/or transfected with PJ reagent (PJ-Control) or *hSIRT4* overexpressing vector. Firstly, there was a significant increase in *hSIRT4* mRNA expression (**Figure 14**) without any change in *rSirt4* mRNA expression (**Figure 15**) in Transfection group, indicating an effective overexpression of *hSIRT4*.

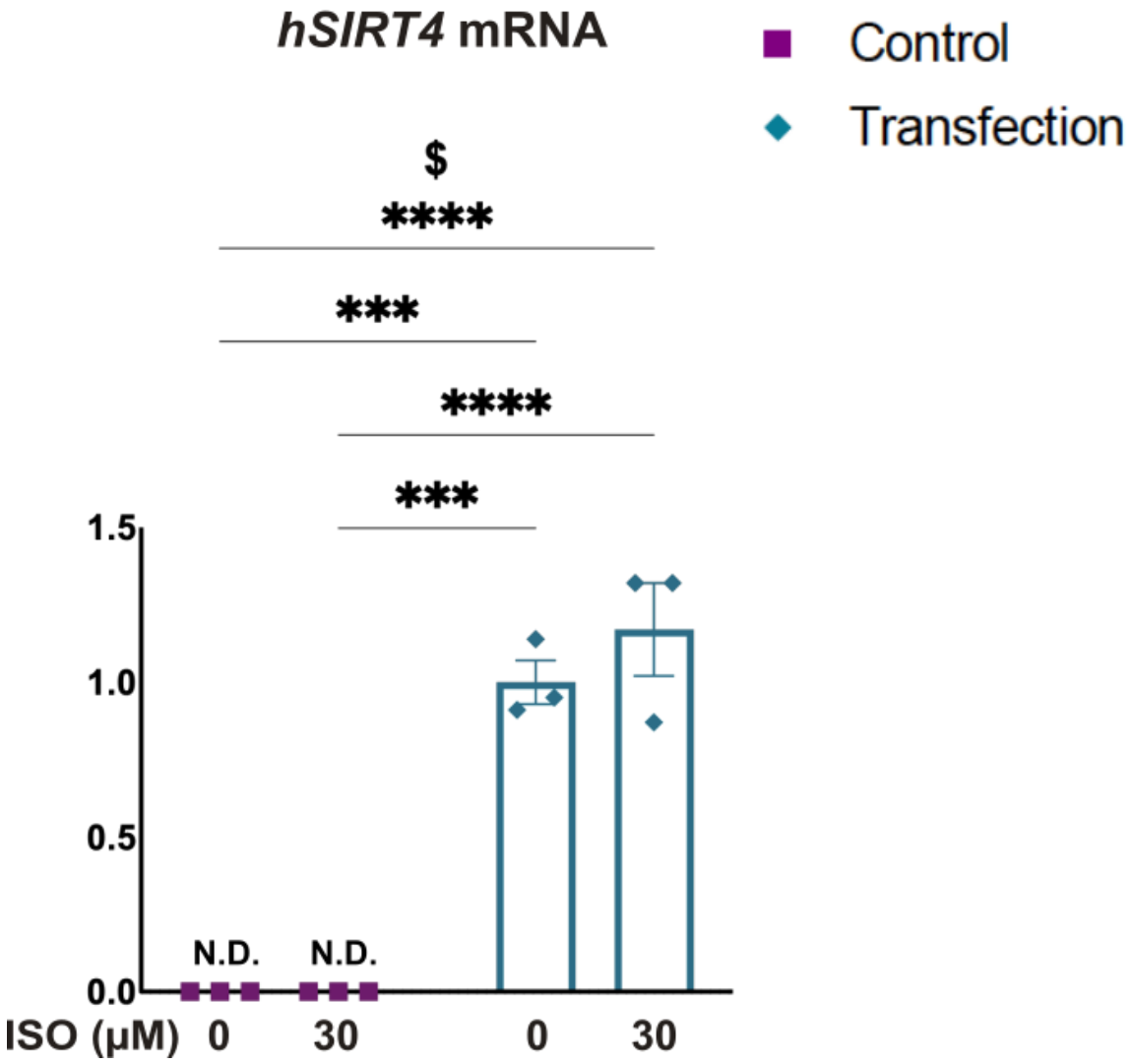

Figure 14: hSIRT4 mRNA level in H9c2 cells following hSIRT4 Transfection and/or ISO-induced hypertrophy.

*The qPCR results are normalized to the reference gene αTub. mRNA in control group were arbitrarily represented as 1; n=3 in all groups. *p<0.05 versus control groups. $ indicates significant transformation effects.*

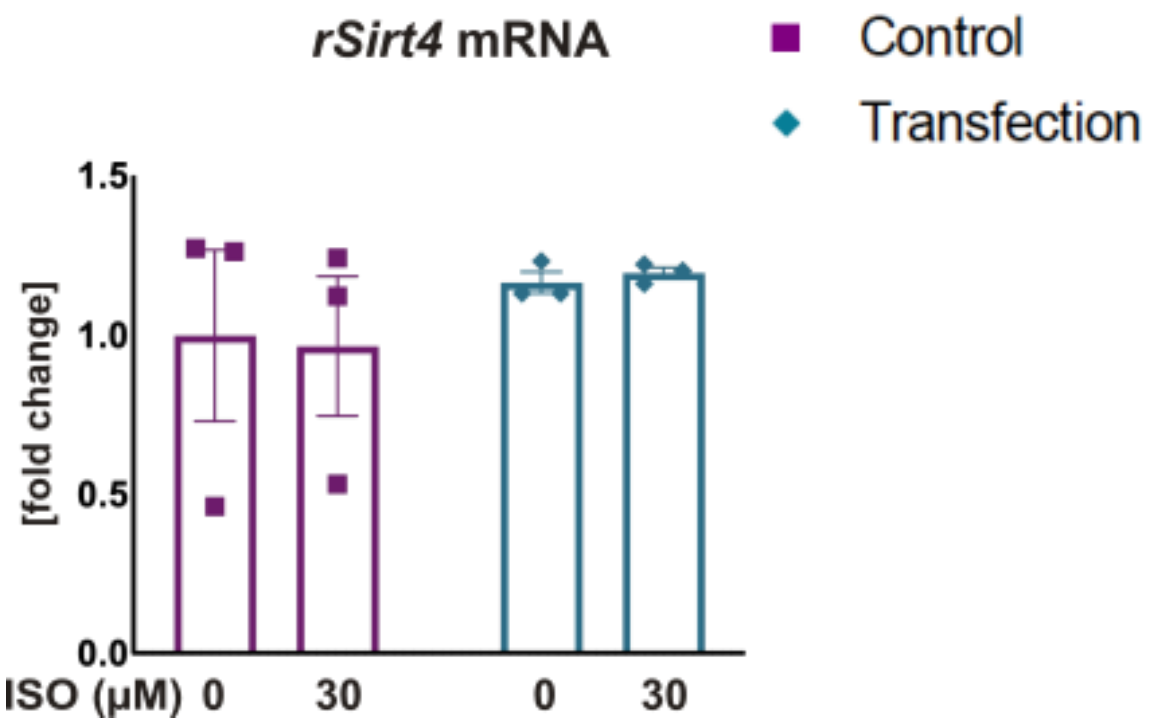

Figure 15: rSirt4 mRNA level in H9c2 cells following hSIRT4 Transfection and/or ISO-induced hypertrophy.

*The qPCR results are normalized to the reference gene αTub. mRNA in control group were arbitrarily represented as 1; n=3 in all groups. *p<0.05 versus control groups. $ indicates significant transformation effects.*

Moreover, this yielded a 5.4-fold increase in SIRT4 protein expression (**Figure 16**). No significant alterations in *hSIRT4* or *rSirt4* mRNA (**Figure 14-15**) or SIRT4 protein (**Figure 16**) levels were observed upon stimulation with ISO, suggesting that hypertrophic stimuli had no effect on cardiomyocyte SIRT4 expression.

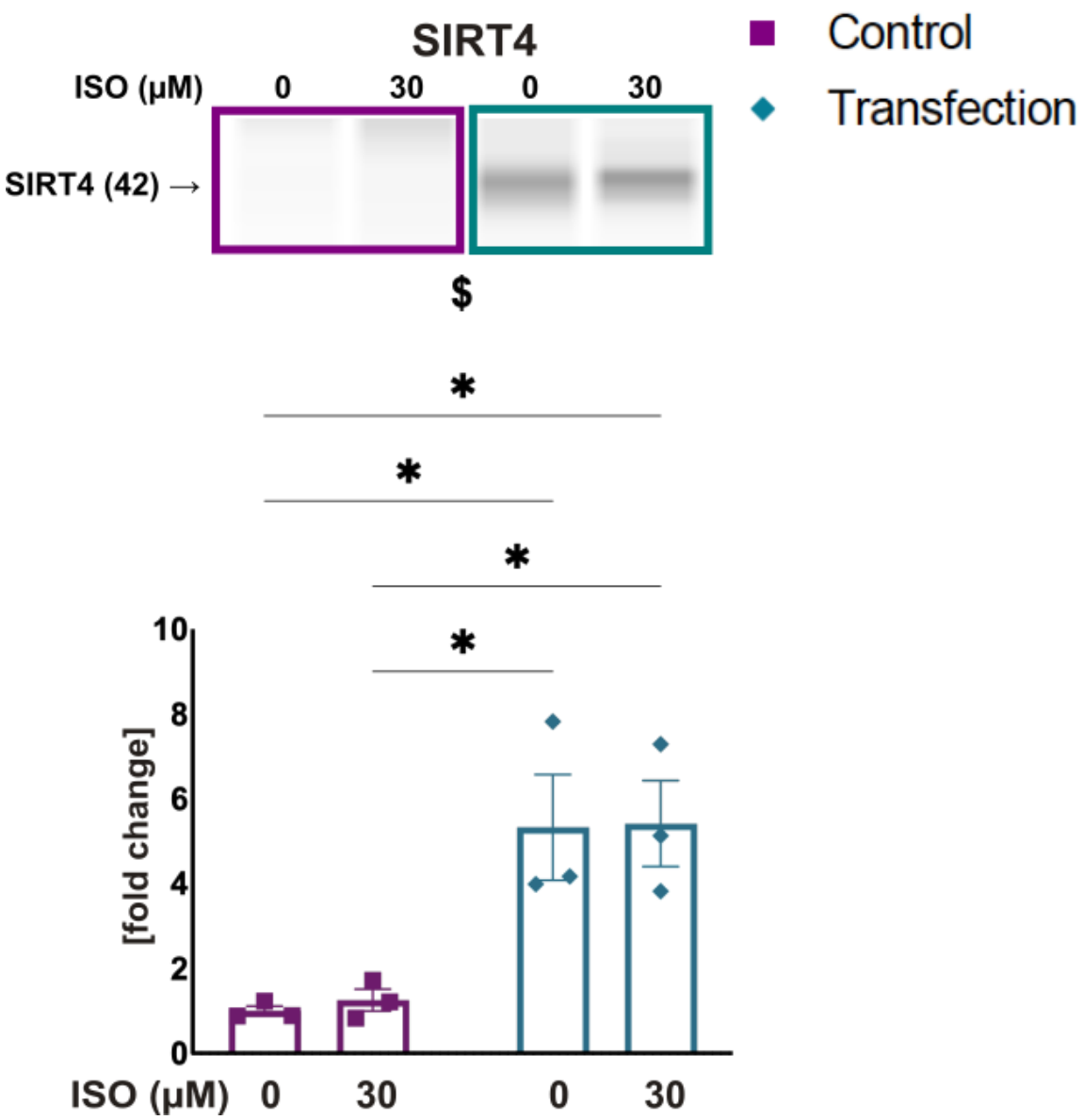

Figure 16: SIRT4 protein level and representative image in H9c2 cells following hSIRT4 Transfection and/or ISO-induced hypertrophy.

*Protein levels in control group were arbitrarily represented as 1; n=3 in all groups. *p<0.05 versus control groups. $ indicates significant transformation effects.*

In order to determine the effect of SIRT4 on hypertrophy, we measured the mRNA level of *Bnp* in H9c2 cardiomyoblast following *hSIRT4* overexpression and ISO-induced hypertrophy.

Transfection induced a significant 4-fold increase in *Bnp* mRNA compared to the PJ-Control, which was slightly, but not significantly, further increased with ISO (**Figure 17**, *p-value 0.6413*).

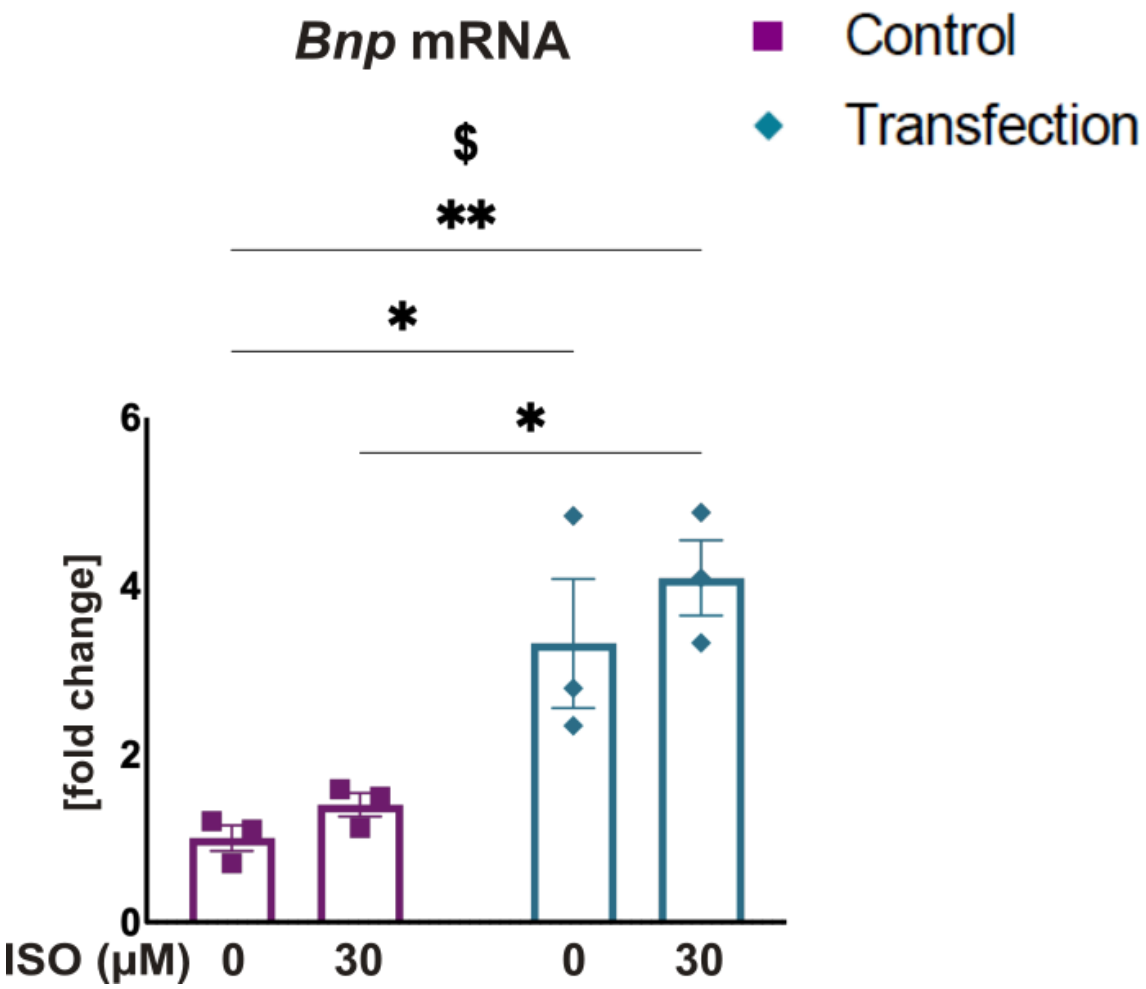

Figure 17: Bnp mRNA level in H9c2 cells following hSIRT4 Transfection and/or ISO-induced hypertrophy.

*The qPCR results are normalized to the reference gene αTub. mRNA in control group were arbitrarily represented as 1; n=3 in all groups. *p<0.05 versus control groups. $ indicates significant transformation effects.*

Whereas *Nox4* mRNA levels were not significantly changed following *hSIRT4* overexpression or ISO treatment (**Figure 18**), NOX4 protein levels were decreased following *hSIRT4* transfection (**Figure 19**).

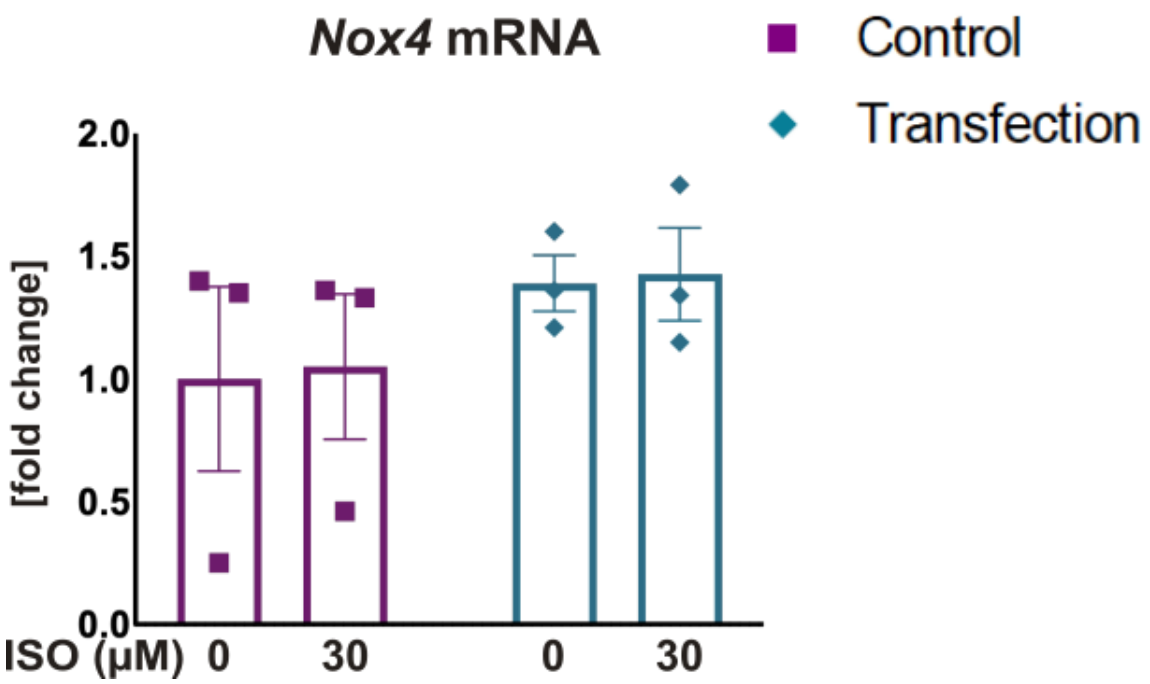

Figure 18: Nox4 mRNA level in H9c2 cells following hSIRT4 Transfection and/or ISO-induced hypertrophy.

*The qPCR results are normalized to the reference gene αTub. mRNA in control group were arbitrarily represented as 1; n=3 in all groups. *p<0.05 versus control groups. $ indicates significant transformation effects.*

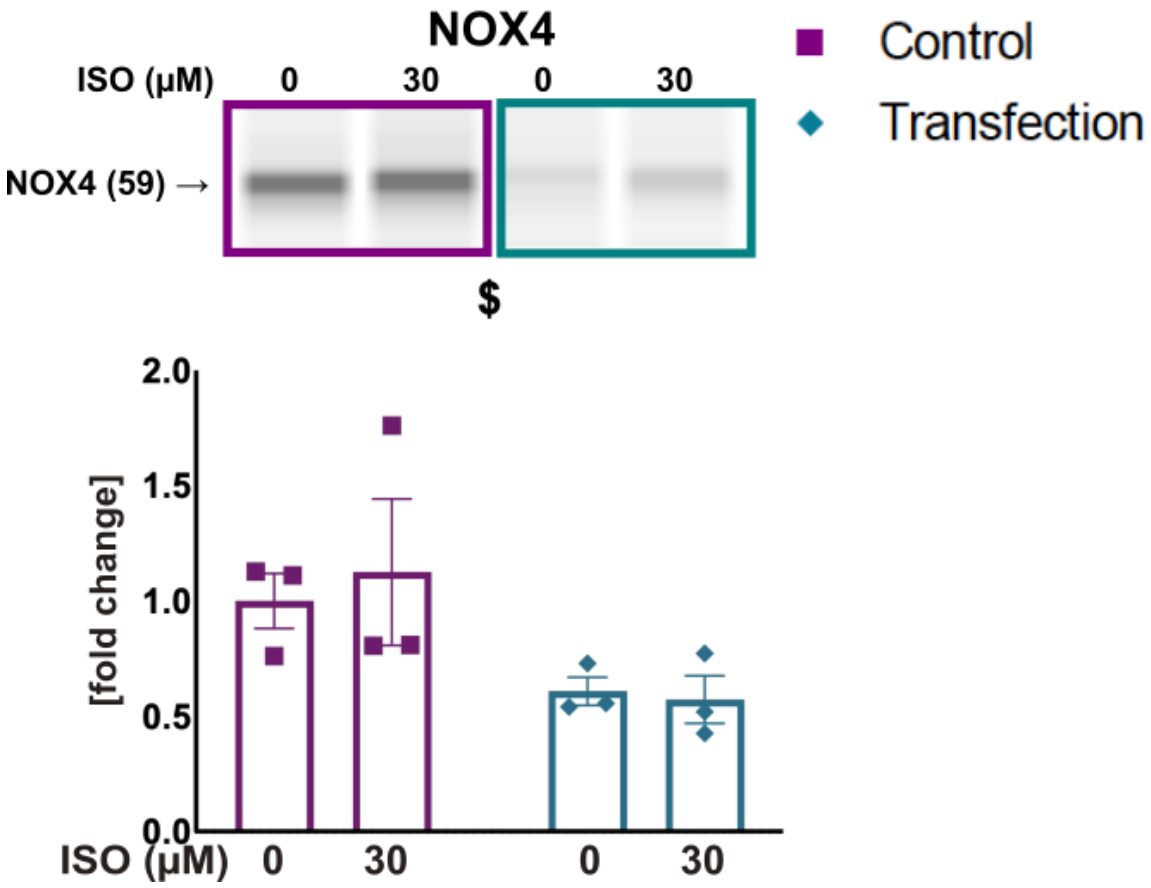

Figure 19: NOX4 protein level and representative image in H9c2 cells following hSIRT4 Transfection and/or ISO-induced hypertrophy.

*Protein levels in control group were arbitrarily represented as 1; n=3 in all groups. *p<0.05 versus control groups. $ indicates significant transformation effects.*

7. Discussion

7.1 H9c2 cells were successfully transfected to overexpress SIRT4.

In the current study, we demonstrate a successful overexpression of *hSIRT4* in H9c2 cardiomyoblasts. Whereas *hSIRT4* mRNA was not detectable before transfection, hSIRT4 mRNA was clearly expressed following transfection. Additionally, this increase in *hSIRT4* mRNA translated into protein expression of SIRT4. In contrast, expression of endogenous *rSirt4* mRNA showed a trend towards a decrease. This could potentially be attributed to a negative feedback mechanism triggered by the overexpression of *hSIRT4*.

7.2 Induction of hypertrophy in H9c2 cells.

We were not able to demonstrate a hypertrophic effect of ANG II in H9c2 cardiomyoblasts, neither by detecting the *Bnp* mRNA levels nor by measuring cardiomyocyte cell size, in contrast to what was previously reported (Pan et al., 2013, Qi et al., 2020, Zheng et al., 2021, Ba et al., 2019, Luo et al., 2017, Watkins et al., 2011, Guan et al., 2017, Alammari et al., 2020). Various studies have shown that doses ranging from 0.2 to 10 µM ANG II increase hypertrophic markers in H9c2 cells, including an increase in cell size (Watkins et al., 2011, Alammari et al., 2020, Teng et al., 2020, Guan et al., 2017, Ma et al., 2019, Wu et al., 2020). Alammari et al. showed that when H9c2 cells are treated with 10 µM ANG II for 24 hours, it leads to a significant increase of the hypertrophic markers *β/α Mhc* and *Bnp,* and to an increase of cell surface by 55%, 60% and 68%, respectively, compared to the control group (Alammari et al., 2020). Possible theories as to why ANG II did not induce hypertrophy in H9c2 cells in our study are that the concentrations of ANG II (i.e. 5 µM, 10 µM and 20 µM) were too high, resulting in reduced cell viability, although future studies would be necessary to confirm this. However, microscopically no differences were visible in the cells compared to the control group in terms of vitality or cell distribution.

In contrast to ANG II, we were able to demonstrate hypertrophic effect of 30 µM ISO in the current study. Firstly, 30 µM ISO led to a significant increase in cardiomyocyte cell size, as determined by WGA stain. Furthermore, we corroborated these results with a significant

elevation in *Bnp* mRNA induced by 30 µM ISO, strengthening our conclusion that ISO treatment effectively induced hypertrophic signaling and pathological hypertrophy in H9c2 cardiomyoblasts. This is consistent with other reports of H9c2 cardiomyoblasts treated with 30 or 100 µM of ISO for 24 hours, which induced an increase in cell diameter (Lingyan et al., 2022). Other examples include Lu et al. and Chowdhury et al., who induced hypertrophic changes like increased cell size and hypertrophy markers (*Anp*, *Bnp* or *ß-Mhc*) using 30µM of ISO for 36h or 25µM of ISO for 48h respectively (Lu et al., 2023a, Chowdhury et al., 2017). The differential effect of two known pro-hypertrophic agents on cell size and *Bnp* levels remains unclear and requires further studies.

7.3 SIRT4 overexpression induces hypertrophy.

In our study, we showed that SIRT4 overexpression in H9c2 cells induced hypertrophy, evident by an upregulation of *Bnp* mRNA, which is in line with previous findings (Luo et al., 2017). SIRT4 was shown to induce hypertrophy in rat neonatal cardiomyocytes, where *Sirt4* overexpression enhanced *Anp* expression when treated with ANG II, whereas *Sirt4* knockdown attenuated *Anp* expression (Luo et al., 2017). Luo et al. were also able to reproduce this result in *Sirt4* overexpressing mice, showing an increased ANG II induced *Anp* expression compared to WT mice, as well as aggravation of hypertrophy and accelerated development of cardiac dysfunction (Luo et al., 2017). Conversely, in *Sirt4* knockdown mice the *Anp* mRNA level is reduced, and they had preserved cardiac function compared to control groups with the same ANG II stimulation (Luo et al., 2017). Luo et al. therefore hypothesized, that *Sirt4* overexpressing mice are hypersensitive to Ang II-induced cardiac hypertrophy (Luo et al., 2017). In a more recent *in vitro* study, Ji et al. showed, that in ANG II-stimulated isolated mice cardiomyocytes the expression of BNP and ANP is again promoted by overexpression of SIRT4 (Ji et al., 2022), further implicating SIRT4s exacerbating role in the development of cardiac hypertrophy, in line with our findings.

In addition to the heart, SIRT4 is also highly expressed in the kidney, brain, and liver (Haigis et al., 2006). However, the effect of SIRT4 on cell size or hypertrophy in other tissues besides the heart is still very limited. Several studies have been published on the influence of SIRT4 on tumor size in various types of cancer, showing that SIRT4 tends to have a tumor-suppressive effect (Bradbury et al., 2005, Jeong et al., 2014, Miyo et al., 2015, Huang et al., 2015, Fu et al., 2017, Min et al., 2018). In line with this, it was shown that expression of

SIRT4 was negatively correlated with tumor size in gastric cancer (Sun et al., 2018). However, this is rather attributed to the antiproliferative effect of SIRT4 through the suppressive effect on glucose and glutamine metabolism, not necessarily to a change in individual cell size, which was not measured (Huang and Zhu, 2018).

However, compared to other sirtuins, SIRT4 appears to be the only sirtuin that has pro-hypertrophic effects on the heart. In fact, SIRT1, SIRT3 and SIRT6 have been shown to be anti-hypertrophic (Oka et al., 2011, Alcendor et al., 2007, Sundaresan et al., 2009, Sundaresan et al., 2012). SIRT3, for example, seems to have protective effects against cardiac hypertrophy. In *Sirt3* knockout mice that are treated with ANG II the myocyte cross sectional area is significantly increased, as well as natriuretic peptide precursor type A (*Anf*) and myosin, heavy chain 7, cardiac muscle, β (*Myh7*), both markers of hypertrophy (Sundaresan et al., 2009). Sundaresan et al. were also able to show a similar result in *Sirt6* knockout mice, where they detected an increase in *Myh7* levels (Sundaresan et al., 2012). They therefore conclude that SIRT6 deficiency is associated with cardiac hypertrophy and degenerative changes in the heart (Sundaresan et al., 2012). *Sirt1* overexpression attenuates cardiac hypertrophy in TAC treated mice, as characterized by heart to body weight ratios (Oka et al., 2011). Interestingly, different levels of *Sirt1* overexpression seems to have varying effects on hypertrophy. Alcendor et al. examined and compared four different levels of *Sirt1* in mice hearts, non-transgenic, 2.5-fold, 7.5-fold, and 12.5-fold (Alcendor et al., 2007). Low (2.5-fold) to moderate (7.5-fold) levels of overexpression attenuated age-related cardiac hypertrophy, whereas a high level (12.5-fold) increased it (Alcendor et al., 2007). This finding might also have some implications on our results. It is possible that the 5.4-fold increase in SIRT4 protein expression used here is so severe that it negates the actual effect of SIRT4. To rule this out, follow-up experiments could be carried out using the work of Alcendor et al. as a model, testing different expression levels of *Sirt4* overexpression.

Additionally, the SIRT4-antibody used here is active against both human and rat SIRT4. Therefore, it is not possible to distinguish whether the increased protein we observed is of human or rat origin. This increases the difficulty to assess whether the overexpressed SIRT4 really exhibits its physiological and pathophysiological effects. For this purpose, rat- or human-specific antibodies would have to be used in future experiments.

7.4 ISO treatment has no effect on NOX4 expression.

We examined the effects of the hypertrophy inducing agent ISO on NOX4 in H9c2 cells, and we were not able to show a significant difference in NOX4 expression when treated with 30 μM of ISO compared to unstimulated cells. This contrasts previous findings. Zhou et al. investigated effects of ISO on NOX4 expression in H9c2 cells (Zhou et al., 2023). In contrast to us, they found a 1.2-fold increase in NOX4 expression when treated with ISO compared to no hypertrophic stimulation (Zhou et al., 2023). In ISO treated WT mice ISO induced a marked 9.1-fold increase in NOX4 expression as evidenced by immunofluorescence staining (Vendrov et al., 2023). ISO treatment also heightened levels of mitochondrial hydrogen peroxide, indicating increased mitochondrial ROS production, but not in NOX4 knockout mice (Vendrov et al., 2023). Similarly, in primary neonatal rat cardiomyocytes, NOX4 was found to be increased after treatment with ISO (Ni et al., 2022b). At the same time, ISO treatment was shown to decrease NOX4 expression in Human umbilical vein endothelial cells, while mitochondrial ROS were increased (Ni et al., 2022a).

In the literature, the effect of ANG II on NOX4 has been examined more extensively compared to ISO and shows contradictory data. When mice were treated with ANG II- (200 ng/kg/min) or phenylephrine (75 mg/kg/day)-infusions Ago et al. were able to show that NOX4 is upregulated 1.5-, 1.9- and 3.4-fold, respectively, in cardiac myocytes (Ago et al., 2010). Higashi et al. treated mice for 4 weeks with ANG II infusions, and then examined the expression profile of thoracic aortas. There they showed that NOX4 was significantly increased (Higashi et al., 2003). The rat aortic smooth muscle cell line A7r5 was treated with 1 μM of ANG II for 4 hours by Wingler et al., which induced a 4-fold increase in *Nox4* mRNA (Wingler et al., 2001). But they observed that the increase in *Nox4* expression was transient, with a maximal induction after 4 hours. After 24 hours, expression returned to control levels. They hypothesized that this may be due to degradation of ANG II in the cell culture media (Wingler et al., 2001). Yamagishi et al. showed an increased expression of *Nox4* in human umbilical vein endothelial cells when treated with 100 μM of ANG II for 24 hours (Yamagishi et al., 2005). However, Lassegue et al. treated vascular smooth muscle cells with 100 nM of ANG II and observed a 40% decrease in *Nox4* expression after 2 h, which remained stable at this level for 12 hours (Lassegue et al., 2001).

The discrepancy between our results and the results in the literature regarding the effect of ISO and ANG II on NOX4 could be due to different doses and incubation times. For example, Zhou et al. used 10µM ISO for 12 hours to stimulate H9c2 cells, and the other groups mentioned here also used different protocols, doses and incubation times compared to us (Zhou et al., 2023, Vendrov et al., 2023, Wingler et al., 2001, Yamagishi et al., 2005, Ni et al., 2022a, Ni et al., 2022b, Ago et al., 2010, Higashi et al., 2003, Lassegue et al., 2001). The degradation of ANG II in cell culture medium described by Wingler et al. could play a role here, as they showed that increased *Nox4* expression was transient with a maximum after 4 hours, returning to control levels after 24 hours (Wingler et al., 2001). This could be investigated in later experiments by measuring *Nox4* expression after different incubation times (e.g. after 4 hours, 6 hours, 8 hours and 24 hours following the example of Wingler et al.).

In conclusion, our results suggest that the regulation of NOX4 expression by hypertrophy-inducing agents such as ISO and ANG II is complex and dependent on multiple variables. Further studies are needed to understand the mechanisms behind these differences. Different cell types, dose-response relationships and treatment durations should be considered.

7.5 SIRT4 overexpression attenuates NOX4.

In an as of yet unpublished study from our group, we have investigated the effect of SIRT4 overexpression and deficiency in chronic pressure-overload in mice, induced with TAC treatment. Oxidative stress, cardiac energetics and global myocardial gene expressions were examined to evaluate possible mechanisms by which SIRT4 influences cardiac remodeling. We found that the expression of NOX4 was increased in SIRT4 overexpressing mice, which was associated with aggravated cardiac hypertrophy. We therefore hypothesized that SIRT4 exacerbates hypertrophy by influencing NOX4. In this present study, however, we show that despite increased *Bnp* due to SIRT4 overexpression, NOX4 expression is decreased. As such, the results of our in vitro study deviated from our initial hypothesis that overexpression of SIRT4 would induce *Nox4* expression in H9c2 cells, as was observed in the heart upon SIRT4 overexpression in our *in vivo* pressure-overload model.

This also stands in contrast to previous findings. Kuroda et al. found that *Nox4* knockout mice exhibited attenuated cardiac hypertrophy when subjected to TAC for 4 weeks, suggesting that decreased *Nox4* expression counteracts hypertrophic remodeling (Kuroda et

al., 2010). A possible explanation for this could lie in a compensatory mechanism by which NOX4 is downregulated during hypertrophy. Interestingly, in other studies NOX4 appeared to be protective against hypertrophic remodeling, as downregulation of NOX4 was associated with exaggerated cardiac hypertrophy (Zhang et al., 2018, Matsushima et al., 2013), which is more in line with our findings. Zhang et al. used global, as well as endothelial- and cardiac-specific *Nox4* knockout mice and induced hypertrophy using TAC for 2 weeks. The mice developed worse pressure overload-induced cardiac remodelling and dysfunction than WT littermates (Zhang et al., 2018).
The discrepancy between our in vivo and in vitro results could be explained by the duration and intensity of the treatment. The duration and intensity of TAC treatment in vivo may not be exactly replicable in vitro. Chronic stress and the associated physiological adaptations may cause differences in gene expression that are not captured in a short-term in vitro treatment. It is also possible that cell-cell interaction with other cell types could play a role in vivo. In vivo, cardiomyocytes interact with a variety of other cell types, such as fibroblasts, endothelial cells and immune cells. These interactions are not present in a cell culture, which may lead to differences in gene expression and cell response.

Interestingly, in the current study we showed no significant difference between *Nox4* mRNA expression in SIRT4 overexpressing cells compared to the control groups, whereas SIRT4 overexpression demonstrated a reduction in NOX4 protein expression. This discrepancy between RNA and protein levels prompts a closer inspection of potential post-transcriptional regulatory mechanisms. One possible explanation could involve alterations in protein stability, degradation, or translation efficiency.

To the best of our knowledge, the relationship between SIRT4 and NOX4 is largely unexplored. However, there is a known connection between SIRT1 and NOX4. Dasgupta et al. proposed a SIRT1-NOX4 signaling pathway, which regulates pancreatic cancer cachexia (Dasgupta et al., 2020). They conclude that tumor-secreted factors decrease SIRT1 in cachectic muscles, which in turn leads to an overexpression of NOX4. NOX4 is significantly negatively correlated with skeletal muscle fiber cross-sectional area in human pancreatic cancer patients (Dasgupta et al., 2020). During pregnancy, maternal activity can improve hypertensive disease in the offspring. The underlying mechanism is based on SIRT1-mediated transcriptional repression of *Nox4* in fetal mesenteric arteries (Zhang et al., 2023). In diabetic mice, SIRT1 supplementation improves vascular dysfunction and blunts

increased arterial stiffness, potentially by decreasing NOX4 expression and suppressing oxidative stress (Yang et al., 2023). In diabetic neuropathy in rats, *Sirt1* is significantly downregulated in the sciatic nerve. Syed et al. propose that hesperidin, a flavonoid, can attenuate the NOX4 mediated inflammation and oxidative stress by upregulating SIRT1 (Syed et al., 2023). Additionally, Zhang et al. showed that cigarette smoking increases mitochondrial ROS, in part due to an imbalance in mitochondrial NOX4 caused by a decrease in SIRT1 in lung fibroblasts (Zhang et al., 2022).

In summary, the interactions between SIRT1 and NOX4 demonstrate an important regulatory role of SIRT1 on NOX4 expression and associated oxidative stress. The established relationship between the sirtuin SIRT1 and NOX4 may suggest that a SIRT4-NOX4 axis is possible and should be further investigated.

7.6 Limitations

The present study has several limitations, the following of which stand out as particularly significant. The relatively small sample size of 3 could limit the statistical power and interpretation of the results. A larger sample size would increase the robustness of the conclusions drawn from the data. Another limitation of our study is that no reference protein was used in the protein analysis with Western blot.

The use of H9c2 cells as an *in vitro* model for cardiac hypertrophy raises questions of relevance due to their proliferative capacity in contrast to non-proliferating cardiomyocytes in the living organism. The transferability of the results from H9c2 cells to conditions in the living heart as well as adult cardiomyocytes or human cell lines, may therefore be impaired (Watkins et al., 2011). To address this limitation in future research, findings could be recapitulated in freshly isolated cells.

We only measured the hypertrophy marker, BNP, following SIRT4 overexpression but did not determine actual cardiomyocyte cell size. To conclude that SIRT4 induces hypertrophy, further quantification of cell size using WGA stain would be required. The use of human *SIRT4* also raises concerns about the transferability of the observed effects to its effects in rat cells. Species-specific differences could influence the biological response. Using a rat specific *Sirt4* overexpression vector may alleviate this problem in future experiments.

Another limitation of this study is that we did not measure ROS production. Our hypothesis was primarily based on the assumption that SIRT4 leads to hypertrophy via NOX4. The

mechanism by which NOX4 activity promotes hypertrophy would appear to be that increased expression of NOX4 leads to increased ROS production. To counteract this in future experiments, ROS should be determined in the cells, e.g. using fluorescent dyes or chemiluminescence assays.

7.7 Conclusions

To evaluate the potential of SIRT4 to mediate NOX4 expression in cardiac hypertrophy, this study investigated whether SIRT4 overexpression increases NOX4 expression in response to pro-hypertrophic signaling in a cell culture model. We successfully induced overexpression of *hSIRT4* in H9c2 cells and were able to successfully demonstrate ISO-induced hypertrophy, as evident by increased cell size and *Bnp* levels. In this model, we showed that SIRT4 overexpression induced *Bnp* mRNA expression, suggesting that SIRT4 drives hypertrophy in H9c2 cells. However, NOX4 expression was not increased in response to SIRT4 overexpression. Thus, increased NOX4 expression in SIRT4 overexpressing mice may not be directly mediated by SIRT4 overexpression but rather the result of another indirect or compensatory mechanism. The precise relationship between SIRT4 and NOX4 in the development of hypertrophy and HF remains to be further explored.

8. References

AGO, T., KURODA, J., PAIN, J., FU, C., LI, H. & SADOSHIMA, J. 2010. Upregulation of Nox4 by hypertrophic stimuli promotes apoptosis and mitochondrial dysfunction in cardiac myocytes. *Circ Res,* 106**,** 1253-64.

AGUILANIU, H., GUSTAFSSON, L., RIGOULET, M. & NYSTROM, T. 2003. Asymmetric inheritance of oxidatively damaged proteins during cytokinesis. *Science,* 299**,** 1751-3.

AHUJA, N., SCHWER, B., CAROBBIO, S., WALTREGNY, D., NORTH, B. J., CASTRONOVO, V., MAECHLER, P. & VERDIN, E. 2007. Regulation of insulin secretion by SIRT4, a mitochondrial ADP-ribosyltransferase. *J Biol Chem,* 282**,** 33583-33592.

ALAMMARI, A. H., SHOIEB, S. M., MAAYAH, Z. H. & EL-KADI, A. O. S. 2020. Fluconazole Represses Cytochrome P450 1B1 and Its Associated Arachidonic Acid Metabolites in the Heart and Protects Against Angiotensin II-Induced Cardiac Hypertrophy. *J Pharm Sci,* 109**,** 2321-2335.

ALCENDOR, R. R., GAO, S., ZHAI, P., ZABLOCKI, D., HOLLE, E., YU, X., TIAN, B., WAGNER, T., VATNER, S. F. & SADOSHIMA, J. 2007. Sirt1 regulates aging and resistance to oxidative stress in the heart. *Circ Res,* 100**,** 1512-21.

ALCENDOR, R. R., KIRSHENBAUM, L. A., IMAI, S., VATNER, S. F. & SADOSHIMA, J. 2004. Silent information regulator 2alpha, a longevity factor and class III histone deacetylase, is an essential endogenous apoptosis inhibitor in cardiac myocytes. *Circ Res,* 95**,** 971-80.

AN, D., ZENG, Q., ZHANG, P., MA, Z., ZHANG, H., LIU, Z., LI, J., REN, H. & XU, D. 2021. Alpha-ketoglutarate ameliorates pressure overload-induced chronic cardiac dysfunction in mice. *Redox Biol,* 46**,** 102088.

ANDERSON, K. A., HUYNH, F. K., FISHER-WELLMAN, K., STUART, J. D., PETERSON, B. S., DOUROS, J. D., WAGNER, G. R., THOMPSON, J. W., MADSEN, A. S., GREEN, M. F., SIVLEY, R. M., ILKAYEVA, O. R., STEVENS, R. D., BACKOS, D. S., CAPRA, J. A., OLSEN, C. A., CAMPBELL, J. E., MUOIO, D. M., GRIMSRUD, P. A. & HIRSCHEY, M. D. 2017. SIRT4 Is a Lysine Deacylase that Controls Leucine Metabolism and Insulin Secretion. *Cell Metab,* 25**,** 838-855 e15.

ARDANAZ, N., YANG, X. P., CIFUENTES, M. E., HAURANI, M. J., JACKSON, K. W., LIAO, T. D., CARRETERO, O. A. & PAGANO, P. J. 2010. Lack of glutathione peroxidase 1 accelerates cardiac-specific hypertrophy and dysfunction in angiotensin II hypertension. *Hypertension,* 55**,** 116-23.

ARRIGO, M., HUBER, L. C., WINNIK, S., MIKULICIC, F., GUIDETTI, F., FRANK, M., FLAMMER, A. J. & RUSCHITZKA, F. 2019. Right

Ventricular Failure: Pathophysiology, Diagnosis and Treatment. *Card Fail Rev,* 5**,** 140-146.

BA, L., GAO, J., CHEN, Y., QI, H., DONG, C., PAN, H., ZHANG, Q., SHI, P., SONG, C., GUAN, X., CAO, Y. & SUN, H. 2019. Allicin attenuates pathological cardiac hypertrophy by inhibiting autophagy via activation of PI3K/Akt/mTOR and MAPK/ERK/mTOR signaling pathways. *Phytomedicine,* 58**,** 152765.

BARTOSCH, C., MONTEIRO-REIS, S., ALMEIDA-RIOS, D., VIEIRA, R., CASTRO, A., MOUTINHO, M., RODRIGUES, M., GRACA, I., LOPES, J. M. & JERONIMO, C. 2016. Assessing sirtuin expression in endometrial carcinoma and non-neoplastic endometrium. *Oncotarget,* 7**,** 1144-54.

BEDARD, K. & KRAUSE, K. H. 2007. The NOX family of ROS-generating NADPH oxidases: physiology and pathophysiology. *Physiol Rev,* 87**,** 245-313.

BENDALL, J. K., CAVE, A. C., HEYMES, C., GALL, N. & SHAH, A. M. 2002. Pivotal role of a gp91(phox)-containing NADPH oxidase in angiotensin II-induced cardiac hypertrophy in mice. *Circulation,* 105**,** 293-6.

BERGMANN, L., LANG, A., BROSS, C., ALTINOLUK-HAMBUCHEN, S., FEY, I., OVERBECK, N., STEFANSKI, A., WIEK, C., KEFALAS, A., VERHULSDONK, P., MIELKE, C., SOHN, D., STUHLER, K., HANENBERG, H., JANICKE, R. U., SCHELLER, J., REICHERT, A. S., AHMADIAN, M. R. & PIEKORZ, R. P. 2020. Subcellular Localization and Mitotic Interactome Analyses Identify SIRT4 as a Centrosomally Localized and Microtubule Associated Protein. *Cells,* 9.

BERNARDI, P., VASSANELLI, S., VERONESE, P., COLONNA, R., SZABO, I. & ZORATTI, M. 1992. Modulation of the mitochondrial permeability transition pore. Effect of protons and divalent cations. *J Biol Chem,* 267**,** 2934-9.

BESKOW, L. M. 2016. Lessons from HeLa Cells: The Ethics and Policy of Biospecimens. *Annu Rev Genomics Hum Genet,* 17**,** 395-417.

BIELLA, G., FUSCO, F., NARDO, E., BERNOCCHI, O., COLOMBO, A., LICHTENTHALER, S. F., FORLONI, G. & ALBANI, D. 2016. Sirtuin 2 Inhibition Improves Cognitive Performance and Acts on Amyloid-beta Protein Precursor Processing in Two Alzheimer's Disease Mouse Models. *J Alzheimers Dis,* 53**,** 1193-207.

BLANK, M. F. & GRUMMT, I. 2017. The seven faces of SIRT7. *Transcription,* 8**,** 67-74.

BORBELY, A., VAN DER VELDEN, J., PAPP, Z., BRONZWAER, J. G., EDES, I., STIENEN, G. J. & PAULUS, W. J. 2005. Cardiomyocyte stiffness in diastolic heart failure. *Circulation,* 111**,** 774-81.

BRADBURY, C. A., KHANIM, F. L., HAYDEN, R., BUNCE, C. M., WHITE, D. A., DRAYSON, M. T., CRADDOCK, C. & TURNER, B. M. 2005. Histone deacetylases in acute myeloid leukaemia show a distinctive pattern of expression that changes selectively in response to deacetylase inhibitors. *Leukemia,* 19**,** 1751-9.

BREDE, M., WIESMANN, F., JAHNS, R., HADAMEK, K., ARNOLT, C., NEUBAUER, S., LOHSE, M. J. & HEIN, L. 2002. Feedback inhibition of catecholamine release by two different alpha2-adrenoceptor subtypes prevents progression of heart failure. *Circulation,* 106**,** 2491-6.

BROUWERS, F. P., DE BOER, R. A., VAN DER HARST, P., VOORS, A. A., GANSEVOORT, R. T., BAKKER, S. J., HILLEGE, H. L., VAN VELDHUISEN, D. J. & VAN GILST, W. H. 2013. Incidence and epidemiology of new onset heart failure with preserved vs. reduced ejection fraction in a community-based cohort: 11-year follow-up of PREVEND. *Eur Heart J,* 34**,** 1424-31.

BRYK, M., BANERJEE, M., MURPHY, M., KNUDSEN, K. E., GARFINKEL, D. J. & CURCIO, M. J. 1997. Transcriptional silencing of Ty1 elements in the RDN1 locus of yeast. *Genes Dev,* 11**,** 255-69.

BUENO, O. F., DE WINDT, L. J., TYMITZ, K. M., WITT, S. A., KIMBALL, T. R., KLEVITSKY, R., HEWETT, T. E., JONES, S. P., LEFER, D. J., PENG, C. F., KITSIS, R. N. & MOLKENTIN, J. D. 2000. The MEK1-ERK1/2 signaling pathway promotes compensated cardiac hypertrophy in transgenic mice. *EMBO J,* 19**,** 6341-50.

BUGGER, H., WITT, C. N. & BODE, C. 2016. Mitochondrial sirtuins in the heart. *Heart Fail Rev,* 21**,** 519-28.

BURCHFIELD, J. S., XIE, M. & HILL, J. A. 2013. Pathological ventricular remodeling: mechanisms: part 1 of 2. *Circulation,* 128**,** 388-400.

CARAFA, V., ROTILI, D., FORGIONE, M., CUOMO, F., SERRETIELLO, E., HAILU, G. S., JARHO, E., LAHTELA-KAKKONEN, M., MAI, A. & ALTUCCI, L. 2016. Sirtuin functions and modulation: from chemistry to the clinic. *Clin Epigenetics,* 8**,** 61.

CHEN, Y., LUO, H. Q., SUN, L. L., XU, M. T., YU, J., LIU, L. L., ZHANG, J. Y., WANG, Y. Q., WANG, H. X., BAO, X. F. & MENG, G. L. 2018. Dihydromyricetin Attenuates Myocardial Hypertrophy Induced by Transverse Aortic Constriction via Oxidative Stress Inhibition and SIRT3 Pathway Enhancement. *Int J Mol Sci,* 19.

CHENG, H. L., MOSTOSLAVSKY, R., SAITO, S., MANIS, J. P., GU, Y., PATEL, P., BRONSON, R., APPELLA, E., ALT, F. W. & CHUA, K. F. 2003. Developmental defects and p53 hyperacetylation in Sir2 homolog (SIRT1)-deficient mice. *Proc Natl Acad Sci U S A,* 100**,** 10794-9.

CHENG, Y., SHEN, A., WU, X., SHEN, Z., CHEN, X., LI, J., LIU, L., LIN, X., WU, M., CHEN, Y., CHU, J. & PENG, J. 2021. Qingda granule

attenuates angiotensin II-induced cardiac hypertrophy and apoptosis and modulates the PI3K/AKT pathway. *Biomed Pharmacother,* 133**,** 111022.
CHOWDHURY, D., KUMAR, D., BHADRA, U., DEVI, T. A. & BHADRA, M. P. 2017. Prohibitin confers cytoprotection against ISO-induced hypertrophy in H9c2 cells via attenuation of oxidative stress and modulation of Akt/Gsk-3beta signaling. *Mol Cell Biochem,* 425**,** 155-168.
CLELAND, J. G. F., BUNTING, K. V., FLATHER, M. D., ALTMAN, D. G., HOLMES, J., COATS, A. J. S., MANZANO, L., MCMURRAY, J. J. V., RUSCHITZKA, F., VAN VELDHUISEN, D. J., VON LUEDER, T. G., BOHM, M., ANDERSSON, B., KJEKSHUS, J., PACKER, M., RIGBY, A. S., ROSANO, G., WEDEL, H., HJALMARSON, A., WIKSTRAND, J., KOTECHA, D. & BETA-BLOCKERS IN HEART FAILURE COLLABORATIVE, G. 2018. Beta-blockers for heart failure with reduced, mid-range, and preserved ejection fraction: an individual patient-level analysis of double-blind randomized trials. *Eur Heart J,* 39**,** 26-35.
COLLABORATORS, G. B. D. R. F. 2020. Global burden of 87 risk factors in 204 countries and territories, 1990-2019: a systematic analysis for the Global Burden of Disease Study 2019. *Lancet,* 396**,** 1223-1249.
COLOMBO, S. L., PALACIOS-CALLENDER, M., FRAKICH, N., CARCAMO, S., KOVACS, I., TUDZAROVA, S. & MONCADA, S. 2011. Molecular basis for the differential use of glucose and glutamine in cell proliferation as revealed by synchronized HeLa cells. *Proc Natl Acad Sci U S A,* 108**,** 21069-74.
CONRAD, N., JUDGE, A., CANOY, D., TRAN, J., PINHO-GOMES, A. C., MILLETT, E. R. C., SALIMI-KHORSHIDI, G., CLELAND, J. G., MCMURRAY, J. J. V. & RAHIMI, K. 2019. Temporal Trends and Patterns in Mortality After Incident Heart Failure: A Longitudinal Analysis of 86 000 Individuals. *JAMA Cardiol,* 4**,** 1102-1111.
CONRAD, N., JUDGE, A., TRAN, J., MOHSENI, H., HEDGECOTT, D., CRESPILLO, A. P., ALLISON, M., HEMINGWAY, H., CLELAND, J. G., MCMURRAY, J. J. V. & RAHIMI, K. 2018. Temporal trends and patterns in heart failure incidence: a population-based study of 4 million individuals. *Lancet,* 391**,** 572-580.
DAI, D. F., JOHNSON, S. C., VILLARIN, J. J., CHIN, M. T., NIEVES-CINTRON, M., CHEN, T., MARCINEK, D. J., DORN, G. W., 2ND, KANG, Y. J., PROLLA, T. A., SANTANA, L. F. & RABINOVITCH, P. S. 2011. Mitochondrial oxidative stress mediates angiotensin II-induced cardiac hypertrophy and Galphaq overexpression-induced heart failure. *Circ Res,* 108**,** 837-46.
DASGUPTA, A., SHUKLA, S. K., VERNUCCI, E., KING, R. J., ABREGO, J., MULDER, S. E., MULLEN, N. J., GRAVES, G., BUETTNER, K.,

THAKUR, R., MURTHY, D., ATTRI, K. S., WANG, D., CHAIKA, N. V., PACHECO, C. G., RAI, I., ENGLE, D. D., GRANDGENETT, P. M., PUNSONI, M., REAMES, B. N., TEOH-FITZGERALD, M., OBERLEY-DEEGAN, R., YU, F., KLUTE, K. A., HOLLINGSWORTH, M. A., ZIMMERMAN, M. C., MEHLA, K., SADOSHIMA, J., TUVESON, D. A. & SINGH, P. K. 2020. SIRT1-NOX4 signaling axis regulates cancer cachexia. *J Exp Med,* 217.

DAYE, D. & WELLEN, K. E. 2012. Metabolic reprogramming in cancer: unraveling the role of glutamine in tumorigenesis. *Semin Cell Dev Biol,* 23**,** 362-9.

DE BOER, R. A., PINTO, Y. M. & VAN VELDHUISEN, D. J. 2003. The imbalance between oxygen demand and supply as a potential mechanism in the pathophysiology of heart failure: the role of microvascular growth and abnormalities. *Microcirculation,* 10**,** 113-26.

DIEZ, J. 2017. Chronic heart failure as a state of reduced effectiveness of the natriuretic peptide system: implications for therapy. *Eur J Heart Fail,* 19**,** 167-176.

DU, J., ZHOU, Y., SU, X., YU, J. J., KHAN, S., JIANG, H., KIM, J., WOO, J., KIM, J. H., CHOI, B. H., HE, B., CHEN, W., ZHANG, S., CERIONE, R. A., AUWERX, J., HAO, Q. & LIN, H. 2011. Sirt5 is a NAD-dependent protein lysine demalonylase and desuccinylase. *Science,* 334**,** 806-9.

EMDIN, M., PASSINO, C., PRONTERA, C., FONTANA, M., POLETTI, R., GABUTTI, A., MAMMINI, C., GIANNONI, A., ZYW, L., ZUCCHELLI, G. & CLERICO, A. 2007. Comparison of brain natriuretic peptide (BNP) and amino-terminal ProBNP for early diagnosis of heart failure. *Clin Chem,* 53**,** 1289-97.

FINKEL, T., DENG, C. X. & MOSTOSLAVSKY, R. 2009. Recent progress in the biology and physiology of sirtuins. *Nature,* 460**,** 587-91.

FIRESTEIN, R., BLANDER, G., MICHAN, S., OBERDOERFFER, P., OGINO, S., CAMPBELL, J., BHIMAVARAPU, A., LUIKENHUIS, S., DE CABO, R., FUCHS, C., HAHN, W. C., GUARENTE, L. P. & SINCLAIR, D. A. 2008. The SIRT1 deacetylase suppresses intestinal tumorigenesis and colon cancer growth. *PLoS One,* 3**,** e2020.

FRYE, R. A. 2000. Phylogenetic classification of prokaryotic and eukaryotic Sir2-like proteins. *Biochem Biophys Res Commun,* 273**,** 793-8.

FU, L., DONG, Q., HE, J., WANG, X., XING, J., WANG, E., QIU, X. & LI, Q. 2017. SIRT4 inhibits malignancy progression of NSCLCs, through mitochondrial dynamics mediated by the ERK-Drp1 pathway. *Oncogene,* 36**,** 2724-2736.

GAN, L. & MUCKE, L. 2008. Paths of convergence: sirtuins in aging and neurodegeneration. *Neuron,* 58**,** 10-4.

GIORDANO, F. J. 2005. Oxygen, oxidative stress, hypoxia, and heart failure. *J Clin Invest,* 115**,** 500-8.

GLOZAK, M. A., SENGUPTA, N., ZHANG, X. & SETO, E. 2005. Acetylation and deacetylation of non-histone proteins. *Gene,* 363**,** 15-23.

GRILLON, J. M., JOHNSON, K. R., KOTLO, K. & DANZIGER, R. S. 2012. Non-histone lysine acetylated proteins in heart failure. *Biochim Biophys Acta,* 1822**,** 607-14.

GUAN, X. H., HONG, X., ZHAO, N., LIU, X. H., XIAO, Y. F., CHEN, T. T., DENG, L. B., WANG, X. L., WANG, J. B., JI, G. J., FU, M., DENG, K. Y. & XIN, H. B. 2017. CD38 promotes angiotensin II-induced cardiac hypertrophy. *J Cell Mol Med,* 21**,** 1492-1502.

HAIGIS, M. C., MOSTOSLAVSKY, R., HAIGIS, K. M., FAHIE, K., CHRISTODOULOU, D. C., MURPHY, A. J., VALENZUELA, D. M., YANCOPOULOS, G. D., KAROW, M., BLANDER, G., WOLBERGER, C., PROLLA, T. A., WEINDRUCH, R., ALT, F. W. & GUARENTE, L. 2006. SIRT4 inhibits glutamate dehydrogenase and opposes the effects of calorie restriction in pancreatic beta cells. *Cell,* 126**,** 941-54.

HAIGIS, M. C. & SINCLAIR, D. A. 2010. Mammalian sirtuins: biological insights and disease relevance. *Annu Rev Pathol,* 5**,** 253-95.

HALESTRAP, A. P., CONNERN, C. P., GRIFFITHS, E. J. & KERR, P. M. 1997. Cyclosporin A binding to mitochondrial cyclophilin inhibits the permeability transition pore and protects hearts from ischaemia/reperfusion injury. *Mol Cell Biochem,* 174**,** 167-72.

HALL, G., HASDAY, J. D. & ROGERS, T. B. 2006. Regulating the regulator: NF-kappaB signaling in heart. *J Mol Cell Cardiol,* 41**,** 580-91.

HARTUPEE, J. & MANN, D. L. 2017. Neurohormonal activation in heart failure with reduced ejection fraction. *Nat Rev Cardiol,* 14**,** 30-38.

HEIDENREICH, P. A., BOZKURT, B., AGUILAR, D., ALLEN, L. A., BYUN, J. J., COLVIN, M. M., DESWAL, A., DRAZNER, M. H., DUNLAY, S. M., EVERS, L. R., FANG, J. C., FEDSON, S. E., FONAROW, G. C., HAYEK, S. S., HERNANDEZ, A. F., KHAZANIE, P., KITTLESON, M. M., LEE, C. S., LINK, M. S., MILANO, C. A., NNACHETA, L. C., SANDHU, A. T., STEVENSON, L. W., VARDENY, O., VEST, A. R. & YANCY, C. W. 2022. 2022 AHA/ACC/HFSA Guideline for the Management of Heart Failure: A Report of the American College of Cardiology/American Heart Association Joint Committee on Clinical Practice Guidelines. *Circulation,* 145**,** e895-e1032.

HEINEKE, J. & MOLKENTIN, J. D. 2006. Regulation of cardiac hypertrophy by intracellular signalling pathways. *Nat Rev Mol Cell Biol,* 7**,** 589-600.

HEYMES, C., BENDALL, J. K., RATAJCZAK, P., CAVE, A. C., SAMUEL, J. L., HASENFUSS, G. & SHAH, A. M. 2003. Increased myocardial

NADPH oxidase activity in human heart failure. *J Am Coll Cardiol,* 41**,** 2164-71.

HIGASHI, M., SHIMOKAWA, H., HATTORI, T., HIROKI, J., MUKAI, Y., MORIKAWA, K., ICHIKI, T., TAKAHASHI, S. & TAKESHITA, A. 2003. Long-term inhibition of Rho-kinase suppresses angiotensin II-induced cardiovascular hypertrophy in rats in vivo: effect on endothelial NAD(P)H oxidase system. *Circ Res,* 93**,** 767-75.

HILL, J. A. & OLSON, E. N. 2008. Cardiac plasticity. *N Engl J Med,* 358**,** 1370-80.

HIROTANI, S., OTSU, K., NISHIDA, K., HIGUCHI, Y., MORITA, T., NAKAYAMA, H., YAMAGUCHI, O., MANO, T., MATSUMURA, Y., UENO, H., TADA, M. & HORI, M. 2002. Involvement of nuclear factor-kappaB and apoptosis signal-regulating kinase 1 in G-protein-coupled receptor agonist-induced cardiomyocyte hypertrophy. *Circulation,* 105**,** 509-15.

HOLTWICK, R., VAN EICKELS, M., SKRYABIN, B. V., BABA, H. A., BUBIKAT, A., BEGROW, F., SCHNEIDER, M. D., GARBERS, D. L. & KUHN, M. 2003. Pressure-independent cardiac hypertrophy in mice with cardiomyocyte-restricted inactivation of the atrial natriuretic peptide receptor guanylyl cyclase-A. *J Clin Invest,* 111**,** 1399-407.

HUANG, G., CHENG, J., YU, F., LIU, X., YUAN, C., LIU, C., CHEN, X. & PENG, Z. 2016. Clinical and therapeutic significance of sirtuin-4 expression in colorectal cancer. *Oncol Rep,* 35**,** 2801-10.

HUANG, G., CUI, F., YU, F., LU, H., ZHANG, M., TANG, H. & PENG, Z. 2015. Sirtuin-4 (SIRT4) is downregulated and associated with some clinicopathological features in gastric adenocarcinoma. *Biomed Pharmacother,* 72**,** 135-9.

HUANG, G. & ZHU, G. 2018. Sirtuin-4 (SIRT4), a therapeutic target with oncogenic and tumor-suppressive activity in cancer. *Onco Targets Ther,* 11**,** 3395-3400.

IGCI, M., KALENDER, M. E., BORAZAN, E., BOZGEYIK, I., BAYRAKTAR, R., BOZGEYIK, E., CAMCI, C. & ARSLAN, A. 2016. High-throughput screening of Sirtuin family of genes in breast cancer. *Gene,* 586**,** 123-8.

IMAI, S., ARMSTRONG, C. M., KAEBERLEIN, M. & GUARENTE, L. 2000. Transcriptional silencing and longevity protein Sir2 is an NAD-dependent histone deacetylase. *Nature,* 403**,** 795-800.

JANICKI, J. S., BROWER, G. L., GARDNER, J. D., CHANCEY, A. L. & STEWART, J. A., JR. 2004. The dynamic interaction between matrix metalloproteinase activity and adverse myocardial remodeling. *Heart Fail Rev,* 9**,** 33-42.

JEONG, S. M., LEE, A., LEE, J. & HAIGIS, M. C. 2014. SIRT4 protein suppresses tumor formation in genetic models of Myc-induced B cell lymphoma. *J Biol Chem,* 289**,** 4135-44.

JEONG, S. M., XIAO, C., FINLEY, L. W., LAHUSEN, T., SOUZA, A. L., PIERCE, K., LI, Y. H., WANG, X., LAURENT, G., GERMAN, N. J., XU, X., LI, C., WANG, R. H., LEE, J., CSIBI, A., CERIONE, R., BLENIS, J., CLISH, C. B., KIMMELMAN, A., DENG, C. X. & HAIGIS, M. C. 2013. SIRT4 has tumor-suppressive activity and regulates the cellular metabolic response to DNA damage by inhibiting mitochondrial glutamine metabolism. *Cancer Cell,* 23**,** 450-63.

JI, H., QU, J., PENG, W. & YANG, L. 2022. Downregulation of lncRNA MALAT1 Inhibits Angiotensin II-induced Hypertrophic Effects of Cardiomyocytes by Regulating SIRT4 via miR-93-5p. *Int Heart J,* 63**,** 602-611.

KAEBERLEIN, M., MCVEY, M. & GUARENTE, L. 1999. The SIR2/3/4 complex and SIR2 alone promote longevity in Saccharomyces cerevisiae by two different mechanisms. *Genes Dev,* 13**,** 2570-80.

KASNER, M., WESTERMANN, D., LOPEZ, B., GAUB, R., ESCHER, F., KUHL, U., SCHULTHEISS, H. P. & TSCHOPE, C. 2011. Diastolic tissue Doppler indexes correlate with the degree of collagen expression and cross-linking in heart failure and normal ejection fraction. *J Am Coll Cardiol,* 57**,** 977-85.

KLINGBEIL, A. U., SCHNEIDER, M., MARTUS, P., MESSERLI, F. H. & SCHMIEDER, R. E. 2003. A meta-analysis of the effects of treatment on left ventricular mass in essential hypertension. *Am J Med,* 115**,** 41-6.

KNOWLES, J. W., ESPOSITO, G., MAO, L., HAGAMAN, J. R., FOX, J. E., SMITHIES, O., ROCKMAN, H. A. & MAEDA, N. 2001. Pressure-independent enhancement of cardiac hypertrophy in natriuretic peptide receptor A-deficient mice. *J Clin Invest,* 107**,** 975-84.

KOENTGES, C., BODE, C. & BUGGER, H. 2016. SIRT3 in Cardiac Physiology and Disease. *Front Cardiovasc Med,* 3**,** 38.

KRAUSE, K. H. 2007. Aging: a revisited theory based on free radicals generated by NOX family NADPH oxidases. *Exp Gerontol,* 42**,** 256-62.

KURODA, J., AGO, T., MATSUSHIMA, S., ZHAI, P., SCHNEIDER, M. D. & SADOSHIMA, J. 2010. NADPH oxidase 4 (Nox4) is a major source of oxidative stress in the failing heart. *Proc Natl Acad Sci U S A,* 107**,** 15565-70.

KUWAHARA, K. 2021. The natriuretic peptide system in heart failure: Diagnostic and therapeutic implications. *Pharmacol Ther,* 227**,** 107863.

LANGENICKEL, T. H., BUTTGEREIT, J., PAGEL-LANGENICKEL, I., LINDNER, M., MONTI, J., BEUERLEIN, K., AL-SAADI, N., PLEHM, R., POPOVA, E., TANK, J., DIETZ, R., WILLENBROCK, R. & BADER, M. 2006. Cardiac hypertrophy in transgenic rats expressing a

dominant-negative mutant of the natriuretic peptide receptor B. *Proc Natl Acad Sci U S A,* 103**,** 4735-40.
LASSEGUE, B., SORESCU, D., SZOCS, K., YIN, Q., AKERS, M., ZHANG, Y., GRANT, S. L., LAMBETH, J. D. & GRIENDLING, K. K. 2001. Novel gp91(phox) homologues in vascular smooth muscle cells : nox1 mediates angiotensin II-induced superoxide formation and redox-sensitive signaling pathways. *Circ Res,* 88**,** 888-94.
LAURENT, G., GERMAN, N. J., SAHA, A. K., DE BOER, V. C., DAVIES, M., KOVES, T. R., DEPHOURE, N., FISCHER, F., BOANCA, G., VAITHEESVARAN, B., LOVITCH, S. B., SHARPE, A. H., KURLAND, I. J., STEEGBORN, C., GYGI, S. P., MUOIO, D. M., RUDERMAN, N. B. & HAIGIS, M. C. 2013. SIRT4 coordinates the balance between lipid synthesis and catabolism by repressing malonyl CoA decarboxylase. *Mol Cell,* 50**,** 686-98.
LI, J. M., GALL, N. P., GRIEVE, D. J., CHEN, M. & SHAH, A. M. 2002. Activation of NADPH oxidase during progression of cardiac hypertrophy to failure. *Hypertension,* 40**,** 477-84.
LI, X., WU, Y., YANG, Y., WU, Y., YU, X. & HU, W. 2024. Omaveloxolone ameliorates isoproterenol-induced pathological cardiac hypertrophy in mice. *Free Radic Res,* 58**,** 57-68.
LIN, S. J., DEFOSSEZ, P. A. & GUARENTE, L. 2000. Requirement of NAD and SIR2 for life-span extension by calorie restriction in Saccharomyces cerevisiae. *Science,* 289**,** 2126-8.
LINGYAN, Z., YIHONG, W., YOUHUA, W., JIANMEI, Y., JIAWEI, L. I., MIN, C. & DUAN, Z. 2022. Protective efficacy of Shenge San on mitochondria in H9c2 cardiomyocytes. *J Tradit Chin Med,* 42**,** 892-899.
LIU, B., CHE, W., XUE, J., ZHENG, C., TANG, K., ZHANG, J., WEN, J. & XU, Y. 2013. SIRT4 prevents hypoxia-induced apoptosis in H9c2 cardiomyoblast cells. *Cell Physiol Biochem,* 32**,** 655-62.
LIU, B. Y., LI, L., LIU, G. L., DING, W., CHANG, W. G., XU, T., JI, X. Y., ZHENG, X. X., ZHANG, J. & WANG, J. X. 2021. Baicalein attenuates cardiac hypertrophy in mice via suppressing oxidative stress and activating autophagy in cardiomyocytes. *Acta Pharmacol Sin,* 42**,** 701-714.
LU, P., ZHANG, D., DING, F., MA, J., XIANG, Y. K. & ZHAO, M. 2023a. Silencing of circCacna1c Inhibits ISO-Induced Cardiac Hypertrophy through miR-29b-2-5p/NFATc1 Axis. *Cells,* 12.
LU, S., LIANG, Y., YANG, S., FU, M., SHAN, X., ZHANG, C., CHEN, H., ZHAO, P. & LU, R. 2023b. Stachydrine Hydrochloride Regulates the NOX2-ROS-Signaling Axis in Pressure-Overload-Induced Heart Failure. *Int J Mol Sci,* 24.
LUO, G., CHEN, L., CHEN, M., MAO, L., ZENG, Q., ZOU, Y., XUE, J., LIU, P., WU, Q., YANG, S. & LIU, M. 2024. Hirudin inhibit the formation

of NLRP3 inflammasome in cardiomyocytes via suppressing oxidative stress and activating mitophagy. *Heliyon,* 10**,** e23077.

LUO, Y. X., TANG, X., AN, X. Z., XIE, X. M., CHEN, X. F., ZHAO, X., HAO, D. L., CHEN, H. Z. & LIU, D. P. 2017. SIRT4 accelerates Ang II-induced pathological cardiac hypertrophy by inhibiting manganese superoxide dismutase activity. *Eur Heart J,* 38**,** 1389-1398.

LYMPEROPOULOS, A., RENGO, G. & KOCH, W. J. 2013. Adrenergic nervous system in heart failure: pathophysiology and therapy. *Circ Res,* 113**,** 739-53.

LYNN, E. G., MCLEOD, C. J., GORDON, J. P., BAO, J. & SACK, M. N. 2008. SIRT2 is a negative regulator of anoxia-reoxygenation tolerance via regulation of 14-3-3 zeta and BAD in H9c2 cells. *FEBS Lett,* 582**,** 2857-62.

MA, Y., HU, Y., WU, J., WEN, J., LI, S., ZHANG, L., ZHANG, J., LI, Y. & LI, J. 2019. Epigallocatechin-3-gallate inhibits angiotensin II-induced cardiomyocyte hypertrophy via regulating Hippo signaling pathway in H9c2 rat cardiomyocytes. *Acta Biochim Biophys Sin (Shanghai),* 51**,** 422-430.

MAILLET, M., VAN BERLO, J. H. & MOLKENTIN, J. D. 2013. Molecular basis of physiological heart growth: fundamental concepts and new players. *Nat Rev Mol Cell Biol,* 14**,** 38-48.

MALIK, S., VILLANOVA, L., TANAKA, S., AONUMA, M., ROY, N., BERBER, E., POLLACK, J. R., MICHISHITA-KIOI, E. & CHUA, K. F. 2015. SIRT7 inactivation reverses metastatic phenotypes in epithelial and mesenchymal tumors. *Sci Rep,* 5**,** 9841.

MALLAT, Z., PHILIP, I., LEBRET, M., CHATEL, D., MACLOUF, J. & TEDGUI, A. 1998. Elevated levels of 8-iso-prostaglandin F2alpha in pericardial fluid of patients with heart failure: a potential role for in vivo oxidant stress in ventricular dilatation and progression to heart failure. *Circulation,* 97**,** 1536-9.

MAO, Z., HINE, C., TIAN, X., VAN METER, M., AU, M., VAIDYA, A., SELUANOV, A. & GORBUNOVA, V. 2011. SIRT6 promotes DNA repair under stress by activating PARP1. *Science,* 332**,** 1443-6.

MATHIAS, R. A., GRECO, T. M., OBERSTEIN, A., BUDAYEVA, H. G., CHAKRABARTI, R., ROWLAND, E. A., KANG, Y., SHENK, T. & CRISTEA, I. M. 2014. Sirtuin 4 is a lipoamidase regulating pyruvate dehydrogenase complex activity. *Cell,* 159**,** 1615-25.

MATSUSHIMA, S., IDE, T., YAMATO, M., MATSUSAKA, H., HATTORI, F., IKEUCHI, M., KUBOTA, T., SUNAGAWA, K., HASEGAWA, Y., KURIHARA, T., OIKAWA, S., KINUGAWA, S. & TSUTSUI, H. 2006a. Overexpression of mitochondrial peroxiredoxin-3 prevents left ventricular remodeling and failure after myocardial infarction in mice. *Circulation,* 113**,** 1779-86.

MATSUSHIMA, S., KINUGAWA, S., IDE, T., MATSUSAKA, H., INOUE, N., OHTA, Y., YOKOTA, T., SUNAGAWA, K. & TSUTSUI, H. 2006b. Overexpression of glutathione peroxidase attenuates myocardial remodeling and preserves diastolic function in diabetic heart. *Am J Physiol Heart Circ Physiol,* 291**,** H2237-45.

MATSUSHIMA, S., KURODA, J., AGO, T., ZHAI, P., PARK, J. Y., XIE, L. H., TIAN, B. & SADOSHIMA, J. 2013. Increased oxidative stress in the nucleus caused by Nox4 mediates oxidation of HDAC4 and cardiac hypertrophy. *Circ Res,* 112**,** 651-63.

MATSUSHIMA, S. & SADOSHIMA, J. 2015. The role of sirtuins in cardiac disease. *Am J Physiol Heart Circ Physiol,* 309**,** H1375-89.

MAULIK, S. K. & KUMAR, S. 2012. Oxidative stress and cardiac hypertrophy: a review. *Toxicol Mech Methods,* 22**,** 359-66.

MCDONAGH, T. A., METRA, M., ADAMO, M., GARDNER, R. S., BAUMBACH, A., BOHM, M., BURRI, H., BUTLER, J., CELUTKIENE, J., CHIONCEL, O., CLELAND, J. G. F., COATS, A. J. S., CRESPO-LEIRO, M. G., FARMAKIS, D., GILARD, M., HEYMANS, S., HOES, A. W., JAARSMA, T., JANKOWSKA, E. A., LAINSCAK, M., LAM, C. S. P., LYON, A. R., MCMURRAY, J. J. V., MEBAZAA, A., MINDHAM, R., MUNERETTO, C., FRANCESCO PIEPOLI, M., PRICE, S., ROSANO, G. M. C., RUSCHITZKA, F., KATHRINE SKIBELUND, A. & GROUP, E. S. C. S. D. 2021. 2021 ESC Guidelines for the diagnosis and treatment of acute and chronic heart failure. *Eur Heart J,* 42**,** 3599-3726.

MCMURRAY, J. J., PACKER, M., DESAI, A. S., GONG, J., LEFKOWITZ, M. P., RIZKALA, A. R., ROULEAU, J. L., SHI, V. C., SOLOMON, S. D., SWEDBERG, K., ZILE, M. R., INVESTIGATORS, P.-H. & COMMITTEES 2014. Angiotensin-neprilysin inhibition versus enalapril in heart failure. *N Engl J Med,* 371**,** 993-1004.

MEYER, S., BROUWERS, F. P., VOORS, A. A., HILLEGE, H. L., DE BOER, R. A., GANSEVOORT, R. T., VAN DER HARST, P., RIENSTRA, M., VAN GELDER, I. C., VAN VELDHUISEN, D. J., VAN GILST, W. H. & VAN DER MEER, P. 2015. Sex differences in new-onset heart failure. *Clin Res Cardiol,* 104**,** 342-50.

MICHISHITA, E., MCCORD, R. A., BERBER, E., KIOI, M., PADILLA-NASH, H., DAMIAN, M., CHEUNG, P., KUSUMOTO, R., KAWAHARA, T. L., BARRETT, J. C., CHANG, H. Y., BOHR, V. A., RIED, T., GOZANI, O. & CHUA, K. F. 2008. SIRT6 is a histone H3 lysine 9 deacetylase that modulates telomeric chromatin. *Nature,* 452**,** 492-6.

MICHISHITA, E., PARK, J. Y., BURNESKIS, J. M., BARRETT, J. C. & HORIKAWA, I. 2005. Evolutionarily conserved and nonconserved

cellular localizations and functions of human SIRT proteins. *Mol Biol Cell,* 16**,** 4623-35.

MIN, Z., GAO, J. & YU, Y. 2018. The Roles of Mitochondrial SIRT4 in Cellular Metabolism. *Front Endocrinol (Lausanne),* 9**,** 783.

MIYO, M., YAMAMOTO, H., KONNO, M., COLVIN, H., NISHIDA, N., KOSEKI, J., KAWAMOTO, K., OGAWA, H., HAMABE, A., UEMURA, M., NISHIMURA, J., HATA, T., TAKEMASA, I., MIZUSHIMA, T., DOKI, Y., MORI, M. & ISHII, H. 2015. Tumour-suppressive function of SIRT4 in human colorectal cancer. *Br J Cancer,* 113**,** 492-9.

MOSTERD, A. & HOES, A. W. 2007. Clinical epidemiology of heart failure. *Heart,* 93**,** 1137-46.

MUEHLEMAN, D. L., CROCINI, C., SWEARINGEN, A. R., OZEROFF, C. D. & LEINWAND, L. A. 2022. Regression from pathological hypertrophy in mice is sexually dimorphic and stimulus specific. *Am J Physiol Heart Circ Physiol,* 322**,** H785-H797.

MUNZEL, T., GORI, T., KEANEY, J. F., JR., MAACK, C. & DAIBER, A. 2015. Pathophysiological role of oxidative stress in systolic and diastolic heart failure and its therapeutic implications. *Eur Heart J,* 36**,** 2555-64.

NAKAGAWA, T. & GUARENTE, L. 2011. Sirtuins at a glance. *J Cell Sci,* 124**,** 833-8.

NAKAGAWA, T., LOMB, D. J., HAIGIS, M. C. & GUARENTE, L. 2009. SIRT5 Deacetylates carbamoyl phosphate synthetase 1 and regulates the urea cycle. *Cell,* 137**,** 560-70.

NAKAHARA, Y., YAMASAKI, M., SAWADA, G., MIYAZAKI, Y., MAKINO, T., TAKAHASHI, T., KUROKAWA, Y., NAKAJIMA, K., TAKIGUCHI, S., MIMORI, K., MORI, M. & DOKI, Y. 2016. Downregulation of SIRT4 Expression Is Associated with Poor Prognosis in Esophageal Squamous Cell Carcinoma. *Oncology,* 90**,** 347-55.

NAKAMURA, M. & SADOSHIMA, J. 2018. Mechanisms of physiological and pathological cardiac hypertrophy. *Nat Rev Cardiol,* 15**,** 387-407.

NASRIN, N., WU, X., FORTIER, E., FENG, Y., BARE, O. C., CHEN, S., REN, X., WU, Z., STREEPER, R. S. & BORDONE, L. 2010. SIRT4 regulates fatty acid oxidation and mitochondrial gene expression in liver and muscle cells. *J Biol Chem,* 285**,** 31995-2002.

NI, Y., DENG, J., BAI, H., LIU, C., LIU, X. & WANG, X. 2022a. CaMKII inhibitor KN-93 impaired angiogenesis and aggravated cardiac remodelling and heart failure via inhibiting NOX2/mtROS/p-VEGFR2 and STAT3 pathways. *J Cell Mol Med,* 26**,** 312-325.

NI, Y., ZHANG, J., ZHU, W., DUAN, Y., BAI, H. & LUAN, C. 2022b. Echinacoside inhibited cardiomyocyte pyroptosis and improved heart function of HF rats induced by isoproterenol via suppressing NADPH/ROS/ER stress. *J Cell Mol Med,* 26**,** 5414-5425.

NICHTOVA, Z., NOVOTOVA, M., KRALOVA, E. & STANKOVICOVA, T. 2012. Morphological and functional characteristics of models of experimental myocardial injury induced by isoproterenol. *Gen Physiol Biophys,* 31**,** 141-51.

NORTH, B. J. & VERDIN, E. 2004. Sirtuins: Sir2-related NAD-dependent protein deacetylases. *Genome Biol,* 5**,** 224.

OKA, S., ALCENDOR, R., ZHAI, P., PARK, J. Y., SHAO, D., CHO, J., YAMAMOTO, T., TIAN, B. & SADOSHIMA, J. 2011. PPARalpha-Sirt1 complex mediates cardiac hypertrophy and failure through suppression of the ERR transcriptional pathway. *Cell Metab,* 14**,** 598-611.

OLDFIELD, C. J., DUHAMEL, T. A. & DHALLA, N. S. 2020. Mechanisms for the transition from physiological to pathological cardiac hypertrophy. *Can J Physiol Pharmacol,* 98**,** 74-84.

PAN, P. W., FELDMAN, J. L., DEVRIES, M. K., DONG, A., EDWARDS, A. M. & DENU, J. M. 2011. Structure and biochemical functions of SIRT6. *J Biol Chem,* 286**,** 14575-87.

PAN, W., ZHONG, Y., CHENG, C., LIU, B., WANG, L., LI, A., XIONG, L. & LIU, S. 2013. MiR-30-regulated autophagy mediates angiotensin II-induced myocardial hypertrophy. *PLoS One,* 8**,** e53950.

PAULUS, W. J. & TSCHOPE, C. 2013. A novel paradigm for heart failure with preserved ejection fraction: comorbidities drive myocardial dysfunction and remodeling through coronary microvascular endothelial inflammation. *J Am Coll Cardiol,* 62**,** 263-71.

PENG, S., LU, X. F., QI, Y. D., LI, J., XU, J., YUAN, T. Y., WU, X. Y., DING, Y., LI, W. H., ZHOU, G. Q., WEI, Y., LI, J., CHEN, S. W. & LIU, S. W. 2020. LCZ696 Ameliorates Oxidative Stress and Pressure Overload-Induced Pathological Cardiac Remodeling by Regulating the Sirt3/MnSOD Pathway. *Oxid Med Cell Longev,* 2020**,** 9815039.

PISOSCHI, A. M. & POP, A. 2015. The role of antioxidants in the chemistry of oxidative stress: A review. *Eur J Med Chem,* 97**,** 55-74.

POTENTE, M., GHAENI, L., BALDESSARI, D., MOSTOSLAVSKY, R., ROSSIG, L., DEQUIEDT, F., HAENDELER, J., MIONE, M., DEJANA, E., ALT, F. W., ZEIHER, A. M. & DIMMELER, S. 2007. SIRT1 controls endothelial angiogenic functions during vascular growth. *Genes Dev,* 21**,** 2644-58.

POTTER, L. R., YODER, A. R., FLORA, D. R., ANTOS, L. K. & DICKEY, D. M. 2009. Natriuretic peptides: their structures, receptors, physiologic functions and therapeutic applications. *Handb Exp Pharmacol***,** 341-66.

QI, H., REN, J., BA, L., SONG, C., ZHANG, Q., CAO, Y., SHI, P., FU, B., LIU, Y. & SUN, H. 2020. MSTN Attenuates Cardiac Hypertrophy through Inhibition of Excessive Cardiac Autophagy by Blocking AMPK

/mTOR and miR-128/PPARgamma/NF-kappaB. *Mol Ther Nucleic Acids,* 19**,** 507-522.
RAAB, W. 1960. Key position of catecholamines in functional and degenerative cardiovascular pathology. *Am J Cardiol,* 5**,** 571-8.
RAGHUBEER, S. 2024. The influence of epigenetics and inflammation on cardiometabolic risks. *Semin Cell Dev Biol,* 154**,** 175-184.
RAINER, P. P. & KASS, D. A. 2016. Old dog, new tricks: novel cardiac targets and stress regulation by protein kinase G. *Cardiovasc Res,* 111**,** 154-62.
RAMADANI-MUJA, J., GOTTSCHALK, B., PFEIL, K., BURGSTALLER, S., RAUTER, T., BISCHOF, H., WALDECK-WEIERMAIR, M., BUGGER, H., GRAIER, W. F. & MALLI, R. 2019. Visualization of Sirtuin 4 Distribution between Mitochondria and the Nucleus, Based on Bimolecular Fluorescence Self-Complementation. *Cells,* 8.
RAZA, U., TANG, X., LIU, Z. & LIU, B. 2024. SIRT7: the seventh key to unlocking the mystery of aging. *Physiol Rev,* 104**,** 253-280.
REN, S., WANG, Y., ZHANG, Y., YAN, P., XIAO, D., ZHAO, Y., JIA, W., DING, L., DONG, H., WEI, C., LIN, S. & LIN, Y. 2023. Paeoniflorin alleviates AngII-induced cardiac hypertrophy in H9c2 cells by regulating oxidative stress and Nrf2 signaling pathway. *Biomed Pharmacother,* 165**,** 115253.
RINE, J., STRATHERN, J. N., HICKS, J. B. & HERSKOWITZ, I. 1979. A suppressor of mating-type locus mutations in Saccharomyces cerevisiae: evidence for and identification of cryptic mating-type loci. *Genetics,* 93**,** 877-901.
ROCKEY, D. C., BELL, P. D. & HILL, J. A. 2015. Fibrosis--A Common Pathway to Organ Injury and Failure. *N Engl J Med,* 373**,** 96.
ROGER, V. L. 2021. Epidemiology of Heart Failure: A Contemporary Perspective. *Circ Res,* 128**,** 1421-1434.
ROGINA, B. & HELFAND, S. L. 2004. Sir2 mediates longevity in the fly through a pathway related to calorie restriction. *Proc Natl Acad Sci U S A,* 101**,** 15998-6003.
RONA, G. 1985. Catecholamine cardiotoxicity. *J Mol Cell Cardiol,* 17**,** 291-306.
RUSTANDI, R. R., LOUGHNEY, J. W., HAMM, M., HAMM, C., LANCASTER, C., MACH, A. & HA, S. 2012. Qualitative and quantitative evaluation of Simon, a new CE-based automated Western blot system as applied to vaccine development. *Electrophoresis,* 33**,** 2790-7.
SABRI, A., HUGHIE, H. H. & LUCCHESI, P. A. 2003. Regulation of hypertrophic and apoptotic signaling pathways by reactive oxygen species in cardiac myocytes. *Antioxid Redox Signal,* 5**,** 731-40.
SADHUKHAN, S., LIU, X., RYU, D., NELSON, O. D., STUPINSKI, J. A., LI, Z., CHEN, W., ZHANG, S., WEISS, R. S., LOCASALE, J. W.,

AUWERX, J. & LIN, H. 2016. Metabolomics-assisted proteomics identifies succinylation and SIRT5 as important regulators of cardiac function. *Proc Natl Acad Sci U S A,* 113**,** 4320-5.

SCHER, M. B., VAQUERO, A. & REINBERG, D. 2007. SirT3 is a nuclear NAD+-dependent histone deacetylase that translocates to the mitochondria upon cellular stress. *Genes Dev,* 21**,** 920-8.

SEDDON, M., LOOI, Y. H. & SHAH, A. M. 2007. Oxidative stress and redox signalling in cardiac hypertrophy and heart failure. *Heart,* 93**,** 903-7.

SELBY, D. E., PALMER, B. M., LEWINTER, M. M. & MEYER, M. 2011. Tachycardia-induced diastolic dysfunction and resting tone in myocardium from patients with a normal ejection fraction. *J Am Coll Cardiol,* 58**,** 147-54.

SERAFINI, M., PELUSO, I. & RAGUZZINI, A. 2010. Flavonoids as anti-inflammatory agents. *Proc Nutr Soc,* 69**,** 273-8.

SHIMAMATSU, M. & TOSHIMA, H. 1987. Impaired coronary vasodilatory capacity after dipyridamole administration in hypertrophic cardiomyopathy. *Jpn Heart J,* 28**,** 387-401.

SHIMIZU, I. & MINAMINO, T. 2016. Physiological and pathological cardiac hypertrophy. *J Mol Cell Cardiol,* 97**,** 245-62.

SHIOMI, T., TSUTSUI, H., MATSUSAKA, H., MURAKAMI, K., HAYASHIDANI, S., IKEUCHI, M., WEN, J., KUBOTA, T., UTSUMI, H. & TAKESHITA, A. 2004. Overexpression of glutathione peroxidase prevents left ventricular remodeling and failure after myocardial infarction in mice. *Circulation,* 109**,** 544-9.

SMEETS, M., VAES, B., MAMOURIS, P., VAN DEN AKKER, M., VAN POTTELBERGH, G., GODERIS, G., JANSSENS, S., AERTGEERTS, B. & HENRARD, S. 2019. Burden of heart failure in Flemish general practices: a registry-based study in the Intego database. *BMJ Open,* 9**,** e022972.

SMITH, J. S. & BOEKE, J. D. 1997. An unusual form of transcriptional silencing in yeast ribosomal DNA. *Genes Dev,* 11**,** 241-54.

SORMUNEN, A., KOIVULEHTO, E., ALITALO, K., SAKSELA, K., LAHAM-KARAM, N. & YLA-HERTTUALA, S. 2023. Comparison of Automated and Traditional Western Blotting Methods. *Methods Protoc,* 6.

SUMIMOTO, H. 2008. Structure, regulation and evolution of Nox-family NADPH oxidases that produce reactive oxygen species. *FEBS J,* 275**,** 3249-77.

SUN, H., HUANG, D., LIU, G., JIAN, F., ZHU, J. & ZHANG, L. 2018. SIRT4 acts as a tumor suppressor in gastric cancer by inhibiting cell proliferation, migration, and invasion. *Onco Targets Ther,* 11**,** 3959-3968.

SUNDARESAN, N. R., GUPTA, M., KIM, G., RAJAMOHAN, S. B., ISBATAN, A. & GUPTA, M. P. 2009. Sirt3 blocks the cardiac hypertrophic response by augmenting Foxo3a-dependent antioxidant defense mechanisms in mice. *J Clin Invest,* 119**,** 2758-71.

SUNDARESAN, N. R., VASUDEVAN, P., ZHONG, L., KIM, G., SAMANT, S., PAREKH, V., PILLAI, V. B., RAVINDRA, P. V., GUPTA, M., JEEVANANDAM, V., CUNNINGHAM, J. M., DENG, C. X., LOMBARD, D. B., MOSTOSLAVSKY, R. & GUPTA, M. P. 2012. The sirtuin SIRT6 blocks IGF-Akt signaling and development of cardiac hypertrophy by targeting c-Jun. *Nat Med,* 18**,** 1643-50.

SYED, A. A., REZA, M. I., YADAV, H. & GAYEN, J. R. 2023. Hesperidin inhibits NOX4 mediated oxidative stress and inflammation by upregulating SIRT1 in experimental diabetic neuropathy. *Exp Gerontol,* 172**,** 112064.

TAKEMOTO, Y., YOSHIYAMA, M., TAKEUCHI, K., OMURA, T., KOMATSU, R., IZUMI, Y., KIM, S. & YOSHIKAWA, J. 1999. Increased JNK, AP-1 and NF-kappa B DNA binding activities in isoproterenol-induced cardiac remodeling. *J Mol Cell Cardiol,* 31**,** 2017-30.

TAKIMOTO, E., CHAMPION, H. C., LI, M., REN, S., RODRIGUEZ, E. R., TAVAZZI, B., LAZZARINO, G., PAOLOCCI, N., GABRIELSON, K. L., WANG, Y. & KASS, D. A. 2005. Oxidant stress from nitric oxide synthase-3 uncoupling stimulates cardiac pathologic remodeling from chronic pressure load. *J Clin Invest,* 115**,** 1221-31.

TAMURA, N., DOOLITTLE, L. K., HAMMER, R. E., SHELTON, J. M., RICHARDSON, J. A. & GARBERS, D. L. 2004. Critical roles of the guanylyl cyclase B receptor in endochondral ossification and development of female reproductive organs. *Proc Natl Acad Sci U S A,* 101**,** 17300-5.

TANG, X., CHEN, X. F., WANG, N. Y., WANG, X. M., LIANG, S. T., ZHENG, W., LU, Y. B., ZHAO, X., HAO, D. L., ZHANG, Z. Q., ZOU, M. H., LIU, D. P. & CHEN, H. Z. 2017. SIRT2 Acts as a Cardioprotective Deacetylase in Pathological Cardiac Hypertrophy. *Circulation,* 136**,** 2051-2067.

TENG, W., ZHENG, X. J., GONG, G. H. & HE, Z. H. 2020. [MicroRNA-23a knockdown attenuates angiotensin II induced hypertrophy in rat H9c2 cells via activating PTEN and AMPK pathway]. *Zhonghua Xin Xue Guan Bing Za Zhi,* 48**,** 329-335.

TIRZIU, D., GIORDANO, F. J. & SIMONS, M. 2010. Cell communications in the heart. *Circulation,* 122**,** 928-37.

TISSENBAUM, H. A. & GUARENTE, L. 2001. Increased dosage of a sir-2 gene extends lifespan in Caenorhabditis elegans. *Nature,* 410**,** 227-30.

TSUJI, T. & KUNIEDA, T. 2005. A loss-of-function mutation in natriuretic peptide receptor 2 (Npr2) gene is responsible for disproportionate dwarfism in cn/cn mouse. *J Biol Chem,* 280**,** 14288-92.

VAKHRUSHEVA, O., SMOLKA, C., GAJAWADA, P., KOSTIN, S., BOETTGER, T., KUBIN, T., BRAUN, T. & BOBER, E. 2008. Sirt7 increases stress resistance of cardiomyocytes and prevents apoptosis and inflammatory cardiomyopathy in mice. *Circ Res,* 102**,** 703-10.

VAN HEEREBEEK, L., BORBELY, A., NIESSEN, H. W., BRONZWAER, J. G., VAN DER VELDEN, J., STIENEN, G. J., LINKE, W. A., LAARMAN, G. J. & PAULUS, W. J. 2006. Myocardial structure and function differ in systolic and diastolic heart failure. *Circulation,* 113**,** 1966-73.

VAN RIET, E. E., HOES, A. W., LIMBURG, A., LANDMAN, M. A., VAN DER HOEVEN, H. & RUTTEN, F. H. 2014. Prevalence of unrecognized heart failure in older persons with shortness of breath on exertion. *Eur J Heart Fail,* 16**,** 772-7.

VENDROV, A. E., XIAO, H., LOZHKIN, A., HAYAMI, T., HU, G., BRODY, M. J., SADOSHIMA, J., ZHANG, Y. Y., RUNGE, M. S. & MADAMANCHI, N. R. 2023. Cardiomyocyte NOX4 regulates resident macrophage-mediated inflammation and diastolic dysfunction in stress cardiomyopathy. *Redox Biol,* 67**,** 102937.

VERMA, M., SHULGA, N. & PASTORINO, J. G. 2013. Sirtuin-4 modulates sensitivity to induction of the mitochondrial permeability transition pore. *Biochim Biophys Acta,* 1827**,** 38-49.

VIRANI, S. S., ALONSO, A., BENJAMIN, E. J., BITTENCOURT, M. S., CALLAWAY, C. W., CARSON, A. P., CHAMBERLAIN, A. M., CHANG, A. R., CHENG, S., DELLING, F. N., DJOUSSE, L., ELKIND, M. S. V., FERGUSON, J. F., FORNAGE, M., KHAN, S. S., KISSELA, B. M., KNUTSON, K. L., KWAN, T. W., LACKLAND, D. T., LEWIS, T. T., LICHTMAN, J. H., LONGENECKER, C. T., LOOP, M. S., LUTSEY, P. L., MARTIN, S. S., MATSUSHITA, K., MORAN, A. E., MUSSOLINO, M. E., PERAK, A. M., ROSAMOND, W. D., ROTH, G. A., SAMPSON, U. K. A., SATOU, G. M., SCHROEDER, E. B., SHAH, S. H., SHAY, C. M., SPARTANO, N. L., STOKES, A., TIRSCHWELL, D. L., VANWAGNER, L. B., TSAO, C. W., AMERICAN HEART ASSOCIATION COUNCIL ON, E., PREVENTION STATISTICS, C. & STROKE STATISTICS, S. 2020. Heart Disease and Stroke Statistics-2020 Update: A Report From the American Heart Association. *Circulation,* 141**,** e139-e596.

VOLPE, M., CARNOVALI, M. & MASTROMARINO, V. 2016. The natriuretic peptides system in the pathophysiology of heart failure: from molecular basis to treatment. *Clin Sci (Lond),* 130**,** 57-77.

VON LUEDER, T. G., KOTECHA, D., ATAR, D. & HOPPER, I. 2017. Neurohormonal Blockade in Heart Failure. *Card Fail Rev,* 3**,** 19-24.

WANG, C., WANG, Y. & SHEN, L. 2021. Mitochondrial proteins in heart failure: The role of deacetylation by SIRT3. *Pharmacol Res,* 172**,** 105802.

WANG, F., NGUYEN, M., QIN, F. X. & TONG, Q. 2007. SIRT2 deacetylates FOXO3a in response to oxidative stress and caloric restriction. *Aging Cell,* 6**,** 505-14.

WANG, Y., HE, J., LIAO, M., HU, M., LI, W., OUYANG, H., WANG, X., YE, T., ZHANG, Y. & OUYANG, L. 2019. An overview of Sirtuins as potential therapeutic target: Structure, function and modulators. *Eur J Med Chem,* 161**,** 48-77.

WANG, Y., LIU, T., CAI, Y., LIU, W. & GUO, J. 2023. SIRT6's function in controlling the metabolism of lipids and glucose in diabetic nephropathy. *Front Endocrinol (Lausanne),* 14**,** 1244705.

WATKINS, S. J., BORTHWICK, G. M. & ARTHUR, H. M. 2011. The H9C2 cell line and primary neonatal cardiomyocyte cells show similar hypertrophic responses in vitro. *In Vitro Cell Dev Biol Anim,* 47**,** 125-31.

WEEKS, K. L. & MCMULLEN, J. R. 2011. The athlete's heart vs. the failing heart: can signaling explain the two distinct outcomes? *Physiology (Bethesda),* 26**,** 97-105.

WINGLER, K., WUNSCH, S., KREUTZ, R., ROTHERMUND, L., PAUL, M. & SCHMIDT, H. H. 2001. Upregulation of the vascular NAD(P)H-oxidase isoforms Nox1 and Nox4 by the renin-angiotensin system in vitro and in vivo. *Free Radic Biol Med,* 31**,** 1456-64.

WOOD, J. G., ROGINA, B., LAVU, S., HOWITZ, K., HELFAND, S. L., TATAR, M. & SINCLAIR, D. 2004. Sirtuin activators mimic caloric restriction and delay ageing in metazoans. *Nature,* 430**,** 686-9.

WU, T., QU, Y., XU, S., WANG, Y., LIU, X. & MA, D. 2023. SIRT6: A potential therapeutic target for diabetic cardiomyopathy. *FASEB J,* 37**,** e23099.

WU, T., WANG, H., XIN, X., YANG, J., HOU, Y., FANG, M., LU, X. & XU, Y. 2020. An MRTF-A-Sp1-PDE5 Axis Mediates Angiotensin-II-Induced Cardiomyocyte Hypertrophy. *Front Cell Dev Biol,* 8**,** 839.

YAMAGISHI, S., NAKAMURA, K., UEDA, S., KATO, S. & IMAIZUMI, T. 2005. Pigment epithelium-derived factor (PEDF) blocks angiotensin II signaling in endothelial cells via suppression of NADPH oxidase: a novel anti-oxidative mechanism of PEDF. *Cell Tissue Res,* 320**,** 437-45.

YANG, K., VELAGAPUDI, S., AKHMEDOV, A., KRALER, S., LAPIKOVA-BRYHINSKA, T., SCHMIADY, M. O., WU, X., GENG, L., CAMICI, G. G., XU, A. & LUSCHER, T. F. 2023. Chronic SIRT1 supplementation in diabetic mice improves endothelial function by suppressing oxidative stress. *Cardiovasc Res,* 119**,** 2190-2201.

YIN, J. Y., LU, X. T., HOU, M. L., CAO, T. & TIAN, Z. 2023. Sirtuin1-p53: A potential axis for cancer therapy. *Biochem Pharmacol,* 212**,** 115543.

YUAN, Y., PENG, W., LIU, Y. & XU, Z. 2017. Palmatine attenuates isoproterenol-induced pathological hypertrophy via selectively inhibiting HDAC2 in rats. *Int J Immunopathol Pharmacol,* 30**,** 406-412.

ZANG, R., TAN, Q., ZENG, F., WANG, D., YU, S. & WANG, Q. 2020. JMJD1A Represses the Development of Cardiomyocyte Hypertrophy by Regulating the Expression of Catalase. *Biomed Res Int,* 2020**,** 5081323.

ZAVILEYSKIY, L. & BUNIK, V. 2022. Regulation of p53 Function by Formation of Non-Nuclear Heterologous Protein Complexes. *Biomolecules,* 12.

ZELARAYAN, L., RENGER, A., NOACK, C., ZAFIRIOU, M. P., GEHRKE, C., VAN DER NAGEL, R., DIETZ, R., DE WINDT, L. & BERGMANN, M. W. 2009. NF-kappaB activation is required for adaptive cardiac hypertrophy. *Cardiovasc Res,* 84**,** 416-24.

ZHANG, M., MONGUE-DIN, H., MARTIN, D., CATIBOG, N., SMYRNIAS, I., ZHANG, X., YU, B., WANG, M., BRANDES, R. P., SCHRODER, K. & SHAH, A. M. 2018. Both cardiomyocyte and endothelial cell Nox4 mediate protection against hemodynamic overload-induced remodelling. *Cardiovasc Res,* 114**,** 401-408.

ZHANG, Y., LI, T., PAN, M., WANG, W., HUANG, W., YUAN, Y., XIE, Z., CHEN, Y., PENG, J., LI, X. & MENG, Y. 2022. SIRT1 prevents cigarette smoking-induced lung fibroblasts activation by regulating mitochondrial oxidative stress and lipid metabolism. *J Transl Med,* 20**,** 222.

ZHANG, Y., SHAN, M., DING, X., SUN, H., QIU, F. & SHI, L. 2023. Maternal exercise represses Nox4 via SIRT1 to prevent vascular oxidative stress and endothelial dysfunction in SHR offspring. *Front Endocrinol (Lausanne),* 14**,** 1219194.

ZHENG, C. B., GAO, W. C., XIE, M., LI, Z., MA, X., SONG, W., LUO, D., HUANG, Y., YANG, J., ZHANG, P., HUANG, Y., YANG, W. & YAO, X. 2021. Ang II Promotes Cardiac Autophagy and Hypertrophy via Orai1/STIM1. *Front Pharmacol,* 12**,** 622774.

ZHOU, D., LIU, W., ZHANG, J., DONG, Y., WU, J., ZHANG, Y., DAI, C., ZHANG, T., YANG, G., ZHANG, Y. & LI, A. 2023. Bellidifolin ameliorates isoprenaline-induced cardiac hypertrophy by the Nox4/ROS signalling pathway through inhibiting BRD4. *Cell Death Discov,* 9**,** 279.

ZIAEIAN, B. & FONAROW, G. C. 2016. Epidemiology and aetiology of heart failure. *Nat Rev Cardiol,* 13**,** 368-78.